Crustal structure of active deformation zones in Africa: Implications for global crustal processes

C.J. Ebinger[1], D. Keir[2,3], I.D. Bastow[4], K. Whaler[5], J.O.S. Hammond[6], A. Ayele[7], M. S. Miller[8], C. Tiberi[9], S. Hautot[10]

1. Department of Earth and Environmental Sciences, Tulane University, USA cebinger@tulane.edu
2. Dipartimento di Scienze della Terra, Università degli Studi di Firenze, Florence, Italy.
3. Ocean and Earth Science, University of Southampton, Southampton, U.K.
4. Department of Earth Science and Engineering, Imperial College, London, U.K.
5. Grant Institute, School of GeoSciences, University of Edinburgh, Edinburgh, U.K.
6. Department of Earth and Planetary Sciences, Birkbeck, University of London, U.K.
7. Institute of Geophysics, Space Science, and Astronomy, Addis Ababa University, Addis Ababa, Ethiopia.
8. Research School of Earth Sciences, The Australian National University, Canberra, Australia
9. Géosciences Montpellier, UMR5243-CNRS, Université Montpellier, France.
10. Imagir sarl, 29200 Brest, France

Final: August 24, 2017

This article has been accepted for publication and undergone full peer review but has not been through the copyediting, typesetting, pagination and proofreading process which may lead to differences between this version and the Version of Record. Please cite this article as doi: 10.1002/2017TC004526

Abstract

The Cenozoic East African rift (EAR), Cameroon Volcanic Line (CVL), and Atlas Mountains formed on the slow-moving African continent, which last experienced orogeny during the Pan-African. We synthesize primarily geophysical data to evaluate the role of magmatism in shaping Africa's crust. In young magmatic rift zones, melt and volatiles migrate from the asthenosphere to gas-rich magma reservoirs at the Moho, altering crustal composition and reducing strength. Within the southernmost Eastern rift, the crust comprises ~20% new magmatic material ponded in the lower crust sills, and intruded as sills and dikes at shallower depths. In the Main Ethiopian rift, intrusions comprise 30% of the crust below axial zones of dike-dominated extension. In the incipient rupture zones of the Afar rift, magma intrusions fed from crustal magma chambers beneath segment centers create new columns of mafic crust, as along slow-spreading ridges. Our comparisons suggest that transitional crust, including seaward-dipping sequences, is created as progressively smaller screens of continental crust are heated and weakened by magma intrusion into 15-20 km-thick crust. In the 30Ma-Recent CVL, which lacks a hotspot age-progression, extensional forces are small, inhibiting the creation and rise of magma into the crust. In the Atlas orogen, localized magmatism follows the strike of the Atlas Mountains from the Canary Islands hotspot towards the Alboran Sea. CVL and Atlas magmatism has had minimal impact on crustal structure. Our syntheses show that magma and volatiles are migrating from the asthenosphere through the plates, modifying rheology and contributing significantly to global carbon and water fluxes.

1. Overview

The geological record of the African continent spans three-quarters of Earth history. Key events occurred in the Archaean when the West African, Congo, Kaapvaal, Zimbabwe, and Tanzanian cratons formed, followed by Palaeoproterozoic accretion of cratons. Unusually, only the northern and northwestern margins of the African plate have been involved in orogeny since the end Pan-African (~500 Ma), when a Himalayan-scale collision formed along eastern Africa, and orogenies ringed the Zimbabwe-Kaapvaal-Congo cratons of southern and western Africa (e.g., Muhongo and Lenoir, 1994; Shackleton, 1986; van Hinsbergen et al., 2011). Each of these processes has left an indelible signature on Africa's crust, and contributed to the formation and destruction of continental topography.

Excluding the collisional belts of NW Africa (e.g., Miller & Becker, 2014), the predominant tectonic processes since the Pan-African have been magmatism and extension that have increased the surface area and volume of African crust, as outlined in this paper. Southeastern Africa was affected by rifting and flood magmatism at 184-179 Ma (Ferrar-Karroo flood basalts) prior to the separation of Africa and Antarctica (e.g., Duncan et al., 1997), and large sectors of western Africa experienced flood magmatism at 137-127 Ma (Etendeka-Parana flood basalts) as the south Atlantic opened (e.g., Turner et al., 1994; Mohriak et al., 2012). Central, southern, and eastern Africa were affected by the Mesozoic rifting and breakup of Gondwana that left scars such as the Central African rift system, and the widespread extensional basins from Somalia to S. Africa (e.g., Burke, 1996; Veevers et al., 1994). Over the past ~45 Ma, Africa again has experienced kimberlitic to flood magmatism and plateau uplift, followed by diachronous rifting from Egypt south to South Africa, and southwest through Botswana (e.g., Ebinger and Scholz, 2012) (Fig. 1). The Tertiary rift basins and magmatic provinces include all stages and styles in the evolution of cratonic rift zones: incipient rifting in the Okavango to incipient seafloor spreading in the Afar Depression; amagmatic sectors in the Western and Southwestern rift to the large igneous province (LIP) in Ethiopia-Yemen; and sectors that transect Paleozoic lithosphere of variable thickness and composition (e.g., Corti, 2009; Ebinger and Scholz, 2012; Rooney, 2017) (Figs. 1-4). Oligocene-Recent magmatism with little extension modifies crustal structure beneath West-Central Africa along the Cameroon Volcanic Line (CVL) (Fig. 3). Perhaps owing to the very slow movement of the African plate since collision with Europe initiated at ~40 Ma, domal uplift and magmatism without faulting also characterize northern Africa (e.g., Hoggar-Tibesti; Bond, 1978; Brown and Girdler, 1980; Rosenbaum & Lister, 2004) (Fig. 1).

Over the past few decades, multiple geoscientific experiments have yielded fundamental new constraints on the structure, composition, and evolution of the crust beneath extensional basin systems in Africa and between Africa and Arabia (e.g., Berckhemer et al., 1975; Prodehl & Mechie, 1991; Wölbern et al., 2010; Tokam et al., 2010). Controlled source seismic experiments provide absolute velocity control and details along largely 2D profiles of crust, and, where seismic sources are large, the upper mantle (e.g., Ruegg et al., 1975; Stuart et al., 1985; Keller et al., 1994; Maguire et al., 2006). Receiver functions provide constraints on velocity contrasts at the Moho and, in some areas, intra-crustal and intra-mantle reflectors, beneath each permanent or temporary seismic station (e.g., Hammond et al., 2011; Gao et al., 2013; Plasman et al., 2017; Hodgson et al., 2017) (e.g., Figs. 2, 3). Crustal tomography provides a 3D image of the velocity structure, and serves to connect velocity variations between the 2D controlled source profiles and receiver function point measurements. Ambient noise and arrival time tomography methods, however, rarely image the lower crust owing to sparse ray coverage from local earthquakes, and array aperture for ambient noise (e.g., Daly et al., 2008; Kim et al., 2012; Korostelev et al., 2015; Accardo et al., 2017). Magnetotelluric data provide 2D profiles and point measurements of crust and upper mantle electrical resistivity properties, including resistivity vs depth and azimuthal anisotropy of electrical conductivity (e.g., Whaler and Hautot, 2006; Selway et al., 2014). Magnetotelluric data are more sensitive to the presence of melt than seismic methods. Although models of gravity anomalies are highly non-unique, when constrained or jointly inverted with independent 2D and 3D data sets, the spatial patterns of gravity anomalies provide additional information on 3D density variations (e.g., Tiberi et al., 2005; Roecker et al., 2017). The combination of magnetotelluric, seismic, and gravity data in separate and joint inversions enables tighter constraints on material properties, and, in some instances, provides new insights into the distinction between magmatic fluids, aqueous fluids and volatiles within the crust, and their role in crustal deformation.

This contribution synthesizes our current understanding of crustal modification in tectonically active cratonic rift zones and mountain belts, and lays out a road road-map for future studies of African rift and orogenic zones. Several large-scale crust and mantle imaging experiments have acquired promising data sets in incipient and weakly extended, magma-poor rift sectors (e.g., Gao et al., 2013; Shillington et al., 2016; Hodgson et al., 2017), but a synthesis of crustal structure of early stage rifts is premature. Our focus is to characterize crustal structure in zones of active deformation in the East

African rift, Cameroon Volcanic Line (CVL), and Atlas Mountains. The review of along-axis variations in the East African rift affords the opportunity to compare and contrast magma-rich rift sectors, providing insights on the evolution of the continental crust in response to stretching and magmatism. This synthesis and comparison offers new insights into the nature of 'transitional' crust beneath late-stage rifts (e.g., Fuis and Mooney, 1990; Persaud et al., 2016) and passive margins worldwide (e.g., van Avendonk et al., 2009; Skogseid et al., 2000). Comparison and contrast with the magmatically modified crust beneath the Atlas Mountains and CVL adds to our understanding of fluid and volatile migration through the African crust.

Section 2 provides a broad-brush summary of the geodynamical context of active deformation in Africa. Section 3 outlines the role of magma intrusion during the first 5-7 My of rifting in cratonic lithosphere, using examples from the southern sector of the Eastern (Gregory) rift. Sections 4 & 5 address the role of magmatism and thinning in the formation of crust transitional between continental and oceanic. The Horn of Africa is one of few areas worldwide where this transition is occurring, and comparisons with the well-studied Salton Trough and northern Gulf of California (e.g., Fuis and Mooney, 1990; Persaud et al., 2016) inform our understanding of magmatic modification along passive margins worldwide. In Section 6, we journey across the continent, where warm asthenosphere rises beneath the eastern edge of the Congo craton and the southern margin of a pre-existing Mesozoic rift zone. This linear belt of Cenozoic eruptive volcanic centers, the CVL, exhibits neither the age-progression, mechanical stretching, magmatic modification displayed in parts of East Africa, nor along linear volcanic tracks in oceanic plates. Here too, volatiles have likely played a central role in magmatic modification of Africa's crust. Section 7 presents a review of crustal structure and its relation to mantle dynamics beneath the Atlas Mountains where compressional tectonics may inhibit upward migration of melt, leading to the localized, linear trend of magmatism linked instead to the Canary Island hotspot. This integration of constraints on crustal structure beneath zones of active rifting and orogenesis in Africa shows that magma and volatiles are migrating from the asthenosphere through the plates, modifying lithospheric rheology and significantly contributing to global carbon and water fluxes.

2. Geodynamic Settings

The slow-moving African continent moves at 3-7 mm y^{-1} NW to WNW and collides with the Eurasian plate (e.g., Serpelloni et al., 2007). Africa has unusually high elevation, in large part owing to the broad plateau uplifts associated with mantle plumes and volcanic construction in the large igneous provinces of the EARS and the CVL, and the un-extended Hoggar and Tibesti volcanic uplifts (Fig. 1). Extension effectively increases the surface area of continental landmasses and creates continental platforms. Magmatism during rifting creates new continental crust through dike and sill intrusion and surface construction, but the rates and volumes of crustal accretion are poorly constrained (Thybo and Artemieva, 2013; Lee et al., 2016), in part motivating this comparative study.

2.1 East African rift system (EARS)

Active faulting and magmatism occur across a large part of the African continent between the Horn of Africa southwest to the Okavango region of Botswana, and in a second diffuse arm that continues from southwestern Ethiopia to southeastern Mozambique, including offshore regions of the Indian Ocean, such as the Davie Ridge (Figs. 1 & 2). The southern Red Sea, Main Ethiopian and Eastern, Western and Southwestern rift systems have developed atop broad topographic plateaus, whereas the Malawi rift and its southeastward continuation transects low elevation regions in Mozambique (Fig. 2).

The broad plateaus, their corresponding negative Bouguer gravity anomalies, low upper-mantle seismic velocities, and the large volume and geochemistry of eruptive volcanic products have been cited as evidence for one or more mantle plumes beneath sections, or all, of the uplifted zones of Africa (e.g., Sengor and Burke, 1978; Nyblade and Robinson, 1994; Marty and Yirgu, 1996; Ebinger & Sleep, 1998). Global and local tomography and geochemical studies reveal low velocity zones caused by one or a combination of elevated temperatures and the presence of melt in the asthenosphere (e.g., Ritsema et al., 1999; Debayle et al., 2001; Weeraratne et al., 2004; Simmons et al., 2007; Fishwick & Bastow, 2011; Adams et al., 2012; Rooney et al., 2011; Mulibo & Nyblade, 2013; O'Donnell et al., 2013). Although gaps remain in our knowledge of the Western rift and beneath the Indian Ocean, the lowest P- and S-wave velocity regions underlie the Main Ethiopian rift (MER) and the Eastern rift zone, and the isolated volcanic provinces of the Western rift (e.g., Bastow et al., 2008; Adams et al., 2012; Fishwick, 2010; O'Donnell et al., 2013). The Ethiopia-Yemen and East African plateaux are separated by a ~300 km-wide topographic depression that is underlain by crust stretched during Mesozoic rifting, allowing the possibility that the two plateaux are actually one uplifted region

extending from southern Africa to the Red Sea: the African superplume province (e.g., Nyblade & Robinson, 1994; Ritsema et al., 1999; Kendall and Lithgow-Bertelloni, 2016).

Thermal-mechanical modeling indicates that widespread Mesozoic rift zones spanning the breadth and length of Africa would have been actively subsiding and underlain by thinned lithosphere at the onset of flood magmatism. At ~40 Ma the earliest flood basalts were erupted in southwestern Ethiopia and northern Kenya, suggesting that these thinned and heated regions may have been inherently weaker than surrounding regions (e.g., Morley et al., 1999; Hendrie et al., 1994) or may have ponded anomalously hot mantle material susceptible to decompression melting (e.g., Ebinger & Sleep, 1998). Edge-driven convection may enhance magma production and lithospheric heating at the edges of the deeply-rooted Tanzania and Congo cratons where kimberlitic and carbonatitic magmatism has occurred since ~40 Ma (e.g., Ebinger & Sleep, 1998; King & Anderson, 1998; King & Ritsema, 2000). The geochemistry of Eocene-Recent eruptive volcanic products points to a mantle plume origin for the Ethiopia-Yemen flood basalt sequences, but the East African plateau region south of Ethiopia shows more spatial variability (e.g., Pik et al., 2006; Furman et al., 2004, 2006b; Chakrabarti et al., 2008; Rooney et al., 2011; Halldorsson et al., 2014).

Although sub-Saharan Africa is widely separated from subducting slabs that carry fluids to the mantle, and the last orogenesis occurred over 500 Myrs ago, African volcanoes and active fault systems transfer large volumes of exsolved volatiles, and xenoliths are heavily metasomatized (e.g., Chesley et al., 1999; Reisberg et al., 2004; Vauchez et al., 2005; Frezzotti et al., 2010; Rooney et al., 2017b; Trestrail et al., 2017). The lithospheric heating and fluid migration modify crust and mantle density, geothermal gradients, and hydration state, which are the primary controls on the lithospheric strength (e.g., Bürgmann & Dresen, 2011; Lowry & Perez-Gussinyé, 2011; Hacker et al., 2015). Mineral physics, seismic and magnetotelluric (MT) imaging, and xenoliths provide increasing evidence that hydration state and high partial pressures of CO_2 as well as temperature significantly influence the rheology, density, seismic velocity and thermodynamics of minerals (e.g., Vauchez et al., 2005; Schmandt & Humphreys, 2010; Wada et al., 2012; Selway et al., 2014; Guerri et al., 2015). Gas and fluid phases also change the frictional properties of fault zones (e.g., Niemeijer & Spiers, 2005). Thus, heat transfer and the migration of magmatic fluids and exsolved gases through the thinning plate beneath rift zones may play a key role in strain localization during early stage rifting (e.g., Buck, 2004;

Maccaferri et al., 2014; Lee et al., 2016; Muirhead et al., 2016; Rooney et al., 2017b), as outlined in this review paper.

2.2 Cameroon Volcanic Line

The CVL formed between the northern edge of the deeply-rooted Congo Craton and the Benue Trough, a highly extended Cretaceous rift system that connected to basins in eastern Sudan and Kenya (e.g., Fairhead and Binks, 1991; Benkhelil, 1989; Poudjom-Djomani et al., 1997) (Fig. 3). The CVL straddles the continent-ocean boundary (Fig. 3). Intriguingly, 42 Ma to Recent volcanism along the CVL displays no clear age progression (e.g., Fitton, 1980; Halliday et al., 1990; Marzoli et al., 2000; Nkouathio et al., 2008), an observation that has prompted numerous workers to explore beyond the classic plate-plume hypothesis for hotspot development to explain the CVL. Alternatives have included decompression melting beneath reactivated shear zones in the lithosphere (e.g., Freeth, 1979; Fairhead, 1988; Fairhead and Binks, 1991; Moreau et al., 1987), small-scale upper-mantle convection that may advect mantle lithosphere (e.g., King & Anderson, 1998; King & Ritsema, 2000), and delamination (e.g., Fourel et al., 2013; De Plaen et al., 2014). It has also been suggested that lateral flow of buoyant asthenosphere, beneath continental lithosphere thinned extensively during Mesozoic rifting, may now be contributing to the younger volcanism along the line (Ebinger and Sleep, 1998). In support of this hypothesis, Pérez-Gussinyé et al. (2009) constrained lithospheric strength via study of effective elastic plate thickness (Te) across the African continent using coherence analysis of topography and Bouguer anomaly data. Their study revealed corridors of relatively weak lithosphere that continue across the African continent from the Afar region to Cameroon, where Te is also depressed in comparison to the surrounding cratons.

2.3 Atlas Mountains

The Atlas Mountains of Morocco are a 2000 km-long intra-continental compressional belt that strikes ENE from Morocco into Algeria and Tunisia (Figs. 1, 3, 4). The structure was formed by reactivation of Triassic-Jurassic age normal faults that originally formed during the opening of the North Atlantic, followed by the Cenozoic collision of Africa with Eurasia (e.g., Gomez et al., 2000; Pique et al., 2002). Unlike some of the other orogenic belts around the Mediterranean, the origin of the topography of the Atlas is not directly linked to slab rollback (e.g., Dewey et al., 1989; Wortel and Spakman, 2000; Faccenna et al., 2004). The unusualyl high topography, modest tectonic

shortening, thin lithosphere and localized alkali volcanism may be explained by upwelling of a hot mantle anomaly linked to the Canary island hotspot (e.g. Duggen et al., 2009; Miller and Becker, 2014; Miller et al., 2015).

3. Embryonic rifting of cratonic lithosphere and the role of volatiles

A long-standing question in plate tectonics involves the initiation of rifting in strong cratonic lithosphere, where the inherent strength of the plate is greater than the far-field and gravitational potential energy forces available (e.g., Bott, 1990; Stamps et al., 2014; Flesch and Bendick, 2014). Where magma is generated, the buoyancy forces of magma add to the tectonic stress, and dike intrusion may accommodate extension at $1/8^{th}$ the force required to overcome friction along a fault (e.g., Buck, 2004; Bialas et al. 2010). Yet, only very small melt volumes can be generated beneath thick lithosphere; magma-assisted rifting is unlikely in lithosphere greater than ca. 100 km thick, unless the upper mantle is anomalously hot, carbonated and hydrated (e.g., Turner et al., 1994; Dixon et al., 2008). The < 7 My-old Eastern rift in southern Kenya and northern Tanzania provides a unique opportunity to address this paradigm: faulting and magmatism occur in deeply-rooted lithosphere, and crust and mantle xenoliths constrain compositions (Fig. 5). This region is one of the most seismically active regions in East Africa, and both teleseismically and locally detected earthquakes span the entire crustal thickness (e.g., Yang and Chen, 2010; Craig et al., 2011; Albaric et al., 2014; Lee et al., 2016) (Fig. 4).

The Eastern (Gregory) rift marks the divergent plate boundary between the slowly-opening (≤ 6 mm/y) Nubia and Somalia plates (e.g., Saria et al., 2014; Birhanu et al., 2016) (Figs. 4, 5). The Eastern rift splays into a broad zone of ~80 km-long, seismically active faults and isolated eruptive centers at its southern termination in northern Tanzania (Figs. 4, 5). The southern sector of the Eastern rift developed after ~6 Ma, based on ^{40}Ar-^{39}Ar dating of volcanic samples, and carbon dating of abundant fossil remains in the Olduvai and Natron basins (e.g., Ashley, 2007; Mana et al., 2012; 2015). Sedimentary basin thicknesses increase to almost 10 km where the East African rift overprints Mesozoic rift basins in northern Kenya (e.g., Hendrie et al., 1994).

Although heat flow data show little-to-no elevation of geotherms beneath the 1.5-2 km rift flanks, magmatic systems within basins have locally elevated geotherms (e.g., Nyblade et al., 1990; Wheildon et al., 1994; Simiyu et al., 2010). The geochemistry and petrology of mantle xenoliths indicate that the lithosphere beneath the craton (west), rift, and Pan-African belt (east) has been metasomatized in large part by magmatic fluids and volatiles (e.g., Rudnick et al., 1993; Aulbach et al.,

2011; Mattson et al., 2013). Uniquely, voluminous CO_2 emissions derived from magma degassing occur along the seismically active border fault systems bounding basins (Lee et al., 2016) at distances >20 km from the active carbonatitic volcano, Oldoinyo Lengai (Fig. 5). The volume of fault zone degassing along faults and from volcanoes may be 11% of the global CO_2 budget (Lee et al., 2016). The localized metasomatism, magma intrusion, and magma degassing may have weakened the cratonic lithosphere to enable rift initiation at the edge of the deeply-rooted Tanzania craton. Crustal xenoliths from Archaean crust (west) and Pan-African crust (east) are mafic granulites (Jones et al., 1983; Mansur et al., 2014) (Fig. 5). Yield strength envelopes for granulitic lower crust indicate that it is too weak to explain the unusual lower crustal seismicity in this rift sector (e.g., Wang et al., 2012; Weinstein et al., 2017).

3.1 ***Crustal velocities, thinning and evidence for intrusions***

Seismic refraction/wide-angle reflection, arrival time and mantle tomography, MT, and gravity data acquired as part of the KRISP94 (Kenya Rift International Seismic Project) with profile locations shown in Figure 5, provide details of Archaean and Late Proterozoic crust, as well as rift structure. Data from two temporary seismic arrays spanning 3 rift segments of the Eastern rift, including the active Oldoinyo Lengai volcano, provide critical insights into magmatic modification and crustal stretching processes within the faulted basins and beneath the numerous eruptive volcanic centers (Ibs-von Seht et al., 2001; Plasman et al., 2017; Roecker et al., 2017) (Figs. 2b, 5).

The uppermost crust is dominated by the ~3-7 km thick sedimentary basins that formed in the Oligocene-Recent zones of crustal stretching (e.g., Hendrie et al., 1994; Morley et al.,1999; Morrissey and Scholz, 2014). Upper-crustal velocities in crystalline basement are 6.0-6.3 km/s. The sometimes-reflective boundary between upper and middle crust is marked by a velocity increase to ~6.5 km/s (Keller et al., 1994; Birt et al., 1997). Lower-crustal velocities are variable, but 6.7-6.9 km/s on average. Last et al. (1997) and Dugda et al. (2005) analyzed receiver functions from widely-spaced stations spanning the Archaean-Pan-African suture in the southernmost (Tanzania) and central (Kenya) sectors of the Eastern rift (Figs. 2, 5). Last et al. (1997) find no change in crustal thickness crossing the Archaean-Proterozoic boundary through the central Manyara rift. Dugda et al. (2005) find slightly thicker crust in the Pan-African belt east of the rift (39-42 km) than west of the rift beneath the Tanzania craton (37-38 km), and normal Poisson's ratios of 0.24-0.27, indicating little or no crustal thinning or magmatic modification outside the rift zones.

Geophysical data from the Magadi-Natron-Manyara sector of the Eastern rift reveal crustal thinning and magma intrusion across the rift zone, and low-velocity, high V_P/V_S bodies beneath some volcanoes. Moho depth determined from receiver functions and the KRISP94 profile varies between 28 and 41 km beneath the rift valley and rift shoulders, respectively (Fig. 2b, Figs. 6a, b). The thickest crust (41 km) underlies the Crater Highlands, a wedge of uplifted basement and < 6 My volcanic constructs (Plasman et al., 2017). The V_P/V_S ratio depicts a lateral variability, with zones of high V_P/V_S strongly correlated with the location of volcanic edifices. Unusually high lower-crustal velocities of 7.1-7.2 km/s in the lowermost crust beneath the Magadi basin have been interpreted as evidence for cooled gabbroic crustal intrusions (e.g., Thybo et al., 2000), or cumulates (Christensen and Mooney, 1994). Beneath the Natron basin, Plasman et al. (2017) find local low-velocity zones with a strong reflective signature, and high V_P/V_S (1.83-1.98) in the lower crust, interpreted as magma bodies. Based on wide-angle reflection-refraction studies, the mantle reflection, PmP, is high amplitude, but only at low frequencies. At high frequencies, reverberative phases are observed and modelled as an approximately 4-km thick series of mafic sills (Thybo et al., 2000).

At a greater depth of ~60 km, an intra-mantle interface roughly mimics the step-like and symmetrically outward-dipping geometry of the Moho (Plasman et al., 2017). Intra-mantle reflectors were also detected in refraction/wide-angle reflection profiling in the northern part of the Eastern rift (Mechie et al., 1994; Keller et al., 1994), and in the Main Ethiopian rift, as outlined in Section 4. A narrow zone of thinned mantle lithosphere is imaged directly beneath the fault bounded rift basins: ~90 km thick versus >125 km outside the rift zone (Green et al., 1991; Ritsema et al., 1999), consistent with P-T conditions of eruptive volcanic products (Macdonald, 1994; Mechie et al., 1994b). Along the length of the rift, velocities in the mantle just below the Moho from Pn analyses are 7.5-7.7 km/s, significantly lower than values beneath the flanks and stable interior: 8.0-8.1 km/s (Mechie et al., 1994a; Maguire et al., 1994). The magnitude of the velocity decrease is 0.3 km/s larger than predicted from higher geothermal gradients, suggesting partial melt within the upper mantle also contributes to the observed velocity reduction beneath the rift (Mechie et al., 1994b).

If we assume an initial crustal thickness of 40 km, the ~28 km–thick crust beneath the Natron and Magadi basins crustal thickness estimated from wide-angle refraction/reflection studies and receiver function studies indicate ~30% extension achieved in <7 My. The volume increase from magma intrusion may bias crustal stretching estimates to smaller values.

3.2 Crustal magmatic plumbing systems

KRISP-94 MT experiments crossing the -Proterozoic suture, the Magadi rift basin and flanks, and the off-rift Quaternary-Recent Chyulu Hills eruptive centers reveal not only the shallow basin structure, but several high conductivity zones interpreted as active and ancient intrusives. Using a 2D inversion, Simpson et al. (2000) report high conductivity lower crust, and Meju and Sakkas (2007) use a 3D inversion to image narrow high conductivity zones rising to ~8 km subsurface beneath the central rift, and beneath the Chyulu hills. Seismic tomography models reveal similar patterns. Tomography models of local earthquake P- and S-wave arrival times indicate a ~10 km-wide, linear low velocity zone beneath the central Magadi basin, which may be a zone of fractured or intruded rock (Ibs-von Seht et al., 2001) (Fig. 6c). For the Magadi-Natron-Manyara sector, Roecker et al. (2017) jointly inverted ambient noise, arrival time, and gravity data to image V_P, V_S, and V_P/V_S in the crust shallower than ~25 km. The most significant features are (1) low P and S wavespeeds underlying the rift zone, (2) a relatively high wavespeed, ~10 km-wide tabular feature located along the western edge of the Natron and Manyara rifts and (3) areas with low (1.65-1.71) values of V_P/V_S in the upper crust, with the lowest ratios along the boundaries of the rift zones (Roecker et al, 2017). The low P and S wavespeeds at mid crustal levels beneath the rift valley correlate with Holocene-Recent eruptive centers, and the tabular (in plan-view), high-wavespeed feature is the uplifted footwall of the Natron basin, with crust on the hanging wall intruded and experiencing magma degassing along the fault zone (Lee et al., 2016; Weinstein et al., 2017) (Fig. 6a). Given the high levels of CO_2 outgassing observed at the surface and the sensitivity of V_P/V_S to pore-fluid compressibility, Roecker et al. (2017) suggest that the low V_P/V_S values that correlate with zones of active CO_2 degassing at the surface are caused by the volcanic plumbing in the upper crust being suffused by a gaseous CO_2 above a deeper, crystalline mush with high V_P/V_S and high reflectivity in some areas (Plasman et al., 2017).

In a detailed study of the off-axis Chyulu hills shield-cone province (Fig. 5), Sakkas et al. (2002) find steeply-dipping high conductivity zones at depths 1-8 km and 9-18 km, interpreted as magma intrusions. Similarly, in a joint gravity-MT study of the Baringo rift segment to the north, Hautot et al. (2000) suggest Mesozoic sediments underlie a ~4 km East African rift sequence, and interpret a high-density magma intrusion with top no shallower than 6 km. Within the southern Natron basin, pancake-shaped zones of persistent $M_L \leq 4.5$ earthquakes above the inferred lower crustal crystal-rich mush zone at depths of 6-11 km below sea level may be stacked sills, with the variable fractionation depths

feeding the wide range of magma compositions at Oldoinyo Lengai and the adjacent monogenetic cone complex (Roecker et al., 2017; Weinstein et al., 2017).

Guth (2016) provides coarse estimates of eruptive magma volumes both from map data and from seismically-imaged basin fill, which combine to 310,000 km^3. Because her work includes only basins in Kenya, and ignores the Eastern rift in northern Tanzania and southwestern Ethiopia, we extrapolate estimates of intrusive volumes to the same region. For a conservative estimate of intrusive volumes, we assume 20% new magmatic material (underplate and intrusions into the central rift zone, 8 km-thick) for a 70 km-wide rift zone that is 600 km-long; intrusive volumes are at least 336,000 km^3. The total volume is at least 43000 km^3 per million years, assuming all sectors are 15 My old (average age of Eastern rift).

3.3. Constraints on Lower Crustal Deformation in Early Stage Rifts

Although lower crustal earthquakes occur in magmatic and amagmatic rift basins in Africa, we focus on lower crustal earthquakes in magmatic rift sectors. The Magadi, Natron, and Manyara basins are all associated with earthquakes in the lower crust, as relocated from local seismic networks (Ibs-von Seht et al., 2001; Albaric et al., 2014; Mulibo and Nyblade, 2010; Roecker et al., 2017) and from teleseismic studies (Shudofsky et al., 1990; Wang and Chen, 2010; Craig et al., 2011). Within the Natron basin, precisely-relocated earthquakes occur at depths of 20-27 km along a projection of the border fault to the base of the crust, consistent with thermo-mechanical models of basin and flank morphology and gravity anomalies (e.g., Ebinger et al., 1991; Sippel et al., 2017). Volumetrically-significant gas fluxes measured near these deeply penetrating fault zones bounding basins indicate that the border faults serve as conduits for CO_2 exsolved from active magma intrusions (Lee et al., 2016). Lower crustal seismicity also occurs around lower crustal mush zones, and the inferred sill complexes where high fluid pressures may induce hydraulic fracture (Weinstein et al., 2017).

Laboratory experiments simulating lower crustal conditions demonstrate that granulite is weak, particularly if the rock contains a small weight percent of water (Wang et al., 2012). Although cooled magmatic underplate or cumulates may locally strengthen the lower crust, the high V_P/V_S ratios in the lower crust and CO_2 degassing along faults that penetrate to the lower crust indicate active intrusion processes, and locally hot, weak lower crust (Plasman et al., 2017; Roecker et al., 2017). A strong, mafic lower crust, therefore, seems an unlikely explanation for widespread lower crustal seismicity in this sector of the Eastern rift. Instead, slip along border faults that penetrate to lower crustal levels and

with locally high pore fluid pressures as indicated by volatile degassing, and active magma intrusion are explanations for the unusual lower crustal earthquakes in magmatically-active early stage rift zones.

3.4 Summary: Early Stage Magmatic Rift Zones

Half-graben basins bounded by steep border faults that penetrate to lower crustal levels characterize the <7 My southern sector of the Eastern (Gregory) rift. Seismic, gravity, MT, seismicity, and xenolith studies show widespread magmatic underplating, with high levels of magmatic CO_2 degassing along border faults, as well as through active volcanoes. Although much of the area was affected by magmatism between 6 and 1 Ma, during the past ~1 Ma, eruptive centers have formed within the central Magadi and Natron basins. Tomographic imaging and seismicity indicate that the central volcanoes and monogenetic cones are sourced by one or more lower crustal magma chamber(s) overlain by stacked sills that may explain the wide range of lava compositions. Dike and sill intrusions have reached 8-10 km subsurface, in patterns similar to the Main Ethiopian rift outlined below. Sharp contrasts in velocity and V_P/V_S between hanging wall and footwall suggest that magmatic modification has localized to the faulted basin area.

4. Magma-rich continental rifting - the Main Ethiopian rift

The Horn of Africa captures the combined processes of crustal stretching and intrusion at various stages of continental breakup. The Ethiopian rift is the northernmost sector of the EARS, which is the incipient boundary between the Nubia and the Somalia plate (Figs. 2a & 7). It encompasses early to mid-stage continental rift sectors, and it captures the transition from deformation along 50-100 km-long border fault systems to zones of magma intrusion. Here we focus our synthesis on how geophysics and petrology are providing improved understanding of where and how magma migrates and ponds in the crust during progressive rift development. Some of these patterns mimic along-strike patterns noted in the <7 My old Natron-Magadi rift sectors (Section 3), and highlight strain and structural changes associated with the rise of magma to upper crustal levels.

The Main Ethiopian rift (MER) formed within the Precambrian metamorphic crustal basement of the Pan-African orogenic belt that exhibits N–S to NNE–SSW suture zones (Vail, 1983; Berhe, 1990) and NW-SE oriented strike-slip faults in Ethiopia (Brown, 1970; Purcell, 1976). The central and

northern sectors of the MER developed between 18 and 10 Ma, respectively (e.g., WoldeGabriel, 1990; Wolfenden et al., 2004; Rooney et al., 2013). Between 18 and 12 Ma, large offset border faults commonly marked by chains of eruptive centers formed along one or both sides of the rift (e.g., Chernet et al., 1998; Rooney et al., 2014) (Fig. 7). South of ~7.5°N, seismically-active faults in a broad depression effectively link the ~30 My Eastern rift to the MER, across a broad zone of sub-parallel and time-transgressive basins (e.g., Morley et al., 1992; Ebinger et al., 2000). Further north, within the basin bounded by Miocene border faults, the rift floor is segmented into a series of Quaternary-to-Recent aligned volcanic centers cut by small offset normal fault systems, referred to as magmatic segments (Ebinger and Casey, 2001; Corti, 2008; 2009; Mazzarini et al., 2013) (Fig. 7). The magmatic segments are the locus of magma intrusion, and are underlain by high velocity zones interpreted as gabbroic intrusions, as outlined below (Fig. 8). GPS data show the axial volcanic segments are the locus of current extension (Bilham et al., 1999), with the surface geology suggesting this has been the case since the Quaternary (Ebinger and Casey, 2001). Plate kinematic models constrained by marine magnetic anomaly patterns and geodetic data require that some extension across the MER took place by about 16 Ma (DeMets and Merkouriev, 2016).

As outlined below, crustal structure in Ethiopia is constrained using receiver functions, wide-angle controlled source seismology, MT, and inversion of gravity data. Combined, these results provide important clues to extensional processes that modify the crust during rifting.

4.1 Crustal velocities, thinning and evidence for intrusion

Stuart et al. (2006) and Hammond et al. (2011) analyzed receiver functions from broadband stations in the Ethiopian rift, building on results of earlier studies of data from widely-spaced networks (Dugda et al., 2005, 2006) (Figs. 2a, 5). The EAGLE controlled source wide-angle experiment constrained across-rift and along-axis variations in crustal structure, as well as the uplifted flanks of the Ethiopian flood basalt province (Figs. 8, 9, 10A). EAGLE comprised two ~400 km-long profiles: one cross-rift (Fig. 9) and one rift axial profile (Maguire et al., 2006). A dense network of stations was deployed over the intersection of the two profiles to provide 3D images of the along-axis segmentation patterns (Keranen et al., 2004; Mackenzie et al., 2005; Maguire et al., 2006) (Fig. 7). Figure 10 compares receiver function results projected onto the line of controlled source and MT profiles to facilitate comparisons of crustal thickness estimates from seismic tomography, reflection, and MT

results. Crustal thicknesses are similar to those determined using receiver functions, but absolute determination of V_P, and variations thereof provide further insights.

The crust beneath the Somalian plate east of the rift is 38–40 km thick (Figs. 2a, 7). The crust on the Nubian plate west of the rift is of similar thickness, but thickens to 41-43 km between ~9°N and 12°N. MT data show significant differences between the lowermost crust beneath the plateaux on either side of the rift (Fig. 9): thicker and resistive beneath the Somalian Plateau, thinner with higher conductivity beneath the Ethiopian Plateau in agreement with the interpretation of underplate there (Mackenzie et al., 2005; Rooney et al., 2016). This region of thicker crust lies at the northern edge of an off-rift upper-mantle low-velocity structure imaged by travel-time tomography (e.g., Bastow et al., 2005; 2008; Hammond et al., 2013). At the surface, this upper mantle low-velocity zone and thicker crust on the northwestern rift shoulder is marked by a chain of Miocene-Quaternary eruptive centers, the Yerer-Tullul Wellel volcanic lineament (YTVL; Abebe, 1998) (Fig. 7). Magmatic underplating during the early stages of rifting may have thickened and strengthened crust to the north, and localized later strain and magmatism (e.g., Keranen and Klemperer, 2008; Kim et al., 2012). It should be borne in mind that receiver function Moho depth estimates for the Ethiopian plateau are shallower than those inferred by wide-angle reflection analysis: receiver functions appear sensitive primarily to the top, not the bottom of the 8-12 km-thick mafic layer(s) in the lower crust (e.g., Stuart et al., 2006).

Along the rift axis, crustal thickness varies from around 38 km in the south to 30 km in the north, with most of the change in Moho depth occurring just south of the Boset-Kone magmatic segment where the rift floor drops in elevation into the Afar depression (Figs. 2a, 7). The change in crustal thickness from ~40 km beneath the rift shoulders to 30 km in the rift implies a minimum stretching factor of 1.5 (28 km), or considerably less than the stretching factor ~2 estimated by plate kinematic models (42 km; DeMets and Merkouriev, 2016). Stretching factors estimated from crustal thickness alone will under-estimate total extension, as outlined below.

The crust is interpreted to be slightly more mafic (V_P/V_S >1.85) beneath the Ethiopian Plateau than the Somalian Plateau (V_P/V_S ≈1.80) (Figs. 2a, 7C). This could either be due to Oligocene to Recent magmatic activity or different pre-rift crustal compositions. Regions of volcanism inside and on the side of the rift (e.g., Silti Debre Zeit Fault zone, SDFZ), are characterized by thinned crust and V_P/V_S >2.0, indicative of partial melt within the crust (Fig. 7C). Seismic, MT, gravity, and petrological data image or require significant magma volumes, particularly in the lower crust of these magmatic rift zones (Field et

al., 2012; Hammond et al., 2011; Desissa et al., 2014; Lewi et al., 2016; Johnson et al., 2016). For example, elevated V_P/V_S ratios in regions of thinning likely indicates both solidified and still partially molten intrusions contribute to extension (Hammond et al., 2011; 2013).

Using spatial variations in V_P imaged by wide-angle controlled source seismology it has been possible to infer spatial variations in amount of intrusion. Along the rift, V_P in the lower crust ranges from 6.6 to 7.2 km/s, peaking at 7.1-7.2 km/s in the lowermost crust between Gedemsa and Fentale volcanoes in the central part of the MER (Figs. 7, 9). Elevated wavespeeds of >6.8 km/s have been interpreted as evidence for gabbroic crustal intrusions (e.g., Keranen et al., 2004; Mackenzie et al., 2005; Maguire et al., 2006). In the upper crust, 3-D controlled source tomography shows significant variation in V_P, with discrete high V_P (>6.4 km/s) zones beneath the magmatic segments (Figs. 8, 9). The > 7 km/s velocities and high densities inferred from forward and inverse models of gravity data indicate that the magmatic segments are underlain by gabbroic material (e.g., Mahatsente et al., 2004; Tiberi et al., 2005; Cornwell et al., 2006). The observed pattern of segmented high velocity zones was reproduced by gabbroic bodies that rise to 10 km below the surface, indicating that 30% of the crust beneath the magmatic segments is new igneous material (Keranen et al., 2004).

The observations corroborate the surface geology evidence that axial magma intrusion, likely in the form of gabbroic cumulates from crustal magma chambers, fed sheeted dykes. The dikes, as well as faults above the dikes, accommodate most of the deformation across the rift, based on time-averaged and active deformation patterns (Keir et al., 2006; Casey et al., 2006). New GPS data confirm that active deformation occurs across the Ethiopian plateau (Birhanu et al., 2016), which hosts aligned chains of Quaternary eruptive centers, high-conductivity lower-crust, and lower-crustal seismicity (Keir et al., 2011) (e.g., Fig. 10).

4.3 Crustal magma plumbing systems

The interpretation of gravity and electrical conductivity anomalies has been used to construct an ever more detailed picture of the crustal magma plumbing system accommodating extension during breakup, and sourcing active off-axis volcanoes (Fig. 9). In the MER, Cornwell et al. (2006) conducted a cross-rift gravity survey and Whaler and Hautot (2006) a cross-rift MT survey, coincident with wide-angle Line 1 (Fig. 9). Major features of the gravity study are an axial low-density upper-mantle or high-density lower-crustal zone which is modeled as a ~50 km wide body with a density of 3190 kg/m^3, supporting interpretations of a mafic underplate layer beneath the northwestern rift flank (Cornwell et

al., 2006). Two high-density (3000 kg/m^3) upper-crustal bodies underlie the MER: a 20 km-wide axial body, and a 12 km-wide off-axis body, both of which are likely gabbroic in composition.

MT data provide some of the best evidence for the emplacement and migration of melt during breakup. Major features of the MT survey are a conductive body at 20-25 km depth beneath the rift axis interpreted as a mid-to-lower crustal magma reservoir (Fig. 9). A second highly conductive region at 25-35 km depth is beneath the rift flank near the SDFZ and YTVL (Figs. 6, 8). The lower-crustal high conductivity zone coincides with seismicity, leading to its interpretation as a pressurized magma reservoir beneath the rift flank volcanoes (Keir et al., 2009) (Fig. 9). Ambient noise tomography reveals low V_S (<3.2 km/s) beneath the magmatic segments, suggesting that the zones of solidified axial intrusions still include a small fraction of partial melt (Kim et al., 2012). Lower-crustal melt retention is also consistent with high V_P/V_S ratios imaged in the upper crust beneath the rift axis using local earthquake tomography (Daly et al., 2008). Petrological analyses along the SDFZ indicate that erupted lavas fractionated at a range of crustal depths, in line with the geophysical observations (Rooney et al., 2007; 2011; 2014). A shallow conductive lens at <1 km depth underlying Boset Volcano is most likely indicative of either a shallow hydrothermal or magmatic system (Whaler & Hautot, 2006).

Farther south in the MER, Samrock et al. (2015) collected broadband MT data over the Aluto volcanic center (Fig. 7a). They found no mid- or lower-crustal conductor there, despite models of geodetic data indicating melt storage and migration at <10 km depths (Biggs et al., 2011). These observations have subsequently been interpreted as resulting from a locked, crystal-rich mush which lacks the connectivity to provide high bulk electrical conductivity (Hutchison et al., 2016). Samrock et al.'s (2015) data did, however, indicate a conductor beneath the SDFZ to the northwest of Aluto, with top surface at ~12 km depth. Both observations have subsequently been confirmed as melt storage beneath rift flank volcanoes by a 110 km-long MT profile centered on Aluto and orthogonal to the rift axis, which included deeper-probing long period MT measurements (Hübert et al., 2016).

4.3 Summary of mature rift crustal structure

Geophysical and petrological studies indicate that intrusion and fluid release into the lower crust occurs beneath the rift and parts of the uplifted plateau region, 40 Myr after the onset of flood magmatism. This long-lived magmatism produces a high-velocity, high P-wave lower crust with or without low S-wave velocities. Within the fault-bounded basins, border faults are largely inactive, and strain is localized to < 20 km-wide magmatic segments: zones of localized magma intrusion, volcanic

construction, and dense faulting. At least 30% of the crust beneath the magmatic segments is new igneous material. Comparison of refraction/wide-angle reflection Moho and receiver function Moho reveals a discrepancy: the receiver function analyses image the top of the high-velocity lower crust in zones of active magma intrusion, and provide minimum constraints on intrusive magma volumes.

5. Late stage continental breakup and initiation of seafloor spreading - the Afar depression

The Afar Depression encompasses the rift-rift-rift triple junction between the Nubian, Somalian, and Arabian plates: The Red Sea (Arabia-Nubia) and Gulf of Aden (Arabia-Somalia) rifts that bound the Arabian plate, and the East African rift (Nubia-Somalia) (e.g., McKenzie and Davies, 1970; Mohr, 1972; Manighetti et al., 1998; Beyene and Abdelsalam, 2005) (Fig. 7). The cumulative extension in Afar is much higher than in the MER, and it therefore is the ideal setting to understand the final stages of continental breakup (e.g., Wolfenden et al., 2005; Doubre et al., 2007; Stab et al., 2016). Well-established seafloor spreading with seafloor spreading anomalies is observed in some sectors of the Red Sea (Ligi et al., 2011) and in the Gulf of Aden (e.g., Leroy et al. 2010).

Rifting of Arabia from Africa to form the Red Sea and Gulf of Aden rift zones preceded rifting in the Main Ethiopian rift by >10 My, based on structural, stratigraphic, and plate kinematic data (e.g., Chernet et al., 1998; Wolfenden et al., 2004; Corti et al., 2009; DeMets and Merkouriev, 2016). Stratal relations of dated volcanic sequences and aligned eruptive centers indicate that some border faults along the western margin of Afar began at 29-31 Ma, approximately coeval with the highest magma production rates in the Ethiopia-Yemen flood basalt province (e.g., Ayalew et al., 2006; Wolfenden et al., 2005). Faulting and basin subsidence had begun by about 35 Ma along large portions of the Gulf of Aden, but without magmatism (Leroy et al., 2010). As in the Ethiopian rift, structural and geomorphological analyses indicate that extensional strain was initially focused on large offset border faults, and subsequently extension has become more localized to axial volcanic segments (Hayward and Ebinger, 1996; Wolfenden et al., 2005; Sembroni et al., 2016) (Fig. 7).

The comparatively long history of flood magmatism and faulting has produced unusual crust; the structure and composition of the 18-25 km-thick crust beneath Afar is transitional between continental and oceanic (e.g., Makris and Ginzburg, 1987; Mohr, 1989). Its structure informs magmatic passive margin studies in the Red Sea and worldwide. Specifically, debate continues regarding the nature of

crust beneath thick sequences of seaward-dipping volcanic layers that mask basement structure (e.g., Franke et al., 2007; van Avendonk et al., 2009). **Is the Afar crust, which isslightly thicker than normal oceanic crust, completely new igneous material intruded as sheeted dikes fed from lower crustal magma chamber(s), as along mid-ocean ridges with slow opening rates, or is it a combination of highly stretched continental crust with magmatic intrusions and metamorphic sediments?**

Active deformation processes in the Afar Depression provide important clues (e.g., Keir et al., 2009; Pagli et al., 2012). Constraints on crustal structure primarily come from teleseismic receiver function studies (Ayele et al., 2004; Dugda et al., 2005; Hammond et al., 2011; Stuart et al., 2006); wide-angle seismic surveys (Berckhemer et al., 1976; Makris and Ginzburg, 1987; Maguire et al., 2006), gravity (Ebinger and Hayward, 1996; Redfield et al., 2004; Tessema and Antoine, 2004; Tiberi et al., 2005; Lewi et al., 2015) and MT studies (van Ngoc et al., 1981; Desissa et al., 2013; Didana et al., 2015, 2016; Johnson et al., 2015). A primary focus is to address the links between crustal thinning, magma intrusion, and subsidence to address a long-standing debate in plate tectonics: **When does seafloor spreading start?**

5.1. Crustal thinning and intrusive bodies

Over the past 30 My, the zone of stretched and subsiding crust has broadened to about 300 km in central Afar, whereas the zone of active deformation has narrowed to intensely faulted, <20 km-wide and ~50 km-long magmatic segments fed from central magma chambers. Similar to the shoulders of the Ethiopian rift, receiver function analysis shows that the crust beneath the Ethiopia-Yemen Plateau is 40-45 km thick. It is ~35 km thick beneath the Somalian Plateau (Dugda et al., 2005; Stuart et al., 2006; Keranen et al., 2009; Hammond et al., 2011), similar to average crustal thickness of 35 km beneath the plateau of western Yemen (Ahmed et al., 2013) (Fig. 2a, 9). The Danakil horst, separating the two sub-parallel arms of the Red Sea rift in the offshore and in Afar, is underlain by ~30 km-thick crust. In general, the Ethiopian, Somalian, and Yemen plateaux have V_P/V_S of 1.7-1.9, whereas localized regions of thicker (~30 km-thick) crust within Afar have V_P/V_S of 1.8-1.9 (Dugda et al., 2005; Stuart et al., 2006; Hammond et al., 2011; Reed et al., 2014) (Fig. 7c). $V_P/V_S \leq 1.85$ can be explained compositionally (Christensen, 1996; Hacker et al., 2015), but observations of V_P/V_S >1.85 strongly suggest present-day melt in rift-parallel fractures and cracks, with anisotropy contributing to

the high V_P/V_S values (Hammond, 2014). Ambient noise tomography images low Vs in the mid to upper crust (Korostelev et al., 2015), consistent with the high V_P/V_S (>1.9) imaged with receiver functions (Hammond et al., 2011), with both indicating melt-filled pore spaces/fractures.

Within the fault-bounded depression that includes the MER, southern Red Sea, and Gulf of Aden rifts, distinct differences occur. The <10 My-old northern sector of the MER in Afar cuts through crust originally stretched and intruded as Arabia and Africa separated to form the third arm of the triple junction. The superposition of two rift systems (Red Sea, MER) causes a striking northward decrease in crustal thickness from ~35 km in the central MER, to ~25 km in southern Afar (e.g., Fig. 7b). What remains unclear, however, is the ratio of intrusive to extrusive volumes, and total mechanical stretching.

In central Afar, the crust is 20-25 km thick beneath the current locus of volcanism and strain in the Manda-Harraro rift (MHR) and Tendaho Graben (TG), which are the southernmost segments of the Red Sea rift arm (Reed et al., 2014) (Fig. 7). Currently-active and abandoned magmatic segments are the locus of the greatest crustal thinning (<20 km), and they are separated by bands of ~30 km thick, intruded crust (Hammond et al., 2011). This 'ridge-jump' pattern was created as the magma storage systems supplying magmatic segments jumped laterally across the broad Afar triple junction zone (Hammond et al., 2011). Further suggestion of ridge migration comes from thermal modelling (Daniels et al., 2014) and Medynski et al.'s (2015) inference of chemically-distinct, alternately active magma chambers. The spatial arrangement of sub-parallel, migrating magma accretion zones are similar to patterns observed on passive margins worldwide, and predicted in ridge-jump seaward-dipping accretion models (Buck, 2017).

As outlined in Section 5.3 and Van Ngoc et al. (1981), MT results indicate at least two of the magmatic segments, the MHR segment in the southern Red Sea, and the Asal-Ghoubbet segment in the Gulf of Aden rifts extend in a fashion similar to a mid-ocean ridge (Fig. 7). During intense faulting and fissural eruption episodes, dikes sourced from magma chambers near the center of magmatic segments achieved meters of rift opening, and created up to 60 km-long columns of mafic crust in periods of days (e.g., Abdallah et al., 1978; Ayele et al., 2009; Keir et al., 2009; Barnie et al., 2016).

Gravity and magnetic data from a 50 km-long, ~1m station density profile across the Tendaho basin provide indirect evidence that the intense dike intrusion events produce narrow columns of new igneous crust, similar to processes on slow-spreading ridges (Bridges et al., 2012). Here the magnetic

data show near symmetrical anomalies across the center of the rift, whose scale, shape and magnitude are similar to those observed in nearby seafloor spreading centers in the Gulf of Aden. These data, together with the Bouguer gravity field are consistent with symmetrical sheeted mafic dike complex intruded into the upper ~10 km of the crust, and capped by 2-3 km-thick basin fill of fissural basalts and sediments (Bridges et al., 2012). The observations provide evidence that most crustal extension is facilitated by magma intrusion, mimicking the extensional processes at slow spreading mid-ocean ridges. Thus, it is possible that the first magnetic anomalies recorded at volcanic rifted margins form in comparatively thick (~15 km-thick) crust originally classified as 'transitional crust' (e.g. Bridges et al., 2012; Bronner et al., 2011; Rooney et al., 2014).

5.2 Magmatic Plumbing System

Constraints on the magma plumbing system come from receiver functions, seismicity, MT, gravity and magnetic studies. MT data provide unprecedented constraints on the locus and scale of magma plumbing systems that feed dyke intrusion and volcanism in the MHR segment (Desissa et al., 2013; Johnson et al., 2015) (Fig. 11). A small-scale, but high melt-fraction (≤22%), conductor lies slightly deeper than the inferred source of magma supplying the recent dyking events, determined from geodesy and seismology (e.g. Ebinger et al., 2008; Hamling et al., 2009; Grandin et al., 2011). A much more substantial magma reservoir straddling the Moho (~22 km deep in this area; Hammond et al., 2011) lies ~25 km to the west of the rift axis (Fig. 11) where Ferguson et al. (2013) find geochemical evidence for ponding and re-equilibration of magma at the top of the mantle, most likely stored in stacked sills. Although the regularized MT inversion model of Figure 11 gives a single conductor, Johnson et al. (2015) show that a series of sills, with a similar total magma volume, fit the data equally well.

A second MT profile in the northwestern MHR was acquired on a trend oblique to the rift, and approaching within 10 km of Dabbahu volcano at the northern end of the magmatic segment (Johnson et al., 2016). At its closest point to the volcano, the model has very high (≥12 S/m) conductivity from depths of ~4 km, peaking at 6.5 km depth. Interpretation of these data is a challenge since model conductivities exceed that of basaltic melt at the appropriate temperatures and pressures, even with high water content (Pommier and Le Trong, 2011). However, Field et al. (2012, 2013) found a wide range of erupted products from the Dabbahu volcano, including very evolved, wet rhyolites, which could have crystallized in the top 6 km of the crust. Recent estimates of rhyolite melt conductivity (Guo

et al., 2016) are 3-4 times higher than conductivities of basaltic melt at the appropriate temperature, pressure, Na_2O and water content, but still less than the maximum observed in our model. Very high conductivities and hence substantial melt volumes (even using the higher melt conductivities of rhyolitic magmas deduced by Guo et al., 2016) are also detected beneath the Dabbahu volcano, where Field et al. (2012) inferred protracted fractional crystallization of parent basaltic magma in a substantial, long-lived storage region, preferably in sills, between 1.5 km and 5.5 km depth, consistent with the pressured zone imaged with seismicity data (Ebinger et al., 2008); however, MT data cannot be satisfied by a conductor confined to such shallow depths (Johnson et al., 2015). Jointly, the data support the view of sill complexes beneath axial and flank volcanic systems. However, petrological constraints suggest fractionation starts in the lower crust beneath flank volcanoes, and in the upper crust beneath axial volcanoes.

The two most recent eruptions at the northernmost magmatic segment, Erta'Ale, were sourced from dikes and sills in the upper 3 km (Pagli et al., 2012; Xu et al., 2017; Magee et al., 2017) (Fig. 7b). The persistent lava lake in the Erta'Ale crater and the frequent eruptions suggest a semi-permanent melt-rich sill, as along the magma-rich slow-spreading Reykjanes ridge. Further south where the MHR segment merges with the Tendaho Graben, high conductivity is again imaged off-axis at lower-crustal depths (Johnson et al., 2015) (Fig. 11), but with smaller inferred volumes than beneath the recently active northern MHR. This coincides with an inferred partially-molten gabbroic body that has been intruded into a thinned lower crust deduced from microgravity data (Lewi et al., 2015) (cf. models of MT and gravity data through the Boset volcano in the northern MER; Whaler and Hautot (2006), Cornwell et al., (2006), section 4.2). Didana (2014; 2015) imaged an upper-crustal zone of extensive partial melt fraction (up to 0.13) beneath the Tendaho Graben geothermal prospect to the east of the southern MHR axis, connected to a large intrusive magmatic body underlying the TG and MHR, fed by a mantle source.

Further south across the currently inactive part of the MHR, lying within the TG, high conductivity is again imaged at lower-crustal depths (Profile 3), in this case ~10 km to the east of the rift axis (Johnson et al., 2015) (Fig. 10). The maximum conductivity and lateral extent of the conductor, and hence inferred partial melt fraction and total melt volume, are lower than in the off-axis reservoir beneath the recently active northern MHR. In a similar location, Lewi et al. (2015) modelled microgravity data to infer that a partially-molten gabbroic body has been intruded into a thinned lower

crust. This agreement between MT and gravity results is reminiscent of that found for the location of dense sub-surface bodies, interpreted as gabbroic, and conductors across the northern MER through Boset volcano. Didana et al. (2014, 2015) have modelled several MT profiles across the TG geothermal prospect to the south-east of the profile of Johnson et al. (2015) and to the east of the southern MHR axis. Seismic surface wave (Guidarelli et al., 2011), Pn (Stork et al., 2013) and body-wave tomography (Hammond et al., 2013) studies image slow upper-mantle velocities throughout the MHR rift segment, with the most extreme reductions centered on the recently-active northern part.

5.3 The shape and distributuion of partial melt

Seismic anisotropy in the upper-crust is constrained from shear-wave splitting from local earthquakes (Keir et al., 2011) and surface waves (Bastow et al., 2010) (Fig. 11D). Large amounts of fault-parallel (NNW) anisotropy are seen only in the area of 2005-2012 diking activity. Outside of this region, anisotropy in the upper-crust is lower, but remains aligned with major faults. These patterns suggest that the presence of melt enhances a pervasive fracture-parallel anisotropy in this region. Seismic anisotropy in the whole crust can be estimated by looking at azimuthal variations in V_P/V_S from receiver functions. V_P/V_S throughout Afar have values >2, implying that melts are also present (Dugda et al., 2005, Stuart et al., 2006, Hammond et al., 2011). However, Hammond (2014) shows that such high values are an effect of seismic anisotropy, suggesting that if melt is the cause, then it must be preferentially aligned. Inverting the azimuthal variations in V_P/V_S suggest that melt in the lower crust must be stored in interconnected sills, consistent with reflectivity studies in rift zones (e.g., Thybo et al., 2000). Estimates of azimuthal anisotropy for the whole crust have the same orientation as that in the upper crust, but with much stronger anisotropy.

Further support for aligned crustal melt pockets comes from measurements of geoelectrical strike orientations determined from the MT profiles outlined in Section 5.2 (Johnson, 2012). The presence of electrical anisotropy implies that the aligned melt is interconnected. For periods synonymous with the mostly low-conductivity upper-crust (1-10 s), the electrical anisotropy strikes are similar to those from upper-crustal earthquake shear-wave splitting, and the magnitude of electrical anisotropy (measured as the difference in MT phase for currents flowing along and across geoelectrical strike; see, e.g. Hamilton et al., 2006; Padilha et al., 2006) is relatively low. For periods synonymous with the conductive lower-crust (100-1000 s) the strike of the electrical anisotropy matches well with fast

directions from receiver function and teleseismic shear-wave splitting, and the amount of electrical anisotropy is higher (Fig. 11). These similarities support the idea that seismic and electrical anisotropy are caused by the preferential alignment of melt, primarily in the lower crust. These patterns suggest that melt can flow within these interconnected networks in the lower crust and feed the relatively localized zones of deformation in the upper crust (Desissa et al., 2013, Hammond, 2014). Note that there are areas with little or no electrical anisotropy, but high conductivities indicating abundant melt, in the upper crust (e.g. close to Dabbahu volcano, Fig. 11), suggesting no particular geometry in its arrangement. Here, the penetration depth is severely limited, and the 100-1000 s periods are probably not penetrating the deeper crust.

5.4 Crustal thinning and subsidence at plate rupture

Wide-angle seismic experiments show that the crust throughout Ethiopia has a consistent layering with lower crustal V_P=6.7-7.0 km/s, an upper crustal V_P= 6.0-6.3 km/s, and cover rocks of lava flows and sediments with V_P=2.2-4.5 km/s (Makris and Ginzburg, 1987; Prodehl and Mechie, 1991) (Figs. 8, 10, 12). Excluding the regularly-spaced volcanoes marking the centers and tips of magmatic segments, the cover rocks are generally thickest where the crust is thinnest suggesting a strong link between crustal thinning, rift valley subsidence and resultant accumulation of basin infill (Fig. 12). The Danakil basin, which hosts the Erta'Ale magmatic segment, has the thinnest crust in Afar at 15 km thick and is also characterized by the thickest sedimentary basins: ~5 km as opposed to 2-3 km elsewhere (Berckhemer et al., 1976; Makris and Ginzburg, 1987) (Fig. 12). The change in crustal thickness along-rift from south to north is primarily accounted for by markedly thinned lower crust, although the upper-crust is also appreciably thinner (Makris & Ginzburg, 1987). Existing controlled source data do not traverse the rough relief of the currently active magmatic segments where intrusion volumes may be largest.

Spatial variations in crustal thickness in Ethiopia correlate with variations in effective elastic thickness, with the strongest plate (Te ≈ 60 km) beneath the plateaus, and the weakest plate (Te ≈ 6 km) beneath the Danakil depression (Ebinger and Hayward, 1996; Pérez-Gussinyé et al., 2009). Both crustal thickness and effective elastic thickness, a measure of strength over time periods much longer than the earthquake cycle, also correlate to variations in seismogenic layer thickness estimated from local seismicity and teleseisms; seismogenic layer thickness is 25-30 km beneath the Ethiopian plateau (Keir et al., 2009), but decreases to ~5 km beneath the Danakil depression (Craig et al., 2011;

Nobile et al., 2012).

There is debate regarding whether the regions of thinnest crust (~15-20 km) in Afar, such as the Danakil depression, are fully oceanic in nature. In the Danakil depression, the basin floor is at ~120m below sea-level and the Holocene stratigraphy is dominated by intercalated basalts and evaporites (Atnafu et al., 2015). The basin stratigraphy and environment of deposition is similar to that interpreted to form the seaward dipping reflector sequences (at fully rifted margins), and therefore the Danakil depression could be a modern analog for their formation (Bastow and Keir, 2011; Corti et al., 2015; Buck, 2017). There is at least 50% more melt available beneath the northern MHR than in the TG segment in the south, and likely up to an order of magnitude more. This change is consistent with regional northward increases in the number of Holocene volcanoes as well as the volume of erupted material (Barberi and Varet, 1977), and it is likely a result of a northward increase in thinning of the plate and resultant decompression melting of asthenosphere (Bastow and Keir, 2011).

The most highly-extended crust beneath the Danakil depression is 5-10 km thicker than normal oceanic crust. There are two endmember hypotheses to explain the structure and composition of the Danakil crust. In one model, heavily intruded and extended crust deforms by brittle failure at the surface, and by magma intrusion and ductile flow in the lower crust (Bastow and Keir, 2011). Unlike thin crust at oceanic rifts, the intrusive material may stall and fractionate to produce peralkaline and rhyolitic lavas, and felsic intrusive material, contributing to the unusual structure. The second model relates to high magma production rates in early-stage seafloor spreading caused by the steep lithosphere-asthenosphere boundary on either side of the rift (e.g., Boutilier et al., 1982; White and McKenzie, 1989; Korenaga et al., 2000; Ligi et al., 2011). The high extrusion rates at the weak spreading ridge cause bending above the ridge and may produce seaward-dipping reflectors. Our syntheses suggest that both processes are important.

5.5 Summary: Defining transitional crust and plate rupture along magmatic margins

Passive and controlled source seismic imaging shows that the crust in Afar varies from 15 to 25 km thick, and the crust is heavily modified by solidified mafic intrusion and partial melt currently residing in magma reservoirs through the crust. MT combined with modeling seismic and electrical anisotropy supports the interpretation that the lower crust is an important region of melt ponding. The melt in the lower crust resides in horizontal sills near segment centers, and it is then transported laterally and

vertically in dikes that accommodate most of the plate boundary deformation. The central magma chamber that maintains the along-axis segmentation over multiple episodes, and the extension via dike intrusion and faulting above the dikes produces columns of new crust with corresponding magnetic stripes. The unusually-thick crust (~15 km) matches the thick crust beneath magmatic rifted margins with seaward-dipping reflector sequences, pointing to a common mode of emplacement. In contrast, the observed seismic velocity and structure of the crust and the low-silica composition of basalts suggests that seafloor spreading processes are still evolving.

Seismic imaging, gravity, and MT all suggest that the whole crust beneath the rift flanks and the rift axis is heavily modified by magma intrusion. Seismic and electrical anisotropy support the view that magma accumulates in the lower crust as networks of interconnected stacked sills, whereas magma in the upper crust may be both in sill networks and sub-vertical dikes. Petrological constraints suggest fractionation starts in the lower-crust beneath flank volcanoes during the early stages of rifting, whereas most fractionation occurs in the upper-crust beneath axial volcanoes as plate rupture initiates (Rooney et al., 2011; 2014).

6. The Cameroon Volcanic Line

Cameroon's crustal structure has been investigated using both passive and active seismic sources (e.g., Stuart et al., 1985; Dorbath et al., 1986; Plomerova et al., 1993; Meyers et al., 1998; Tokam et al., 2010; Gallacher and Bastow, 2012) and potential field studies (e.g., Fairhead and Okereke, 1987; Toteu et al., 2004; Tadjou et al., 2009) (Figs. 3b, 13). Thinned crust (~25 km) resulting from extension is imaged beneath the Garoua Rift (Fig. 12), while the transition from the CVL to the Congo Craton is heralded by a transition in Moho depth from ~36 km to 43–48 km depth (Tokam et al., 2010; Gallacher and Bastow, 2012) (Fig. 13). Crustal shear-wave velocities also increase into the craton from the CVL, from ~3.7 km/s to ~3.9 km/s (Tokam et al., 2010). Bulk-crustal V_P/V_S ratios along the CVL are comparable to those of cratons worldwide (~1.74), an observation that Gallacher and Bastow (2012) cited as evidence for the lack of melt fractionation and intrusion during the ~30 Ma development of the CVL. These seismological results thus corroborate petrological studies that attribute low volume, high-pressure magmas to melting of sub-continental lithospheric mantle that has experienced only small amounts of crustal fractionation (e.g., Fitton, 1980; Halliday et al., 1988; Marzoli et al., 2000; Suh et al.,

2003; Yokoyama et al., 2007). Such low-volume, high-pressure magmas are expected to form within the sub-continental lithospheric mantle and exhibit relatively little fractionation within the crust (e.g., Suh et al., 2003).

Gravity studies in Cameroon (e.g., Poudjom-Djomani et al., 1992, 1997; Fairhead and Okereke, 1987; Tadjou et al., 2009) highlight various major tectonic features in the region, including the Benue Trough (+ve Bouguer anomaly), uplift of the Adamawa plateau (-ve anomaly), and the Congo Craton (-ve Bouguer anomaly). Evidence for continental collision was found at the northern margin of the Congo Craton, as well as a positive anomaly associated with the Central African Shear Zone, which bisects the Adamawa uplift (Fig 13: e.g., Poudjom-Djomani et al., 1997; Tadjou et al., 2009).

Recent work by Milelli et al. (2012) and Fourel et al. (2013) has used scaled laboratory models and analytical solutions to investigate the effects of large lateral variations in lithospheric thickness on lithospheric stability. Their work demonstrates that lithospheric instabilities can develop over long timescales with small rates of upwelling and decompression melting as is observed in Cameroon, and consistent with recent hybrid models for magmatism along the CVL (e.g., Reusch et al., 2010; Gallacher et al., 2012; De Plaen et al., 2014).

7. The Atlas Orogen

In contrast to the Mediterranean arcs (Alps, Apennine, Carpathian, Hellenic, and Betic-Rif), the Atlas are subparallel to and south of the convergent margin, and on the African plate (Figs. 1, 3a). The mountain belt has high topography (>4100 m), yet there is no apparent deep crustal root to isostatically support the high elevations of the Atlas (e.g. Sandvol et al., 1998; Ayarza et al., 2005; 2014; Zeyen et al., 2005; Missenard et al., 2006; Miller and Becker, 2014; Jessell et al., 2016) (Figure 3a). Furthermore, only a modest amount of tectonic shortening has been estimated and has been suggested to be achieved through thick-skinned thrusting and folding (e.g. Gomez et al., 1998; Teixell et al., 2003).

Many recent efforts have focused on understanding the crustal- and lithospheric-scale structure of the Atlas to understand the orogenesis. Structural seismological imaging suggests that the lithosphere beneath the Atlas is particularly thin or perhaps the uppermost mantle is abnormally warm with low seismic velocities found at depths of ~65-160 km (e.g., Fullea et al., 2010; Palomeras et al., 2014; Bezada et al., 2014; Sun et al., 2014; Miller et al., 2015). Figure 14 shows S receiver function

estimates of the Moho and lithosphere-asthenosphere depths along a profile across the Atlas from Miller and Becker (2014). Geophysical modelling indicates that the lithosphere is thin (~65 km) compared with the topographically high, thick lithosphere of the Saharan Platform (≥150km) and the Morocco Atlantic Margin along a corridor that is aligned with the highest topography in the Atlas (Teixell et al., 2003; Teixell et al., 2005; Missenard et al., 2006; Fullea et al., 2010; Missenard and Cadoux, 2012; Miller and Becker, 2014; Miller et al., 2015) (see Fig. 3a). The combination of thinned lithosphere and mantle upwelling have been invoked to explain the unusual high topography, low seismic velocities in the uppermost mantle, and lack of a significant crustal root (Arboleya et al., 2004; Teixell et al., 2005; Missenard et al., 2006; Frizon de Lamotte et al., 2009; Fullea et al., 2010; Miller and Becker, 2014; Zlotnik et al., 2014). The source of the upwelling has been suggested to be part of the Canary plume from geochemical analyses of Quaternary alkali basalts in the Atlas and their spatial location above the low velocity material beneath the mountain range (Anguita and Hernan, 2000; Duggen et al., 2009).

Shear-wave splitting analyses (Miller et al., 2013; Diaz and Gallart, 2014) also indicate a strong change in azimuthal anisotropy strength at the northern edge of the Middle Atlas, as well as an alignment of fast polarization orientations parallel to the strike of the Atlas Mountains, suggesting shearing in a mantle channel guided by lithospheric topography (Miller et al., 2013; Miller and Becker, 2014) and deflected by the high velocity slab beneath the Alboran Sea (Alpert et al., 2013; Diaz and Gallart, 2014). Miller et al. (2015) interpret the localized volcanism and low velocity anomalies in the sub-lithospheric mantle to be the result of the Canary Island plume flowing sub-horizontally beneath the Atlas. This seismologically based interpretation is supported by numerical experiments of mantle flow that incorporate the effects of the stiff, deep West African cratonic keel and nearly vertical, narrow slab beneath the Alboran (Alpert et al., 2013), numerical experiments of strongly tilted plumes and resulting instabilities (Mériaux et al., 2011), and by scaled analogue models of the Alboran slab and Canary plume interaction (Mériaux et al., 2015). Other hypotheses explaining the Cenozoic uplift of the Atlas and the links to recent volcanism and to upper-mantle structure include: lithospheric delamination (Duggen et al., 2009; Bezada et al., 2014; Levander et al., 2014) and edge-driven convection (Missenard and Cadoux, 2012; Kaislaniemi and van Hunen, 2014). The two edge-driven convection studies (Missenard and Cadoux, 2012; Kaislaniemi and van Hunen, 2014) are based on numerical experiments, which are designed to evaluate the dynamics of the thinned lithosphere and

mantle melting processes in the Moroccan Atlas. They also find good agreement with observations of lithospheric thickness and volcanism, but neither incorporate the presence of the subducted slab beneath the Alboran Sea.

Despite the lack of consensus on the origin of the Atlas topography, various recent studies using a range of methods, from the SIMA active source seismic experiment (Ayarza et al., 2014), broadband waveform analysis (Sun et al., 2014), MT (Anahnah et al., 2011; Ledo et al., 2011), body wave (e.g. Bezada et al., 2014) and surface wave (Palomaras et al., 2013) tomography for example, have suggested the presence of anomalous low-velocity material beneath the lithosphere and in the crust. The temperature of this material is also inferred to be warm and be due to the presence of partial melt (Anahnah et al, 2011; Ledo et al., 2011; Sun et al., 2014; Ayarza et al., 2014).

8. Summary

Our synthesis of geophysical studies that aim to image the crust beneath zones of active rifting and orogenesis in Africa show that magma and volatiles are migrating from the asthenosphere through the plate, leading to changes in rheology, and making large contributions to H_2O and CO_2 fluxes globally. The addition of magmatic fluids permanently alters the composition of continental crust accreted during the and Proterozoic, and it increases the continental crustal volume. The magma intrusion accommodates plate boundary deformation and masks crustal stretching. In young, weakly extended sectors of the East African rift, volatiles released from upwelling asthenosphere, heated mantle lithosphere, and magma intrusions alter crustal composition and rheology. Even in rifts that formed within the last 7 My, ~20% of the crust is new magmatic material intruded as sills in the lower crust (underplate) and as more localized zones of dike intrusion in the mid- and upper-crust as imaged with seismic, MT, and gravity methods. In the mature Main Ethiopian rift (MER), the surface area of the rift has doubled in the past ca. 10 My, and intrusive volumes are 30%, increasing into the central Afar rift zone where dike intrusion accommodates much of the active extension, and symmetric magnetic anomalies mimic seafloor spreading. Intrusive to extrusive volumes (surface flows plus basin fill) are roughly equivalent, but increase with increasing age of rifting and amount of extension, and proximity to pre-rift flood magmatism. In the older, more evolved Horn of Africa, intense episodes of magma intrusion fed from crustal magma chambers beneath segment centers create new columns of mafic crust up to 8 m-wide in a process akin to that along slow-spreading ridges. The magma intrusion and

faulting above the dikes accommodates centuries of plate boundary opening, and suggests that plate rupture is achieved through catastrophic magma intrusion events in 15-20 km-thick transitional crust. Regional analyses suggest that progressively smaller screens of continental crust are heated and weakened by repeated episodes of magma intrusion immediately prior to seafloor spreading.

On the western side of the African continent, magmatism with very minor extension over the past 30 My has formed the Cameroon Volcanic Line (CVL) - a linear chain of basaltic volcanoes that formed on the broad Adamawa plateau that lacks the age-progression predicted by the traditional hot-spot track hypothesis. Intrusive volumes are much smaller than in the Eastern, MER, and Afar rifts, and magmas largely fractionate at sub-crustal depths. The comparison with East African crustal structure suggests that extensional forces are much smaller in the CVL, inhibiting the creation and rise of magma into the crust, and preventing full-scale rifting. In the Atlas orogen of northwestern Africa, recent magmatism is also primarily along a linear trend from the Canary Islands to the Alboran Sea and linked to the Canary Island hotspot. In contrast to the magma-rich Horn of Africa, however, magmatism in Cameroon and Morocco has had relatively little impact on crustal structure, but the mantle flow and lithospheric heating cause dynamic uplift supporting the high Atlas mountain range.

Our work highlights consistent patterns and new insights into continental lithospheric deformation processes. Based on our results and complementary crust and mantle xenolith studies, future studies would benefit from constraints on physical properties across a broader range of crustal and magmatic rock compositions, and in particular, relatively low silica and gas-rich melts. Our work focuses on areas with sometimes dense data coverage, but large sectors of the African continent remain virtually unexplored in terms of crust and upper mantle structure through seismic, MT, heat flow, and detailed structural analyses. Gap-filling studies will tighten context for studies of active deformation, and they promise new insights into continental lithospheric behavior, given the relative stability of the African continent. Critical areas include the largely amagmatic but remote Western and Southwestern rift zones, the Turkana gap between the Ethiopian and East African plateaux, the seismically active Indian Ocean margin, and the boundaries of thick Archaean cratons, which have been the locus of plate deformation through multiple Wilson Cycles.

Acknowledgements

We thank two anonymous referees and editors Jeff Gu and John Geissman for feedback that greatly improved text and figures. CE was supported by NSF grant EAR-1113355 and EAR-1109302. DK is supported by NERC grant NE/L013932/1. CE and DK also were supported by a grant from Beach Petroleum and Tanzania Development Corporation. CT and SH were supported by ANR grant 12-JS06-000. CE, CT, and DK conducted studies with approval of the Commission for Science and Technology (Tanzania) and the National Council for Science and Technology (Kenya). KAW was supported by NERC grants NER/B/S/2001/00863 and NE/E007147/1 and is currently supported by NERC grant NE/L013932/1. Her MT fieldwork used equipment loaned by the NERC Geophysical Equipment Facility and from University of Brest and the Geophysical Instrument Pool Potsdam, and was supported logistically by Addis Ababa University, the Geological Survey of Ethiopia, and the Petroleum Operations Department of the Ethiopian Ministry of Mines. MSM is supported by NSF Continental Dynamics Program EAR-0809023 and NSF CAREER award EAR-1054638. The facilities of SEIS-UK are supported by the Natural Environment Research Council under agreement R8/H10/64. The facilities of IRIS Data Services, and specifically the IRIS Data Management Center, were used for access to waveforms, related metadata, and/or derived products used in this study. Broadband seismic data collected in Morocco utilized PASSCAL instrumentation and were supported by IRIS. IRIS Data Services are funded through the Seismological Facilities for the Advancement of Geoscience and EarthScope (SAGE) Proposal of the National Science Foundation under Cooperative Agreement EAR-1261681. CRAFTI data (XJ) are available at the IRIS-DMC in 2017 (http://ds.iris.edu/ds/nodes/dmc/).

References

Abdallah, A., Courtillot, V., Kasser, M., Le Dain, A.Y., Lépine, J.C., Robineau, B., Ruegg, J.C., Tapponnier, P. and Tarantola, A. (1979), Relevance of Afar seismicity and volcanism to the mechanics of accreting plate boundaries. *Nature*, *282*(5734), 17-23.

Abdelfettah, Y., Tiercelin, J.J., Tarits, P., Hautot, S., Maia, M. and Thuo, P., (2016), Subsurface structure and stratigraphy of the northwest end of the Turkana Basin, Northern Kenya Rift, as revealed by magnetotellurics and gravity joint inversion. *J. Afri. Earth Sci.*, *119*, 120-138.

Abebe, T., Mazzarini, F., Innocenti, F. and Manetti, P. (1998), The Yerer-Tullu Wellel volcanotectonic lineament: A transtensional structure in central Ethiopia and the associated magmatic activity. *Journal of African Earth Sciences*, *26*(1), pp.135-150.

Accardo, N., J.B. Gaherty, D. J. Shillington, C.J. Ebinger, A. A. Nyblade, G. J. Mbogoni, PRN Chindandali, R. Ferdinand-Wambura, G. D. Mulibo, G. Kamihanda, D. Keir, C. Scholz, K. Selway, J. P. O'Donnell, G. Tepp, R. Gallacher, K. Mtelela, J. Salmina, A. Mruma (2017), Surface-wave imaging of the weakly-extended Malawi Rift from ambient-noise and teleseismic Rayleigh waves, *Geophys. J. Int., 209*(3), 1892-1905.

Adams, A., Nyblade, A. and Weeraratne, D., (2012), Upper mantle shear wave velocity structure beneath the East African plateau: evidence for a deep, plateauwide low velocity anomaly. *Geophys. J. Int.*, *189*(1),123-142.

Ahmed, A., C. Tiberi, S. Leroy, G. W. Stuart, D. Keir, J. Sholan, K. Khanbari, I. Al- Ganad, and C. Basuyau (2013), Crustal structure of the rifted volcanic margins and uplifted plateau of Western Yemen from receiver function analysis, *Geophys. J. Int*., doi:10.1093/gji/ggt072.

Ahmed, S. Leroy, D. Keir, F. Korostelev, K. Khanbari, F. Rolandone, G. Stuart, & M. Obrebski (2014), Crustal structure of the Gulf of Aden southern margin: Evidence from receiver functions on Socotra Island (Yemen), *Tectonophysics*, 637, 251-267.

Albaric, J., J. Déverchère, J. Perrot, A. Jakovlev, and A. Deschamps (2014), Deep crustal earthquakes in North Tanzania, East Africa: Interplay between tectonic and magmatic processes in an incipient rift. Geochem., Geophys., Geosyst*.,* 15, 374-394.

Alpert, L. A., M. S. Miller, T. W. Becker, and A. Allam (2013), Structure beneath the Alboran from Geodynamic Flow Models and Seismic Anisotropy, *J. Geophys. Res*., 118(8), DOI:10.1002/jgrb.50309.

Anahnah, F., Galindo-Zald var, J., Chalouan, A., Pedrera, A., Ruano, P., Pous, J., Heise, W., Ruiz Constan, A., Benmakhlouf, M., L pez-Garrido, A. C., Ahmamou, M., Sanz de Galdeano, C., Arzate, J., Ibarra, P., Gonz lez-Castillo, L., Bouregba, N., Corbo, F., and Asensio, E. (2011), Deep resistivity cross section of the intraplate Atlas Mountains (NW Africa): New evidence of anomalous mantle and related Quaternary volcanism. *Tectonics* 30, doi:10.1029/2010TC002859.

Anguita, F. and Hernán, F., (2000), The Canary Islands origin: a unifying model. *J. Volc. Geotherm. Res.*, *103*(1),1-26.

Arboleya, M.L., Teixell, A., Charroud, M. and Julivert, M. (2004), A structural transect through the High and Middle Atlas of Morocco. *Journal of African Earth Sciences*, *39*(3), 319-327.

Ashley, G. M., Tactikos, J. C., & Owen, R. B. (2009), Hominin use of springs and wetlands: paleoclimate and archaeological records from Olduvai Gorge (~ 1.79–1.74 Ma). *Palaeogeography, Palaeoclimatology, Palaeoecology*, *272*(1), 1-16.

Atnafu, B., T. Kidane, A. Foubert, D. Jaramillo-Vogel, J-C. Schaegis, and J-P. Henriet (2015), Reading history in Afar. EOS 96, 12-15.

Aulbach, S.R.L. Rudnick, R.L. and W. F. McDonough, (2011), Evolution of the lithospheric mantle beneath the East African Rift in Tanzania and its potential signatures in rift magmas. *Geol. Soc. Am. Spec. Papers*, *478*,105-125.

Ayalew, D., C. Ebinger, E. Bourdon, E. Wolfenden, G. Yirgu, and N. Grassineau (2006), Temporal compositional variation of syn-rift rhyolites along the western margin of the southern Red Sea and northern Main Ethiopian Rift, *Geol. Soc. Lond. Spec. Publ*., 259, 121-130.

Ayarza, P., F. Alvarez-Lobato, A. Teixell, M. L. Arboleya, E. Tesón, M. Julivert, and M. Charroud (2005), Crustal Structure under the Central High Atlas Mountains (Morocco) from Geological and Gravity Data, *Tectonophys*., 400(1–4), 67-84,

Ayarza, P., R. Carbonell, A. Teixell, I. Palomeras, D. Martí, A. Kchikach, M. Harnafi, A. Levander, J. Gallart, M. L. Arboleya, J. Alcalde, M. Fernández, M. Charroud, and M. Amrhar, (2014), Crustal Thickness and Velocity Structure across the Moroccan Atlas from Long Offset Wide-Angle Reflection Seismic Data: The Sima Experiment, *Geochem., Geophys., Geosyst.*, 15(5), 1698-1717, 10.1002/2013GC005164.

Ayele, A.A., Stuart, G., and Kendall, J-M., (2004), Insights into rifting from shear wave splitting and receiver functions: an example from Ethiopia, *Geophys. J. Int*., 157, 354-362.

Ayele, A., Keir, D., Ebinger, C., Wright, T.J., Stuart, G.W., Buck, W.R., Jacques, E., Ogubazghi, G. and Sholan, J. (2009), September 2005 mega-dike emplacement in the Manda-Harraro nascent oceanic rift (Afar depression). *Geophysical Research Letters*, *36*(20), 10.1029/2009GL039605.

Barberi, F., and J. Varet, (1977), Volcanism of Afar: Small-scale plate tectonics implications, *Geol. Soc. Am. Bull.*, 88(9), 1251–1266.

Barnie, T.D., Keir, D., Hamling, I., Hofmann, B., Belachew, M., Carn, S., Eastwell, D., Hammond, J.O.S., Ayele, A., Oppenheimer, C. and Wright, T., (2016), A multidisciplinary study of the final episode of the Manda Hararo dyke sequence, Ethiopia, and implications for trends in volcanism during the rifting cycle, *Geol. Soc. Lon. Spec. Publ.*, 420, 149-163

Bastow, I., G. Stuart, J.-M. Kendall, and C. Ebinger, (2005), Upper-mantle seismic structure in a region of incipient continental breakup: northern Ethiopian rift, *Geophys. J. Int.,* 162, 479–493, doi:10.1111/j.1365-246X.2005.02666.x.

Bastow, I., A. Nyblade, G. Stuart, T. Rooney, and M. Benoit, (2008), Upper Mantle Seismic Structure Beneath the Ethiopian Hotspot: Rifting at the Edge of the African Low Velocity Anomaly, *Geochem. Geophys. Geosyst*., 9(12), Q12022, doi: 10.1029/2008GC002107.

Bastow, I., S. Pilidou, J.-M. Kendall, and G. Stuart, (2010), Melt-induced seismic anisotropy and magma assisted rifting in Ethiopia: evidence from surface waves, *Geochem. Geophys. Geosyst*., 11, Q0AB05, doi:10.1029/2010GC003036.

Bastow, I., D. Keir, and E. Daly, (2011), The Ethiopia Afar Geoscientific Lithospheric Experiment (EAGLE): Probing the transition from continental rifting to incipient seafloor spreading, Geol. Soc. Am. Spec. Papers, 478, 51–76, doi: 10.1130/2011.2478(04).

Bastow, I., and D. Keir, (2011), The protracted development of the continent-ocean transition in Afar, *Nat. Geosci.*, 4, 248–250, doi:10.1038/NGEO01095.

Benkhelil, J., (1989), The origin and evolution of the Cretaceous Benue Trough (Nigeria). *J. Afri. Earth Sci.* (and the Middle East), 8(2), 251-282.

Berckhemer, H., B. Baier, H. Bartlesen, A. Behle, H. Burkhardt, H. Gebrande, J. Makris, H. Menzel, H. Miller, and R. Vees, (1975), Deep seismic soundings in the Afar region and on the highland of Ethiopia. In: A. Pilger and A Rosler (Editors), Afar Depression of Ethiopia, Schweizerbart, Stuttgart, I, 89-107.

Berhe, S., (1990), Ophiolites in northeast and East Africa: Implications for Proterozoic crustal growth,

J. Geol. Soc. London, 147 (1), 41–57.

Beyene, A., and M. Abdelsalam, (2005), Tectonics of the Afar Depression: A review and synthesis*, J. Afr. Earth Sci.*, 41 (1), 41–59.

Bezada, M. J., E. D. Humphreys, J. M. Davila, R. Carbonell, M. Harnafi, I. Palomeras, and A. Levander, (2014), Piecewise Delamination of Moroccan Lithosphere from beneath the Atlas Mountains, *Geochem., Geophys., Geosyst.*, 15(4), 975-985, 10.1002/2013GC005059.

Bialas, R., W. Buck, and R. Qin, (2010), How much magma is required to rift a continent?, *Earth Planet. Sci. Lett.*, 292 (1), 68–78.

Biggs, J., I. Bastow, D. Keir, and E. Lewi, (2011), Pulses of deformation reveal frequently recurring shallow magmatic activity beneath the Main Ethiopian Rift, *Geochem. Geophys. Geosyst.*, doi:10.1029/2011GC003662.

Bilham, R., R. Bendick, K. Larson, P. Mohr, J. Braun, S. Tesfaye, and L. Asfaw, (1999), Secular and tidal strain across the Main Ethiopian Rift*, Geophys. Res. Lett.,* 26, 2789–2792.

Birhanu, Y., Bendick, R., Fisseha, S., Lewi, E., Floyd, M., King, R., & Reilinger, R., (2016), GPS constraints on broad scale extension in the Ethiopian Highlands and Main Ethiopian Rift. *Geophys. Res. Lett.*, *43*(13), 6844-6851.

Bird, P., (2003), An updated digital model of plate boundaries, Geochem**.** Geophys**.** Geosyst**.**, 4(3), 1027, doi:10.1029/2001GC000252.

Birt, C.S., P.K.H. Maguire, M. A. Khan, H. Thybo, G. R. Keller, J. Patel, (1997), The influence of pre-existing structures on theS evolution of the southern Kenya Rift Valley—evidence from seismic and gravity studies. *Tectonophysics*, 278(1), 211-242. URL http://dx.doi.org/10.1016/S0040-1951(97)00105-4

Bond, G., (1978), Evidence for late Tertiary uplift of Africa relative to North America, South America, Australia and Europe. *J. Geol.*, *86*(1), 47-65.

Bott, M.H.P. (1990), Stress distribution and plate boundary force associated with collision mountain ranges. *Tectonophysics*, *182*(3-4), 193-209.

Boutilier, R.R. and Keen, C.E., (1999), Small-scale convection and divergent plate boundaries. *J. Geophys. Res.*, *104*(B4), 7389-7403.

Bridges, D., K. Mickus, S. Gao, M. Abdelsalam, and A. Alemu (2012), Magnetic stripes of a transitional continental rift in Afar, *Geology*, 40(3), 203–206.

Bronner, A., D. Sauter, G. Manatschal, G. Peron-Pinvidic, & M. Munschy (2011), Magmatic breakup as an explanation for magnetic anomalies at magma-poor rifted margins, *Nat. Geosci*., 4, 549-553, doi: 10.1038.ngeo1201.

Brown, C. and Girdler, R.W. (1980), Interpretation of African gravity and its implication for the breakup of the continents. *J. Geophys. Res.*, *85*(B11), 6443-6455.

Brown, G., (1970), Eastern margin of Red Sea and coastal structures in Saudi Arabia, *Phil. Trans. R. Soc. Lond. A*, 267, 75–87.

Buck, W. R. (2004), Consequences of asthenospheric variability on continental rifting. *Rheology and deformation of the lithosphere at continental margins*, *62*, 1-30.

Buck, W.R., (2017), The role of magmatic loads and rift jumps in generating seaward dipping reflectors on volcanic rifted margins. *Earth Planet. Sci. Lett*, *466*, 62-69.

Bürgmann, R. and Dresen, G., (2008), Rheology of the lower crust and upper mantle: Evidence from rock mechanics, geodesy, and field observations. *Annu. Rev. Earth Planet. Sci.*, *36*, 531-567.

Burke, K., (1996), The African plate. *S. Afri. J. Geol.,* 99, 341–409.

Casey, M., Ebinger, C., Keir, D., Gloaguen, R. and Mohamed, F., (2006), Strain accommodation in transitional rifts: extension by magma intrusion and faulting in Ethiopian rift magmatic segments. *Geol. Soc., Lond., Spec. Pub.*, *259*(1), 143-163.

Chakrabarti, R., Basu, A.R., Santo, A.P., Tedesco, D. and Vaselli, O., (2009), Isotopic and geochemical evidence for a heterogeneous mantle plume origin of the Virunga volcanics, Western rift, East African Rift system. *Chemical Geology*, *259*(3), 273-289.

Chernet, T., W. Hart, J. Aronson, and R. Walter (1998), New age constraints on the timing of volcanism and tectonism in the northern Main Ethiopian Rift — southern Afar transition zone (Ethiopia), J*. Volcanol. Geotherm. Res.*, 80, 267–280.

Chesley, J.T., Rudnick, R.L. and Lee, C.T., (1999), Re-Os systematics of mantle xenoliths from the East African Rift: Age, structure, and history of the Tanzanian craton. *Geochim. Cosmochim. Acta*, *63*(7), 1203-1217.

Christensen, N., (1996), Poisson's ratio and crustal seismology, *J. Geophys. Res*., 101(B2), 3139–

3156, doi:10.1029/95JB03446.

Christensen, N.I. and Mooney, W.D., (1995), Seismic velocity structure and composition of the continental crust: A global view. *J Geophys. Res.*, *100*(B6), 9761-9788.

Cornwell, D G, Mackenzie, G D, Maguire, P K H, England, R W, Asfaw, L M & Oluma, B, (2006), Northern Main Ethiopian Rift crustal structure from new high-precision gravity data, in Yirgu, G, Ebinger, C J and Maguire, P K M (eds.), Structure and Evolution of the East African Rift System in the Afar volcanic province, *Geol. Soc. London Spec. Pub*., 259, 269–291.

Corti, G., (2008), Control of rift obliquity on the evolution and segmentation of the main Ethiopian rift, *Nat. Geosci.*, 1, 258-262.

Corti, G., (2009), Continental rift evolution: From rift initiation to incipient breakup in the Main Ethiopian Rift, East Africa, *Earth Sci. Rev*., 96, 1-53, doi: 10.1038/ngeo160.

Corti, G., A. Agostini, D. Keir, J. van Wijk, I.D. Bastow, and G. Ranalli, (2015), Magma-induced axial subsidence during final-stage rifting: Implications for the development of seaward-dipping reflectors. *Geosphere*, 11, 563-571, doi: 10.1130/GES01076.1.

Cooper, C. M., and M. S. Miller, (2014), Craton formation: internal structure inherited from closing of the early oceans, *Lithosphere*, 6(1), 35-42, 10.1130/l321.1.

Craig, T., J. Jackson, K. Priestley, and D. McKenzie, (2011), Earthquake distribution patterns in africa: their relationship to variations in lithospheric and geological structure, and their rheological implications, *Geophys. J. Int.*, 403–434, doi: 10.1111/j.1365-246X.2011.04950.x.

Daly, E., D. Keir, CJ.. Ebinger, G.W. Stuart, I.D. Bastow, & A. Ayele, (2008), Crustal tomographic imaging of a transitional continental rift: the Ethiopian rift, *Geophys. J. Int.,* 172, 1033-1048, doi: 10.1111/j.1365-246X.2007.03682.x.

Daniels, K., I. Bastow, D. Keir, R. Sparks, and T. Menand, (2014), Thermal models of dyke intrusion during development of continent-ocean transition, *Earth Planet. Sci. Lett*., 385, 145–153, doi:10.1016/j.epsl.2013.09.018.

Debayle, E., Lévêque, J.J. and Cara, M. (2001), Seismic evidence for a deeply rooted low-velocity anomaly in the upper mantle beneath the northeastern Afro/Arabian continent. *Earth Planet. Sci. Lett*, *193*(3), 423-436.

DeMets, C., and S. Merkouriev (2016), High-resolution estimates of Nubia–Somalia plate motion since 20 Ma from reconstructions of the Southwest Indian Ridge, Red Sea and Gulf of Aden. *Geophys. J. Int.*, 207, 317-332.

De Plaen, R., I. Bastow, E. Chambers, D. Keir, R. Gallacher, and J. Keane (2014), The development of magmatism along the Cameroon Volcanic Line: Evidence from seismicity and seismic anisotropy, *J. Geophys. Res.*, 119, 4233–4252, doi: 10.1002/2013JB010583.

Desissa, M., N. Johnson, K. Whaler, S. Hautot, S. Fisseha, and G. Dawes, (2013), A mantle magma reservoir beneath an incipient mid-ocean ridge in Afar, Ethiopia, *Nat. Geosci*., 6(10), 861-865.

Dewey, J.F., Helman, M.L., Knott, S.D., Turco, E. and Hutton, D.H.W., (1989), Kinematics of the western Mediterranean. *Geol. Soc., Lond., Spec. Pubs.*, *45*(1), 265-283.

Díaz, J., and J. Gallart, (2014), Seismic anisotropy from the Variscan Core of Iberia to the Western African Craton: New constraints on upper mantle flow at regional scales, *Earth Planet. Sci. Lett.,* 394(0), 48-57.

Didana, Y. L., S. Thiel, and G. Heinson, (2014), Magnetotelluric imaging of upper crustal partial melt at Tendaho graben in Afar, Ethiopia, *Geophys. Res. Lett.,* 41, 3089–3095, doi:10.1002/2014GL060000.

Didana, Y.L., Thiel, S. and Heinson, G., (2015), Three dimensional conductivity model of the Tendaho High Enthalpy Geothermal Field, NE Ethiopia, *J. Volc. Geotherm. Res*., 290, 53-62

Dixon, J., Clague, D.A., Cousens, B., Monsalve, M.L. and Uhl, J., (2008), Carbonatite and silicate melt metasomatism of the mantle surrounding the Hawaiian plume: Evidence from volatiles, trace elements, and radiogenic isotopes in rejuvenated-stage lavas from Niihau, Hawaii. *Geochem. Geophys., Geosyst*. 9(9).

Dorbath, C., L. Dorbath, J. Fairhead, and G. Stuart, (1986), A teleseismic delay time study across the Central African Shear Zone in the Adamawa Region of Cameroon, West Africa, *Geophys. J. R. Astr. Soc*., 86(3), 751–766.

Doubre, C., Manighetti, I., Dorbath, L., Dorbath, C., Bertil, D. and Delmond, J.C., (2007), Crustal structure and magmato-tectonic processes in an active rift (Asal-Ghoubbet, Afar, East Africa): 2.

Insights from the 23-year recording of seismicity since the last rifting event. *J. Geophys. Res., 112*(B5).

Dugda, M., A. Nyblade, J. Julià, C. Langston, C. Ammon, and S. Simiyu, (2005), Crustal structure in Ethiopia and Kenya from receiver function analysis*, J. Geophys. Res*., 110(B1),

doi:10.1029/2004JB003065.

Dugda, M., and Nyblade, A.A., (2006), New constraints on crustal structure in eastern Afar from the analysis of receiver functions and surface wave dispersion in Djibouti. *Geol. Soc. Lond. Spec. Pubs.*, *259*(1), 239-251.

Duggen, S., K. A. Hoernle, F. Hauff, A. Klügl, M. Bouabdellah, and M. Thirlwall, (2009), Flow of Canary mantle plume material through a subcontinental lithospheric corridor beneath Africa to the Mediterranean, *Geology*, 37(3), 283-286,

Duncan, R.A., Hooper, P.R., Rehacek, J., Marsh, J.S. and Duncan, A.R., (1997), The timing and duration of the Karoo igneous event, southern Gondwana. *J. Geophys. Res., 102*, p.18.

Ebinger, C., and N. Sleep, (1998), Cenozoic magmatism throughout East Africa resulting from impact of a single plume, *Nature*, 395, 788–791.

Ebinger, C. and Scholz, C.A., (2012), Continental rift basins: the East African perspective. In Busby, C and A. Azor (eds.), *Tectonics of Sedimentary Basins: Recent Advances*, pp.183-208.

Ebinger, C., T. Yemane, D. Harding, S. Tesfaye, S. Kelley, and D. Rex, (2000), Rift deflection, migration, and propagation: Linkage of the Ethiopian and Eastern rifts, Africa, *Bull. Geol. Soc. Am.,* 112(2), 163–176.

Ebinger, C., D. Keir, A. Ayele, E. Calais, T. Wright, M. Belachew, J. Hammond, E. Campbell, and W. Buck, (2008), Capturing magma intrusion and faulting pro- cesses during continental rupture: seismicity of the Dabbahu (Afar) rift, *Geophys. J. Int.,* 174(3), 1138–1152, doi:10.1111/j.1365-246X.2008.03877.x.

Ebinger, C., and M. Casey, (2001), Continental breakup in magmatic provinces: an Ethiopian example, *Geology*, 29, 527–530.

Faccenna, C., C. Piromallo, A. Crespo-Blanc, L. Jolivet, and F. Rossetti, (2004), Lateral slab deformation and the origin of the western Mediterranean Arcs, *Tectonics*, 23(TC1012),

Fairhead, J., (1988), Mesozoic plate tectonic reconstructions of the Central South Atlantic Ocean: The role of the West and Central African Rift System, *Tectonophysics*, 155(1-4), 181–191.

Fairhead, J., and R. Binks, (1991), Differential Opening of the Central and South Atlantic Oceans and the Opening of the West African Rift System, *Tectonophysics*, 187(1-3), 191–203.

Fairhead, J., and C. Okereke (1987), A regional gravity study of the West African Rift System in Nigeria and Cameroon and its tectonic interpretation, *Tectonophysics*, 143(1-3), 141–159.

Ferguson, D.J., Maclennan, J., Bastow, I.D., Pyle, D.M., Keir, D., Blundy, J.D., Plank, T., and Yirgu, G. (2013), Melting during late stage rifting in Afar is hot and deep, *Nature*, 499, 60-73.

Field, L P, Blundy, J, Brooker, R A, Wright, T J and Yirgu, G., (2012), Magma storage conditions beneath Dabbahu Volcano (Ethiopia) constrained by petrology, seismicity and satellite geodesy**,** *Bull. Volc*., 74, 981–1004

Field, L P, Blundy, J, Calvert A and Yirgu, G. (2013), Magmatic history of Dabbahu, a composite volcano in the Afar Rift, Ethiopia, *GSA Bull*., **125**, 128-147, doi: 10.1130/B30560.1

Fishwick, S. (2010), Surface wave tomography: Imaging of the lithosphere–asthenosphere boundary beneath central and southern Africa?. Lithos, *120*(1), 63-73.

Fishwick, S. and Bastow, I.D., (2011), Towards a better understanding of African topography: a review of passive-source seismic studies of the African crust and upper mantle. *Geol. Soc., Lond, Spec. Publs*, *357*(1), 343-371.

Fitton, J., (1980), The Benue Trough and Cameroon Line–A migrating rift system in West Africa, *Earth Planet. Sci. Lett.*, 51 (1), 132–138.

Fitton, J., and H. Dunlop, (1985), The Cameroon Line, West Africa, and its Bearing on the Origin of Oceanic and Continental Alkali Basalt, *Earth Planet. Sci. Lett*., 72(1), 23–38.

Flesch, L. and Bendick, R., (2012), The relationship between surface kinematics and deformation of the whole lithosphere. *Geology*, *40*(8), 711-714.

Fourel, L., L. Milelli, C. Jaupart, and A. Limare (2013), Generation of continental rifts, basins, and swells by lithosphere instabilities, *J. Geophys. Res*., 118, 3080-3100, doi:10.1002/jgrb.50218.

Franke, D., S. Neben, S. Ladage, B. Schreckenberger, and K. Hinz., (2007), Margin segmentation and volcano-tectonic architecture along the volcanic margin off Argentina/Uruguay, South Atlantic. *Marine Geolog,y* 244(1), 46-67.

Freeth, S., (1979). Deformation of the African Plate as a consequence of membrane stress domains generated by Post-Jurassic Drift, *Earth Planet. Sci. Lett*., 45(1), 93–104.

Frezzotti, M.L., S. Ferrando, A. Peccerillo, M. Petrelli, F. Tecce, A. Perucchi (2010), Chlorine-rich

metasomatic H_2O–CO_2 fluids in amphibole-bearing peridotites from Injibara (Lake Tana region, Ethiopian plateau): Nature and evolution of volatiles in the mantle of a region of continental flood basalts. *Geochim. Cosmochim. Acta*, 74(10): 3023-3039.

Frizon de Lamotte, D.F., Leturmy, P., Missenard, Y., Khomsi, S., Ruiz, G., Saddiqi, O., Guillocheau, F. and Michard, A. (2009), Mesozoic and Cenozoic vertical movements in the Atlas system (Algeria, Morocco, Tunisia): an overview. *Tectonophysics*, *475*(1), 9-28.

Fuis, G.S., Mooney, W.D. (1990), Lithospheric structure and tectonics from seismic-refraciton and other data, in Wallace, R.E., ed., The San Andreas fault system, California; U.S. Geological Survey Professional Paper 1515, 207-236.

Fullea, J., Fernandez, M., Zeyen, H. and Vergés, J. (2007), A rapid method to map the crustal and lithospheric thickness using elevation, geoid anomaly and thermal analysis. Application to the Gibraltar Arc System, Atlas Mountains and adjacent zones. *Tectonophysics*, *430*(1), 97-117.

Furman, T., Bryce, J., Rooney, T., Hanan, B., Yirgu, G. and Ayalew, D. (2006), Heads and tails: 30 million years of the Afar plume. *Geol. Soc. Lond. Spec. Pubs.*, *259*(1), 95-119.

Furman, T. (2007), Geochemistry of East African Rift basalts: an overview. *J. Afri. Earth Sci.*, *48*(2), 147-160.

Gallacher, R., and I. Bastow (2012), The development of magmatism along the Cameroon Volcanic Line: Evidence from teleseismic receiver functions, *Tectonics*, 31, TC3018, doi:10.1029/2011TC003028.

Gallacher, R., D. Keir, N. Harmon, G. Stuart, S. Leroy, J. Hammond, J-M. Kendall, A. Ayele, B. Goitom, G. Ogubazghi, and A. Ahmed (2016), The initiation of segmented buoyancy-driven melting during continental breakup, *Nat. Comms*, 7, doi: 10.1038/ncomms13110.

Gao S.S., K.H. Liu, C.A. Reed, Y. Yu, B. Massinque, H. Mdala, M. Moidaki, D. Mutamina, E.A. Atekwana, S. Ingate, and A.M. Reusch (2013), SAFARI-Seismic Arrays for African Rift, *Eos Trans. AGU*, 94, 213-214, doi: 10.1002/2013EO240002.

Gao, S., Davis, P.M., Liu, H., Slack, P.D., Rigor, A.W., Zorin, Y.A., Mordvinova, V.V., Kozhevnikov, V.M. and Logatchev, N.A. (1997), SKS splitting beneath continental rift zones. *Journal of Geophysical Research: Solid Earth*, *102*(B10), pp.22781-22797.

Gomez, F., W. Beauchamp, and M. Barazangi (2000), Role of the Atlas Mountains (Northwest Africa) within the African-Eurasian Plate-Boundary Zone, *Geology*, *28*(9), 775-778.

Grandin, R., E. Jacques, A. Nercessian, A. Ayele, C. Doubre, A. Socquet, D. Keir, M. Kassim, A. Lemarchand, and G. King (2011), Seismicity during lateral dike propagation: Insights from new data in the recent Manda Hararo–Dabbahu rifting episode (Afar, Ethiopia), *Geochem. Geophys. Geosyst*., 12(4), doi: 10.1029/2010GC003434.

Green, W.V., Achauer, U. and Meyer, R.P. (1991), A three-dimensional seismic image of the crust and upper mantle beneath the Kenya rift. *Nature*, *354*(6350), 199.

Guerri, M., Cammarano, F. and Connolly, J.A. (2015), Effects of chemical composition, water and temperature on physical properties of continental crust. *Geochem., Geophys., Geosyst.*, *16*(7), 2431-2449.

Guidarelli, M., Stuart, G., Hammond, J.O.S., Kendall, J.M., Ayele, A. and Belachew, M. (2011), Surface
wave tomography across Afar, Ethiopia: Crustal structure at a rift triple-junction zone, *Geophys. Res. Lett.,* **38**, L24313, doi:10.1029/2011GL046840.

Guo, X., Zhang, L., Behrens, H. and Ni, H. (2016), Probing the status of felsic magma reservoirs: Constraints from the P–T–H 2 O dependences of electrical conductivity of rhyolitic melt. *Earth Planet. Sci. Letts*, *433*, 54-62.

Guth, A.L. (2016), Volcanic volumes associated with the Kenya Rift: recognition and correction of preservation biases. *Geol. Soc. Lond. Spec. Pubs.*, *420*(1), 31-42.

Hacker, B.R., Kelemen, P.B. and Behn, M.D. (2015), Continental lower crust. *Ann. Rev. Earth Planet. Sci*., 43, pp.167-205.

Halldórsson, S.A., Hilton, D.R., Scarsi, P., Abebe, T. and Hopp, J. (2014), A common mantle plume source beneath the entire East African Rift System revealed by coupled helium-neon systematics. *Geophys. Res. Letts*, *41*(7), 2304-2311.

Halliday, A., J. Davidson, P. Holden, C. DeWolf, D. Lee, and J. Fitton (1990), Trace-Element Fractionation in Plumes and the Origin of HIMU Mantle Beneath the Cameroon Line, *Nature*, 347, 523–528.

Hamilton, M. P., Jones, A. G., Evans, R. L., Evans, S., Fourie, C. J. S., Garcia, X., Mountford, A., Spratt, J. E., and Team, S. M. (2006), Electrical anisotropy of South African lithosphere compared with seismic anisotropy from shear-wave splitting analyses, *Phys. Earth Planet.* In., 158, 226-239.

Hamling, I., A. Ayele, L. Bennati, E. Calais, C. Ebinger, D. Keir, E. Lewi, T. Wright, and G. Yirgu (2009), Geodetic observations of the ongoing Dabbahu rifting episode: new dyke intrusions in 2006 and 2007, *Geophys. J. Int*., doi:10.1111/j.1365- 246X.2009.04163.x.

Hammond, J., J.-M. Kendall, G. Stuart, D. Keir, C. Ebinger, A. Ayele, and M. Belachew (2011), The nature of the crust beneath the Afar triple junction: Evidence from receiver functions, *Geochem. Geophys. Geosyst*., 12(12), doi: 10.1029/2011GC003738.

Hammond, J., J.-M. Kendall, G. Stuart, C. Ebinger, I. Bastow, D. Keir, A. Ayele, M. Belachew, B. Goitom, G. Ogubazghi, T. J. Wright (2013), Mantle upwelling and initiation of rift segmentation beneath the Afar Depression, *Geology*, 41(6), 635–638, doi:10.1130/G33925.1.

Hammond, J.O.S., J-M. Kendall, J. Wookey, G.W. Stuart, D. Keir, D. & A. Ayele (2014), Differentiating flow, melt, or fossil seismic anisotropy beneath Ethiopia, *Geochem. Geophys. Geosyst*., 15, 1878-1894, doi: 10.1002/2013GC005185.

Hammond, J.O.S. (2014), Constraining melt geometries beneath the Afar depression, Ethiopia from teleseismic receiver functions: The anisotropic H-K stacking technique, *Geochem. Geophys. Geosyst*., 15, doi: 10.1002/2013GC005186.

Hautot, S., Tarits, P., Whaler, K., Le Gall, B., Tiercelin, J.J. and Le Turdu, C. (2000), Deep structure of the Baringo Rift Basin (central Kenya) from three-dimensional magnetotelluric imaging: Implications for rift evolution. *J. Geophys. Res.*, *105*(B10), 23493-23518.

Hautot, S. and Tarits, P. (2015), Rift Structure and basin control revealed by 3-D magneto telluric data: Examples of Turkana and Northern Tanzania. In *First EAGE Eastern Africa Petroleum Geoscience Forum*.

Hayward, N., and C. Ebinger (1996), Variations in the along–axis segmentation of the Afar rift system, *Tectonics*, 15, 244–257.

Hendrie, D.B., Kusznir, N.J., Morley, C.K. and Ebinger, C.J. (1994). Cenozoic extension in northern Kenya: a quantitative model of rift basin development in the Turkana region. *Tectonophysics*, *236*(1-4), 409-438.

Hodgson, I., F. Illsley-Kemp, D. Keir, C. J. Ebinger, K. Mtelela (2017), Crustal structure at a young continental rift: A receiver function study from the Tanganyika Rift, *Tectonics*, doi:10.1002/2017TC004477, in press.

Hübert, J., Whaler, K. and Fisseha, S. (2016), From 'shoulder to shoulder' – A cross-rift Magnetotelluric Transect through Aluto volcano, Ethiopia, Abstract for the 23rd Electromagnetic Induction in the Earth Workshop, Chiang Mai, Thailand.

Hutchison, W., J. Biggs, T. A. Mather, D. M. Pyle, E. Lewi, G. Yirgu, S. Caliro, G. Chiodini, L. E. Clor, and T. P. Fischer (2016), Causes of unrest at silicic calderas in the East African Rift: New constraints from InSAR and soil-gas chemistry at Aluto volcano, Ethiopia, *Geochem. Geophys. Geosyst*., 17, 3008–3030, doi:10.1002/2016GC006395.

Ibs-von Seht, M., S. Blumenstein, R. Wagner, D. Hollnack, J. Wohlenberg (2001), Seismicity, seismotectonics and crustal structure of the southern Kenya Rift-new data from the Lake Magadi area. *Geophys. J. Int.*, *146*(2), pp.439-453.

Jessell, M.W., Begg, G.C., and Miller, M.S. (2016), The geophysical signatures of the West African Craton, Precam. Res., 274, 3-24.

Johnson, N.E. (2012), Magnetotelluric studies of the crust and upper mantle in a zone of active continental breakup, Afar, Ethiopia, unpublished PhD thesis, University of Edinburgh

Johnson, N.E., Whaler, K.A., Hautot, S., Fisseha, S., Desissa, M. and Dawes, G.J.K. (2016), Magma imaged magnetotellurically beneath an active and an inactive magmatic segment in Afar, Ethiopia. *Geol. Soc. , Lond., Spec. Pubs.*, *420*(1), 105-125.

Jones, A.P., Smith, J.V., Dawson, J.B. and Hansen, E.C. (1983), Metamorphism, partial melting, and K-metasomatism of garnet-scapolite-kyanite granulite xenoliths from Lashaine, Tanzania. *J. Geology*, *91*(2),143-165.

Kaislaniemi, L., and J. van Hunen (2014), Dynamics of lithospheric thinning and mantle melting by edge-driven convection: Application to Moroccan Atlas mountains, *Geochem., Geophys., Geosyst.* 15.8, 3175-3189.

Keir, D., M. Belachew, C.J. Ebinger, J-M. Kendall, J.O.S. Hammond, G.W. Stuart, A. Ayele, and J.V. Rowland (2011), Mapping the evolving strain field during continental breakup from crustal anisotropy in the Afar Depression, *Nat. Comms*., 2, doi: 10.1038/ncomms1287.

Keir, D., I. Bastow, K. Whaler, E. Daly, D. Cornwell, and S. Hautot (2009), Lower crustal earthquakes near the Ethiopian rift induced by magmatic processes, Geochem. Geophys. Geosyst., 10, Q0AB02, doi:10.1029/2009GC002382.

Keir, D., M. Belachew, C. Ebinger, J.-M. Kendall, J. Hammond, G. Stuart, A. Ayele, and J. Rowland (2011), Mapping the evolving strain field during continental breakup from crustal anisotropy in the Afar Depression, *Nat. Comms*., 2, 285.

Keir, D., I. Bastow, G. Corti, F. Mazzarini, and T. Rooney (2015), The origin of along-rift variations in faulting and magmatism in the Ethiopian Rift, *Tectonics*, 34(3), 464–477, doi:10.1002/2014TC003698.

Keller, G.R., Mechie, J., Braile, L.W., Mooney, W.D. and Prodehl, C. (1994), Seismic structure of the uppermost mantle beneath the Kenya rift. *Tectonophysics*, *236*(1-4), 201-216.

Kendall, J.-M., S. Pilidou, D. Keir, I. Bastow, G. Stuart, and A. Ayele (2006), Mantle upwellings, melt migration and the rifting of Africa: Insights from seismic anisotropy, in The Afar Volcanic Province within the East African Rift System, eds. Yirgu, G. Ebinger, C.J. & Maguire, P.K.H., *Geol. Soc. Lond. Spec. Pub*., 259, 271–293.

Kendall, J.M. and Lithgow-Bertelloni, C. (2016), Why is Africa rifting?. *Geological Society, London, Special Publications*, *420*(1), 11-30.

Keranen, K., S. Klemperer, R. Gloaguen, and EAGLE Working Group (2004), Three-dimensional seismic imaging of a protoridge axis in the main Ethiopian rift, Geology, 32, 949–952, doi:10.1130/G20737.1.

Keranen, K. and Klemperer, S.L. (2008), Discontinuous and diachronous evolution of the Main Ethiopian Rift: Implications for development of continental rifts. *Earth and Planetary Science Letters*, *265*(1), 96-111.

Keranen, K.M., Klemperer, S.L., Julia, J., Lawrence, J.F. and Nyblade, A.A. (2009), Low lower crustal velocity across Ethiopia: Is the Main Ethiopian Rift a narrow rift in a hot craton?. *Geochemistry, Geophysics, Geosystems*, *10*(5), 10.1029/2008GC002293.

Khan, M.A., Mechie, J., Birt, C., Byrne, G., Gaciri, S., Jacob, B., Keller, G.R., Maguire, P.K.H., Novak, O., Nyambok, I.O. and Patel, J.P. (1999), The lithospheric structure of the Kenya Rift as revealed by wide-angle seismic measurements. *Geological Society, London, Special Publications*, *164*(1),.257-269.

Kim, S., A.A. Nyblade, J. Rhie, C-E. Baag, & T-S. Kang (2012), Crustal S-wave velocity structure of the Main Ethiopian Rift from ambient noise tomography, Geophys. J. Int., 191, 865-878, doi: 10.1111/j.1365-246x.2012.05664.x.

King, S., and D. Anderson (1998), Edge–driven convection, Earth Planet. Sci. Lett., 160, 289–296.

King, S., and J. Ritsema (2000), African hot spot volcanism: small–scale convection in the upper mantle beneath cratons, Science, 290, 1137–1140.

Korenaga, J., W.S. Holbrook, G.M. Kent, P.B. Kelemen, R.S. Detrick, H.-C. Larsen, J.R. Hopper, & T. Dahl-Jensen (2000), Crustal structure of the southeast Greenland margin from joint refraction and reflection seismic tomography, J. Geophys. Res., 105, 21591-21614.

Korostelev, F., C. Weemstra, S. Leroy, L. Boschi, D. Keir, Y. Ren, I. Molinari, A. Ahmed, G.W. Stuart, F. Rolandone, K. Khanbari, J.O.S. Hammond, J-M. Kendall, C. Doubre, I. Al Ganad, B. Goitom, & A. Ayele (2015), Magmatism on rift flanks: insights from ambient-noise phase velocity in Afar region, Geophys. Res. Lett, 42, 2179-2188, doi: 10.1002/2015GL063259.

Last, R.J., Nyblade, A.A., Langston, C.A. and Owens, T.J. (1997), Crustal structure of the East African Plateau from receiver functions and Rayleigh wave phase velocities. J. Geophys. Res, 102(B11), 24469-24483

Lee, H., J. D. Muirhead, T. Fischer, C. J. Ebinger, S. Kattenhorn, G. Kianji (2016), Tectonic degassing of mantle-derived CO2 along faults in the East African Rift, Nature Geoscience, **9**,145–149**.**

Ledo, J., Jones, A.G., Siniscalchi, A., Campanyà, J., Kiyan, D., Romano, G., Rouai, M. and TopoMed MT Team (2011), Electrical signature of modern and ancient tectonic processes in the crust of the Atlas mountains of Morocco. *Phys. Earth Planet. Int.*, *185*(3), 82-88.

Leroy, S., E. d'Acremont, C. Tiberi, C. Basuyau, J. Autin, F. Lucazeau, and H. Sloan (2010), Recent off-axis volcanism in the eastern Gulf of Aden: implications for plume–ridge interaction, *Earth Planet. Sci. Lett.,* 293 (1), 140–153.

Levander, A., Bezada, M. J., Niu, F., Humphreys, E. D., Palomeras, I., Thurner, S. M., Masy, J., Schmitz, M., Gallart, J., Carbonell, R., and Miller, M. S. (2014), Subduction-driven recycling of continental margin lithosphere. 515, 253–256. doi:10.1038/nature13878.

Lewi, E., Keir, D., Birhanu, Y., Blundy, J., Stuart, G. Wright, T. and Calais, E. (2015), Use of a high-precision gravity survey to understand the formation of oceanic crust and the role of melt at the southern Red Sea rift in Afar, Ethiopia, in 'Magmatic Rifting and Active Volcanism', ed. Wright, T J, Ayele, A, Ferguson, D J, Kidane, T & Vye-Brown, C, *Geol. Soc. Lond. Spec. Pub*., 420:165-180, doi:10.1144/SP420.13.

Ligi, M., E. Bonatti, F.C. Tonotini, A. Cipriani, L. Cocchi, A. Schettino, G. Bortoluzzi, V. Ferrante, S. Khalil, N.C. Mitchell, & N. Rasul (2011), Initial burst of oceanic crust accretion in the Red Sea due to edge-driven mantle convection, *Geology*, 39, 1019-1022, doi: 10.1130/G32243.1.

Lowry, A.R. and Pérez-Gussinyé, M. (2011), The role of crustal quartz in controlling Cordilleran deformation. *Nature*, *471*(7338), 353-357.

Maccaferri, F., Bonafede, M. and Rivalta, E. (2011), A quantitative study of the mechanisms governing dike propagation, dike arrest and sill formation. *J. Volc. Geotherm. Res.*, *208*(1), 39-50.

Macdonald, R. (1994), Petrological evidence regarding the evolution of the Kenya Rift Valley. *Tectonophysics*, *236*(1-4), pp.373-390.

Mackenzie, G., H. Thybo, and P. Maguire (2005), Crustal velocity structure across the Main Ethiopian Rift: Results from 2-dimensional wide-angle seismic modelling, *Geophys. J. Int*., 162, 994–1006, doi:10.1111/j.1365-246X.2005.02710.x.

Magee, C., I.D. Bastow, B.V.W. de Vries, C.A.L. Jackson, R. Hetherington, M. Hagos, and M. Hoggett (2017), Structure and dynamics of surface uplift induced by incremental sill emplacement. *Geology*, *45*(5), 431-434, doi: 10.1130/G38839.1.

Maguire, P.K.H., Swain, C.J., Masotti, R. and Khan, M.A. (1994), A crustal and uppermost mantle cross-sectional model of the Kenya Rift derived from seismic and gravity data. *Tectonophysics*, *236*(1-4), pp.217-249.

Maguire, P., C. Ebinger, G. Stuart, G. Mackenzie, K. Whaler, J.-M. Kendall, M. Khan, C. Fowler, S. Klemperer, G. Keller, S. Harder, T. Furman, K. Mickus, L. Asfaw, A. Ayele, and B. Abebe (2003), Geophysics project in Ethiopia studies continental breakup, *EOS Trans. AGU*, 84 (35), 342–343.

Maguire, P., G. Keller, S. Klemperer, G. Mackenzie, S. Harder, B. O'Reilly, T. H., L. Asfaw, M. Khan, and M. Amha (2006), Crustal structure of the northern Main Ethiopian Rift from the EAGLE controlled-source survey; a snapshot of incipient lithospheric break-up, in The Afar Volcanic Province within the East African Rift System, eds. Yirgu, G. Ebinger, C.J. & Maguire, P.K.H., *Geol. Soc. Lond. Spec. Pub*., 259, 271–293.

Mahatsente, R., Jentzsch, G. and Jahr, T. (1999), Crustal structure of the Main Ethiopian Rift from gravity data: 3-dimensional modeling. *Tectonophysics*, *313*(4), 363-382.

Makris, J., and A. Ginzburg (1987), The Afar Depression: transition between continental rifting and sea floor spreading, *Tectonophysics*, 141, 199–214.

Mana, S., Furman, T., Carr, M.J., Mollel, G.F., Mortlock, R.A., Feigenson, M.D., Turrin, B.D. and Swisher, C.C. (2012), Geochronology and geochemistry of the Essimingor volcano: melting of metasomatized lithospheric mantle beneath the North Tanzanian Divergence zone (East African Rift). *Lithos*, *155*, 310-325.

Mana, S., Furman, T., Turrin, B.D., Feigenson, M.D. and Swisher, C.C. (2015), Magmatic activity across the East African North Tanzanian Divergence Zone. *J. Geol. Soc.*, 2014-072.

Mancilla, F., & Diaz, J. (2015), High resolution Moho topography map beneath Iberia and Northern Morocco from receiver function analysis. *Tectonophysics*, 663, 203–211

Manighetti, I., Tapponnier, P., Gillot, P.Y., Jacques, E., Courtillot, V., Armijo, R., Ruegg, J.C. and King, G. (1998), Propagation of rifting along the Arabia-Somalia plate boundary: Into Afar. *J. Geophys. Res.*, *103*(B3), 4947-4974.

Mansur, A.T., Manya, S., Timpa, S. and Rudnick, R.L. (2014), Granulite-facies xenoliths in rift basalts of northern Tanzania: Age, composition and origin of lower crust. *J. Petrol.*, *55*(7), 1243-1286.
Marty, B. and Yirgu, G. (1996), Helium isotopic variations in Ethiopian plume lavas: nature of magmatic sources and limit on lower mantle contribution. *Earth Planet. Sci. Lett.*, *144*(1-2), 223-237.

Marzoli, A., E. Piccirillo, P. Renne, G. Bellieni, M. Iacumin, J. Nyobe, and A. Tongwa (2000), The Cameroon Volcanic Line Revisited: Petrogenesis of Continental Basaltic Magmas From Lithospheric and Asthenospheric Mantle Sources, *J. Petrol*., 41(1), 87–109.

Mattsson, H.B., R. H. Nandedkar, & P. Ulmer (2013), Petrogenesis of the melilititic and nephelinitic rock suites in the Lake Natron–Engaruka monogenetic volcanic field, northern Tanzania. *Lithos*, *179*, 175-192.

Mazzarini, F., T. Rooney, and I. Isola (2013), The intimate relationship between strain and magmatism: A numerical treatment of clustered monogenetic fields in the Main Ethiopian Rift, *Tectonics*, doi:10.1029/2012TC003146.

McKenzie, D., and D. Davies (1970), Plate tectonics of the Red Sea and east Africa, *Nature*, 226, 243–248.

Mechie, J., Keller, G.R., Prodehl, C., Gaciri, S., Braile, L.W., Mooney, W.D., Gajewski, D. and Sandmeier, K.J. (1994a), Crustal structure beneath the Kenya Rift from axial profile data. *Tectonophysics*, *236*(1-4), 179-200.

Mechie, J., Fuchs, K. and Altherr, R. (1994b), The relationship between seismic velocity, mineral composition and temperature and pressure in the upper mantle—with an application to the Kenya Rift and its eastern flank. *Tectonophysics*, *236*(1-4), 453-464.

Medynski, S., Pik, R., Burnard, P., Vye-Brown, C., France, L., Schimmelpfennig, I., Whaler, K., Johnson, N., Benedetti, L., Ayalew, D. and Yirgu, G. (2015), Stability of rift axis magma reservoirs:

spatial and temporal evolution of magma supply in the Dabbahu rift segment (Afar, Ethiopia) over the past 30 kyr. *Earth Planet. Sci. Letts.*, *409*, 278-289.

Meju, M.A. and Sakkas, V. (2007), Heterogeneous crust and upper mantle across southern Kenya and the relationship to surface deformation as inferred from magnetotelluric imaging. *Journal of Geophysical Research: Solid Earth*, *112*(B4).

Mériaux, C. A., Mansour, J. A., Moresi, L. N., Kerr, R. C., and May, D. A. (2011), On the rise of strongly tilted mantle plume tails. *Phys. Earth Planet. Inter.* 184, 63–79. doi:10.1016/j.pepi.2010.10.013.

Mériaux, C. A., Duarte, J. C., Duarte, S. S., Schellart, W. P., Chen, Z., Rosas, F., Mata, J., and Terrinha, P. (2015), Capture of the Canary mantle plume material by the Gibraltar arc mantle wedge during slab rollback. *Geophys. J. Internat.* 201, 1717–1721. doi:10.1093/gji/ggv120.

Meyers, J., B. Rosendahl, G. Harrison, and Z.-D. Ding (1998), Deep–imaging seismic and gravity results from the offshore Cameroon Volcanic Line, and speculation of African hotlines, *Tectonophysics*, 284(1-2) 31–63.

Milelli, L., L. Fourel, and C. Jaupart (2012), A lithospheric instability origin for the Cameroon Volcanic Line, Earth Planet. Sci. Lett., 335-336, 80–87, doi: 10.1016/j.epsl.2012.04.028.

Miller, M. S., A. Allam, T. W. Becker, J. F. Di Leo, and J. Wookey (2013), Constraints on the tectonic evolution of the westernmost Mediterranean and Northwestern Africa from shear wave splitting analysis, *Earth Planet. Sci. Lett.*, 375, 234-243, 10.1016/j.epsl.2013.05.036.

Miller, M. S., and T. W. Becker (2014), Reactivated Lithospheric-Scale Discontinuities Localize Dynamic Uplift of the Moroccan Atlas Mountains, *Geology*, 42(1), 35-38, 10.1130/g34959.1.

Miller, M.S., O'Driscoll, L.J, Butcher, A.J., and Thomas, C. (2015), Imaging Canary Island hotspot material beneath the lithosphere of Morocco and Spain, *Earth Planet. Sci. Lett.*, 431, 186-194.

Missenard, Y., Zeyen, H., Frizon de Lamotte, D., Leturmy, P., Petit, C., Sébrier, M. and Saddiqi, O. (2006), Crustal versus asthenospheric origin of relief of the Atlas Mountains of Morocco. *J. Geophys. Res.*, *111*(B3).

Missenard, Y., and A. Cadoux (2012), Can Moroccan Atlas lithospheric thinning and volcanism be induced by edge-driven convection?, *Terra Nova*, 24(1), 27-33, 10.1111/j.1365-3121.2011.01033.x.

Mohr, P. (1972), Surface structure and plate tectonics of Afar, *Tectonophysics*, 15 (1), 3–18.

Mohr, P. (1989), Nature of the crust under Afar – new igneous, not thinned continental,

Tectonophysics, 167, 1–11.

Mohriak, W.U., Szatmari, P. and Anjos, S. (2012), Salt: geology and tectonics of selected Brazilian basins in their global context. *Geol. Soc., Lond., Spec. Pubs.*, *363*(1), 131-158.

Moreau, C., J. Regnoult, B. Déruelle, and B. Robineau (1987), A new tectonic model for the Cameroon Line, Central Africa, *Tectonophysics*, 141(4), 317–334.

Morley, C.K., Wescott, W.A., Stone, D.M., Harper, R.M., Wigger, S.T. and Karanja, F.M. (1992), Tectonic evolution of the northern Kenyan Rift. *J. Geol. Soc. London*, *149*(3), 333-348.

Morley, C.K., Karanja, F.M., Wescott, W.A., Stone, D.M., Harper, R.M., Wigger, S.T. and Day, R.A. (1999), AAPG Studies in Geology# 44, Chapter 2: Geology and Geophysics of the Western Turkana Basins, Kenya, 19-54.

Morrissey, A. and Scholz, C.A. (2014), Paleohydrology of Lake Turkana and its influence on the Nile River system. *Palaeogeography, Palaeoclimatology, Palaeoecology*, *403*, 88-100.

Muhongo, S. and Lenoir, J.L. (1994), Pan-African granulite-facies metamorphism in the Mozambique Belt of Tanzania: U-Pb zircon geochronology. *J. Geol. Soc*., 151(2), 343-347.

Muirhead, J.D., S. A. Kattenhorn, H. Lee, T. P. Fischer, S. Mana, B. Turrin, G. Kianji, E. Dindi, D. S. Stamps (2016), Evolution of upper crustal faulting assisted by magmatic volatile release during continental rift initiation in the East Africa Rift: Geosphere*, v.* 12, doi: 10.1130/GES01375.1.

Mulibo, G.D. and Nyblade, A.A. (2009), The 1994–1995 Manyara and Kwamtoro earthquake swarms: Variation in the depth extent of seismicity in Northern Tanzania. *South African Journal of Geology*, *112*(3-4), pp.387-404.

Mulibo, G.D. and Nyblade, A.A. (2013), The P and S wave velocity structure of the mantle beneath eastern Africa and the African superplume anomaly. *Geochem., Geophys., Geosyst.*, *14*(8), 2696-2715.

Nguuri, T.K., Gore, J., James, D.E., Webb, S.J., Wright, C., Zengeni, T.G., Gwavava, O. and Snoke, J.A. (2001), Crustal structure beneath southern Africa and its implications for the formation and evolution of the Kaapvaal and Zimbabwe cratons. *Geophys. Res. Lett*., 28(13), 2501-2504.

Niemeijer, A.R. and Spiers, C.J. (2006), Velocity dependence of strength and healing behaviour in simulated phyllosilicate-bearing fault gouge. *Tectonophysics*, *427*(1), 231-253.

Nkouathio, D., A. Kagou Dongmo, J. Bardintzeff, P. Wandji, H. Bellon, and A. Pouclet (2008),

Evolution of volcanism in graben and horst structures along the Cenozoic Cameroon Line (Africa): Implications for tectonic evolution and nantle source composition, *Min. Petr*, 94(3), 287–303.

Nobile, A., C. Pagli, D. Keir, T. Wright, A. Ayele, J. Ruch, & V. Acocella (2012), Dike-fault interaction during the 2004 Dallol intrusion at the northern edge of the Erta Ale Ridge (Afar, Ethiopia), Geophys. Res. Lett., 39, doi: 10.1029/2012GL053152.

Nyblade, A.A., Pollack, H.N., Jones, D.L., Podmore, F. and Mushayandebvu, M. (1990), Terrestrial heat flow in east and southern Africa. *J. Geophys. Res.*, *95*(B11), 17371-17384.

Nyblade, A.A. and Robinson, S.W. (1994), The African Superswell. *Geophys. Res. Lett.*, *21*(9), 765-768.

O'Donnell, J.P., Adams, A., Nyblade, A.A., Mulibo, G.D. and Tugume, F. (2013), The uppermost mantle shear wave velocity structure of eastern Africa from Rayleigh wave tomography: Constraints on rift evolution. *Geophysical Journal International*, *194*(2), 961-978.

Padilha, A., Vitorello, I., Pádua, M., and Bologna, M. (2006), Lithospheric and sublithospheric anisotropy beneath central-southeastern Brazil constrained by long period magnetotelluric data, Phys. Earth Planet. In., 158 (2), 190-209.

Pagli, C., Wright, T.J., Ebinger, C.J., Yun, S.H., Cann, J.R., Barnie, T. and Ayele, A. (2012), Shallow axial magma chamber at the slow-spreading Erta Ale Ridge. *Nature Geoscience*, *5*(4), 284-288.

Palomeras, I., S. Thurner, A. Levander, K. Liu, A. Villasenor, R. Carbonell, and M. Harnafi (2014), Finite-frequency Rayleigh wave tomography of the Western Mediterranean: Mapping its lithospheric structure, Geochem., Geophys., Geosyst., 15(1), 140-160, 10.1002/2013GC004861.

Perez-Gussinyé, M., M. Metois, M. Fernandez, J. Verges, J. Fullea, and A. Lowry (2009), Effective elastic thickness of Africa and its relationship to other proxies for lithospheric structure and surface tectonics, Earth Planet. Sci. Lett., 287 (1-2), 152–167.

Persaud, P., Ma, Y., Stock, J.M., Hole, J.A., Fuis, G.S. and Han, L. (2016), Fault zone characteristics and basin complexity in the southern Salton Trough, California. *Geology*, *44*(9), 747-750.

Pik, R., Marty, B. and Hilton, D.R. (2006), How many mantle plumes in Africa? The geochemical point of view. *Chemical Geology*, *226*(3), 100-114.

Pique, A., P. Tricart, R. Guiraud, E. Laville, S. Bouaziz, M. Amrhar, and R. Ait Ouali (2002), The Mesozoic–Cenozoic Atlas Belt (North Africa): An Overview, *Geodinamica Acta*, *15*(3), 185-208.

Plasman, M., C. Tiberi, C. Ebinger, S. Roecker, S. Gautier, J. Albaric, S. Peyrat, S. Perrot, J. Déverchère, B. LeGall., P. Tarits, S. Hautot, R. Ferdinand-Wambura, A. Muzuka, G. Mulibo, K. Mtelela, M. Msabi, G. Kianji, N. Rasendra, R. Gama (2017), Lithospheric structure of the North Tanzanian Divergence, East African rift, estimated from receiver functions, Geophys. J. Int., 210, 465–481.

Plomerova, J., V. Babuska, C. Dorbath, L. Dorbath, and R. Lillie (1993), Deep Lithospheric Structure Across the Central African Shear Zone in Cameroon, Geophys. J. Int., 115(2), 381–390.

Prodehl, C. and Mechie, J. (1991), Large-scale variation in lithospheric structure along and across the Kenya rift. *Nature*, *354*(6350), p.223.

Pommier, A and Le Trong, E. (2011), SIGMELTS: A web portal for electrical conductivity calculations in geosciences, Comp. Geosci., **37**, 1450-1459

Poudjom Djomani, Y., M. Diament, and Y. Albouy (1992), Mechanical behaviour of the lithosphere beneath the Adamawa Uplift (Cameroon, West Africa) based on gravity data, J. Afr. Earth Sci., 15 (1), 81–90.

Poudjom Djomani, Y., M. Diament, and M. Wilson (1997), Lithospheric structure across the Adamawa Plateau (Cameroon) from gravity studies, Tectonophysics, 273(3-4), 317–327.

Prodehl, C., Jacob, A.W.B., Thybo, H., Dindi, E. and Stangl, R. (1994), Crustal structure on the northeastern flank of the Kenya rift. *Tectonophysics*, *236*(1-4), 271-290.

Prodehl, C., and J. Mechie (1991), Crustal thinning in relationship to the evolution of the Afro-Arabian rift system: a review of seismic refraction data, Tectonophysics, 198, 311–327.

Prodehl, C., Ritter, J.R.R., Mechie, J., Keller, G.R., Khan, M.A., Jacob, B., Fuchs, K., Nyambok, I.O., Obel, J.D. and Riaroh, D. (1997), The KRISP 94 lithospheric investigation of southern Kenya—the experiments and their main results. *Tectonophysics*, *278*(1), 121-147.

Purcell, P. (1976), The Marda fault zone, Ethiopia, Nature, 261, 569–571.

Redfield, T., W. Wheeler, and M. Often (2003), A kinematic model for the development of the Afar Depression and its paleogeographic implications, Earth Planet. Sci. Lett., 216(3), 383–398.

Reed, C. A., S. Almadani, S. S. Gao, A. A. Elsheikh, S. Cherie, M. G. Abdelsalam, A. K. Thurmond, and K. H. Liu (2014), Receiver function constraints on crustal seismic velocities and partial melting

beneath the Red Sea rift and adjacent regions, Afar Depression, J. Geophys. Res., 119 (3), 2138–2152.

Reisberg, L., Lorand, J.P. and Bedini, R.M. (2004), Reliability of Os model ages in pervasively metasomatized continental mantle lithosphere: a case study of Sidamo spinel peridotite xenoliths (East African Rift, Ethiopia). *Chemical Geology*, *208*(1), 119-140.

Reusch, A., A. Nyblade, D. Wiens, P. Shore, B. Ateba, C. Tabod, and J. Nnange (2010), Upper mantle structure beneath Cameroon from body wave tomography and the origin of the Cameroon Volcanic Line, Geochem. Geophys. Geosyst., 11 (10), Q10W07.

Ritsema, J., H. J. van Heijst, & J, H. Woodhouse (1999), Complex shear wave velocity structure imaged beneath Africa and Iceland. Science, 286(5446), 1925-1928.

Roecker, S., C. Ebinger**,** C. Tiberi, G. Mulibo, R. Ferdinand-Wambura, K. Mtelela, A. Muzuka, G. Kianji, S. Gautier, J. Albaric, S. Peyrat (2017), Subsurface images of the Eastern Rift, Africa, from the joint inversion of body waves, surface waves, and gravity: Investigating the role of fluids in early-stage continental rifting, Geophys. J. Int., *210*(2), 931-950.

Rooney, T., T. Furman, I. Bastow, D. Ayalew, and G. Yirgu (2007), Lithospheric modification during crustal extension in the Main Ethiopian Rift, J. Geophys. Res., doi:10.1029/2006JB004916.

Rooney, T., I. Bastow, and D. Keir (2011), Insights into extensional processes during magma assisted rifting: Evidence from aligned scoria cones, J. Volcanol. Geotherm. Res., 201, 83–96, doi:10.1016/j.jvolgeores.2010.07.019.

Rooney, T.O., P. Mohr, L. Dosso, and C. Hall (2013), Geochemical evidence of mantle reservoir evolution during progressive rifting along the western Afar margin. Geochim. Cosmochim. Acta, 102, 65-88.

Rooney, T., I. Bastow, D. Keir, F. Mazzarini, E. Movsesian, E. Grosfils, J. Zimbelman, M. Ramsey, D. Ayalew, and G. Yirgu (2014), The protracted development of focused magmatic intrusion during continental rifting, Tectonics, 33, 1–23, doi: 10.1002/2013TC003514.

Rooney, T., A. Lavigne, C. Svoboda, G. Girard, G. Yirgu, D. Ayalew, and J. Kappelman (2017a), The making of an underplate: Pyroxenites from the Ethiopian lithosphere, Chem. Geol., doi:10.1016/j.chemgeo.2016.09.011.

Rooney, T.O., W.R. Nelson, D. Ayalew, B. Hanan, G. Yirgu, and J. Kappelman (2017b), Melting the lithosphere: metasomes as a source for mantle-derived magmas, Earth Planet. Sci. Letts. 461, 105-118

Rosenbaum, G. and Lister, G.S. (2004), Formation of arcuate orogenic belts in the western Mediterranean region. *Geological Society of America Special Papers*, *383*, 41-56.

Rudnick, R. L., W. F. McDonough, B. W. Chappell (1993), Carbonatite metasomatism in the northern Tanzanian mantle: petrographic and geochemical characteristics. *Earth Planet. Sci. Lett.,* 114(4), 463-475.

Ruegg, J.C. (1975), Main results about the crustal and upper mantle structure of the Djibouti region (TFAI). *Afar Depression of Ethiopia*, *1*, 120-134.

Sakkas, V., Meju, M.A., Khan, M.A., Haak, V. and Simpson, F. (2002), Magnetotelluric images of the crustal structure of Chyulu Hills volcanic field, Kenya. *Tectonophysics*, *346*(3), 169-185.

Sandvol, E., D. Seber, A. Calvert, and M. Barazangi (1998), Grid search modelling of receiver functions: Implications for crustal structure in the Middle East and North Africa, J. Geophys. Res., 103, 26899-26917.

Samrock, F., Kuvshinov, A., Bakker, J., Jackson, A. and Fisseha, S. (2015), 3-D analysis and interpretation of magnetotelluric data from the Aluto-Langano geothermal field, Ethiopia, Geophys. J. Int., **202,** 1923–1948.

Saria, E., Calais, E., Stamps, D.S., Delvaux, D. and Hartnady, C.J.H. (2014), Present-day kinematics of the East African Rift. *J. Geophys. Res.*, *119*(4), 3584-3600.

Schmandt, B. and Humphreys, E. (2010), Complex subduction and small-scale convection revealed by body-wave tomography of the western United States upper mantle. *Earth Planet. Sci. Lett.*, *297*(3), 435-445.

Selway, K., Yi, J. and Karato, S.I. (2014), Water content of the Tanzanian lithosphere from magnetotelluric data: implications for cratonic growth and stability. *Earth Planet. Sci. Lett.*, *388*, 175-186.

Sembroni, A., Faccenna, C., Becker, T.W., Molin, P. and Bekele, A. (2016), Long-term, deep-mantle support of the Ethiopia-Yemen Plateau. *Tectonics, 35, 469-488*.

Sengör, A.M. and Burke, K. (1978), Relative timing of rifting and volcanism on Earth and its tectonic implications. Geophys. Res. Lett., 5(6), 419-421.

Serpelloni, E., Vannucci, G., Pondrelli, S., Argnani, A., Casula, G., Anzidei, M., Baldi, P. and Gasperini, P., (2007), Kinematics of the Western Africa-Eurasia plate boundary from focal mechanisms and GPS data. *Geophysical Journal International*, *169*(3), pp.1180-1200.

Shackleton, R.M. (1986), Precambrian collision tectonics in Africa. *Geological Society, London, Special Publications*, *19*(1), 329-349.

Shillington, D.J., Gaherty, J.B., Ebinger, C.J., Scholz, C.A., Selway, K., Nyblade, A.A., Bedrosian, P.A., Class, C., Nooner, S.L., Pritchard, M.E. and Elliott, J. (2016), Acquisition of a Unique Onshore/Offshore Geophysical and Geochemical Dataset in the Northern Malawi (Nyasa) Rift. Seismological Research Letters, 87(6), 1406-1416.

Shudofsky, G.N., Cloetingh, S., Stein, S. and Wortel, R. (1987), Unusually deep earthquakes in East Africa: Constraints on the thermo-mechanical structure of a continental rift system. Geophys. Res. Lett., 14(7), 741-744.

Simiyu, S.M. (2010), Status of geothermal exploration in Kenya and future plans for its development. In Proceedings World Geothermal Congress, pp. 25-29.

Simmons, N.A., Forte, A.M. and Grand, S.P. (2007), Thermochemical structure and dynamics of the African superplume. *Geophys. Res. Lett.*, *34*(2), 10.1029/2006GL028009.

Simpson, F. (2000), A three-dimensional electromagnetic model of the southern Kenya Rift: Departure from two dimensionality as a possible consequence of a rotating stress field. *J. Geophys. Res.*, *105*(B8), 19321-19334.

Sippel, J., Meeßen, C., Cacace, M., Mechie, J., Fishwick, S., Heine, C., Scheck-Wenderoth, M. and Strecker, M.R. (2017), The Kenya rift revisited: insights into lithospheric strength through data-driven 3-D gravity and thermal modelling. *Solid Earth*, *8*(1), p.45.

Skogseid, J., Planke, S., Faleide, J.I., Pedersen, T., Eldholm, O. and Neverdal, F. (2000), NE Atlantic continental rifting and volcanic margin formation. Geol. Soc. Lond. Spec. Publ., 167(1), 295-326.

Spieker, K., I. Wölbern, C. Thomas, M. Harnafi, and L. El Moudnib (2014), Crustal and upper-mantle structure beneath the Western Atlas Mountains in SW Morocco derived from receiver functions, Geophys. J. Int., 198, 1474-1485.

Stab, M., Bellahsen, N., Pik, R., Quidelleur, X., Ayalew, D. and Leroy, S. (2015), Modes of rifting in magma-rich settings: Tectono-magmatic evolution of Central Afar. *Tectonics,* 35(1), 2-38.

Stamps, D.S., Flesch, L.M., Calais, E. and Ghosh, A. (2014), Current kinematics and dynamics of Africa and the East African Rift System. *Journal of Geophysical Research: Solid Earth*, *119*(6), 5161-5186.

Stork, A.L., Stuart, G.W., Henderson, C.M., Keir, D. and Hammond, J.O.S. (2013), Uppermost mantle (Pn) velocity model for the Afar region, Ethiopia: an insight into rifting processes. *Geophysical Journal International*, *193*(1), 321-328.

Stuart, G.W., Fairhead, J.D., Dorbath, L. and Dorbath, C. (1985), A seismic refraction study of the crustal structure associated with the Adamawa Plateau and Garoua Rift, Cameroon, West Africa. *Geophysical Journal International*, *81*(1), 1-12.

Stuart, G.W., Bastow, I.D. and Ebinger, C.J. (2006), Crustal structure of the northern Main Ethiopian Rift from receiver function studies. *Geological Society, London, Special Publications*, *259*(1), pp.253-267.

Suh, C., S. Ayonghe, R. Sparks, C. Annen, J. Fitton, R. Nana, and A. Luckman (2003), The 1999 and 2000 Eruptions of Mount Cameroon: Eruption Behaviour and Petrochemistry of Lava, Bull. Volc., 65(4), 267–281.

Sun, D., M. S. Miller, A. Holt, and T. W. Becker (2014), Hot upwelling conduit beneath the Atlas Mountains, Morocco, Geophys. Res. Lett., 41, 8037-8044.

Tadjou, J., R. Nouayou, J. Kamguia, H. Kande, and E. Manguelle-Dicoum (2009), Gravity analysis of the boundary between the Congo Craton and the Pan-African Belt of Cameroon, Austrian J. Earth Sci, 102(1), 71–79.

Teixell, A., M.-L. Arboleya, M. Julivert, and M. Charroud (2003), Tectonic shortening and topography in the Central High Atlas (Morocco), Tectonics, 22(5), doi:10.1029/2002TC001460.

Teixell, A., P. Ayarza, H. Zeyen, M. Fernandez, and M.-L. Arboleya (2005), Effects of mantle upwelling in a compressional setting: The Atlas Mountains of Morocco, Terra Nova, 17, 456-461.

Tessema, A. and Antoine, L.A.G. (2004), Processing and interpretation of the gravity field of the East African Rift: implication for crustal extension. *Tectonophysics*, *394*(1), 87-110.

Thybo, H. and Artemieva, I.M. (2013), Moho and magmatic underplating in continental lithosphere. *Tectonophysics*, *609*, 605-619.

Thybo, H., Maguire, P.K.H., Birt, C. and Perchuć, E. (2000), Seismic reflectivity and magmatic underplating beneath the Kenya Rift. *Geophys. Res. Lett.*, *27*(17), 2745-2748.

Thybo, H., and C. Nielsen (2009), Magma-compensated crustal thinning in continental rift zones, Nature, 457, 7231.

Tiberi, C., C. Ebinger, V. Ballu, G. Stuart, and B. Oluma (2005), Inverse models of gravity data from the Red Sea-Aden-East African rifts triple junction zone, *Geophys. J. Int.*, 163(2), 775–787.

Tokam, A., C. Tabod, A. Nyblade, J. Julià, D. Wiens, and M. Pasyanos (2010), Structure of the crust beneath Cameroon, West Africa, from the joint inversion of Rayleigh wave group velocities and receiver functions, Geophys. J. Int., 183(2), 1061–1076.

Toteu, S., J. Penaye, and Y. Djomani (2004), Geodynamic evolution of the Pan-African Belt in central Africa with special reference to Cameroon, *Can. J. Earth Sci*., 41(1), 73–85.

Trestrail, K.R., T.O. Rooney, G. Girard, C. Svoboda, G. Yirgu, D. Ayalew, and J. Kappelman (2017), Sub-continental lithospheric mantle deformation in the Yerer-Tullu Wellel Volcanotectonic Lineament: A study of peridotite xenoliths: Chemical Geology, *455*, 249-263, doi: 10.1016/j.chemgeo.2016.10.013.

Tugume, F., Nyblade, A. and Julià, J. (2012), Moho depths and Poisson's ratios of Precambrian crust in East Africa: evidence for similarities in Archean and Proterozoic crustal structure. *Earth and Planetary Science Letters*, *355*, pp.73-81.

Turner, S., Regelous, M., Kelley, S., Hawkesworth, C. and Mantovani, M. (1994), Magmatism and continental break-up in the South Atlantic: high precision 40Ar-39Ar geochronology. *Earth Planet. Sci. Lett.*, *121*(3-4), 333-348.

Vail, J. (1983), Pan-African crustal accretion in northeast Africa, J. Afr. Earth Sci., 1, 285–294.

Van Avendonk, H.J., Lavier, L.L., Shillington, D.J. and Manatschal, G. (2009), Extension of continental crust at the margin of the eastern Grand Banks, Nwefoundland, *Tectonophysics*, 468, 131-148.

Van Ngoc, P., Boyer, D., Le Mouél, J-L. and Courtillot, V. (1981), Identification of a magma chamber in the Ghoubbet-Asal rift (Djibouti) from a magnetotelluric experiment, *Earth Planet. Sci. Lett*., 372, 372-380

Van Hinsbergen, D.J.J., S.J.H. Buiter, T.H. Torsvik, C. Gaina, & S.J. Webb (2011), The formation and evolution of Africa from the Archaean to Present: introduction, *Geol. Soc. Lond. Spec. Publ*., 357, 1-8, doi: 10.1144/SP357.1.

Vauchez, A., Dineur, F. and Rudnick, R. (2005), Microstructure, texture and seismic anisotropy of the lithospheric mantle above a mantle plume: insights from the Labait volcano xenoliths (Tanzania). *Earth Planet. Sci. Lett.*, *232*(3), 295-314.

Veevers, J.J., Cole, D.I. and Cowan, E.J. (1994), Southern Africa: Karoo basin and Cape fold belt. Geol. Soc. Am. Mem., 184, 223-280.

Velasco, A., G. Kaip, A. Wamalwa, E. Patlan (2011), Seismic characterization of Menengai Crater, Kenya (Menengai), FDSN Database, doi:10.7914/SN/1C.

Wada, I., Wang, K., He, J. and Hyndman, R.D. (2008), Weakening of the subduction interface and its effects on surface heat flow, slab dehydration, and mantle wedge serpentinization. *J. Geophys. Res.*, *113*, 10.1029/2007JB005190.

Wang, Y.F., J. F. Zhang, J. M. Jin, H. W. Green (2012), Mafic granulite rheology: Implications for a weak continental lower crust. *Earth Planet. Sci. Lett.*, *353*, 99-107.

Weeraratne, D.S., Forsyth, D.W., Fischer, K.M. and Nyblade, A.A. (2003), Evidence for an upper mantle plume beneath the Tanzanian craton from Rayleigh wave tomography. *J. Geophys. Res.*, *108*(B9).

Weinstein, A., S. J. Oliva, C.J. Ebinger, S. Roecker, C. Tiberi, C., E. Witkin, M. Aman, R. Hadfield, S. Gautier, A. Muzuka, G. Mulibo, G. Kianji, M. Msabi, R. Ferdinand-Wambura, J. Albaric, C. Lambert, A. Rodzianko (2017), Active deformation and magmatism during early stage rifting of Archaean lithosphere in the Eastern rift, Africa, *Geochem, Geopys. Geosyst.,* 10.1002/2017GC007027.

Whaler, K., and S. Hautot (2006), The electrical resistivity structure of the crust beneath the northern Ethiopian rift, in The Afar Volcanic Province within the East African Rift System, eds. Yirgu, G. Ebinger, C.J. & Maguire, P.K.H*., Geol. Soc. Lond. Spec. Pub*., 256, 293–305.

Wheildon, J., Morgan, P., Williamson, K.H., Evans, T.R. and Swanberg, C.A. (1994), Heat flow in the Kenya rift zone. *Tectonophysics*, *236*(1-4), 131-149.

White, R., L. Smith, A. Roberts, P. Christie, N. Kusznir, and the rest of the iSIMM Team (2008), Lower-crustal intrusion on the North Atlantic continental margin, *Nature*, 452, 7186.

White, R. and McKenzie, D. (1989), Magmatism at rift zones: the generation of volcanic continental margins and flood basalts. *J. Geophys. Res.*, *94*(B6), 7685-7729.

Wölbern, I., Rümpker, G., Schumann, A. and Muwanga, A. (2010), Crustal thinning beneath the Rwenzori region, Albertine rift, Uganda, from receiver-function analysis. Int. J. Earth Sci., 99(7), 1545-1557.

WoldeGabriel, G. (1988), Volcanotectonic history of the central sector of the main Ethiopian rift; a geochronological, geochemical and petrological approach., Ph.D. thesis, Case Western Reserve University.

Wolfenden, E., C. Ebinger, G. Yirgu, A. Deino, and D. Ayalew (2004), Evolution of the northern main Ethiopian rift: birth of a triple junction, *Earth Planet. Sci. Lett*., 224, 213–228.

Wolfenden, E., C. Ebinger, G. Yirgu, P. Renne, and S. Kelley (2005), Evolution of a volcanic rifted margin: Southern Red Sea, Ethiopia, Bull. Geol. Soc. Am., 117(7-8), 846–864.

Wortel, M.J.R. and Spakman, W. (2000), Subduction and slab detachment in the Mediterranean-Carpathian region. *Science*, *290*(5498),1910-1917.

Xu, W., Rivalta, E. and Li, X., 2017. Magmatic architecture within a rift segment: Articulate axial magma storage at Erta Ale volcano, Ethiopia. Earth and Planetary Science Letters, 476, pp.79-86.

Yang, Z. and Chen, W.P. (2010), Earthquakes along the East African Rift System: A multiscale, system-wide perspective. *J. Geophys. Res.*, *115*(B12).

Yokoyama, T., M. Kusakabe, and E. Nakamura (2007), Plume-lithosphere interaction beneath Mt. Cameroon volcano, West Africa: Constraints from 238U- 230Th-226Ra and Sr-Nd-Pb isotope systematics, Geochim. Cosmochim. Acta, 71(7), 1835–1854.

Zeyen, H., P. Ayarza, M. Fernandez, and A. Rimi (2005), Lithospheric structure under the western African-European plate boundary: A transect across the Atlas Mountains and the Gulf of Cadiz, Tectonics, 24, doi:10.1029/2004TC001639.

Zlotnik, S., Jiménez-Munt, I. and Fernàndez, M. (2014), Coupled mantle dripping and lateral dragging controlling the lithosphere structure of the NW-Moroccan margin and the Atlas Mountains: A numerical experiment. *Lithos*, *189*, 16-27.

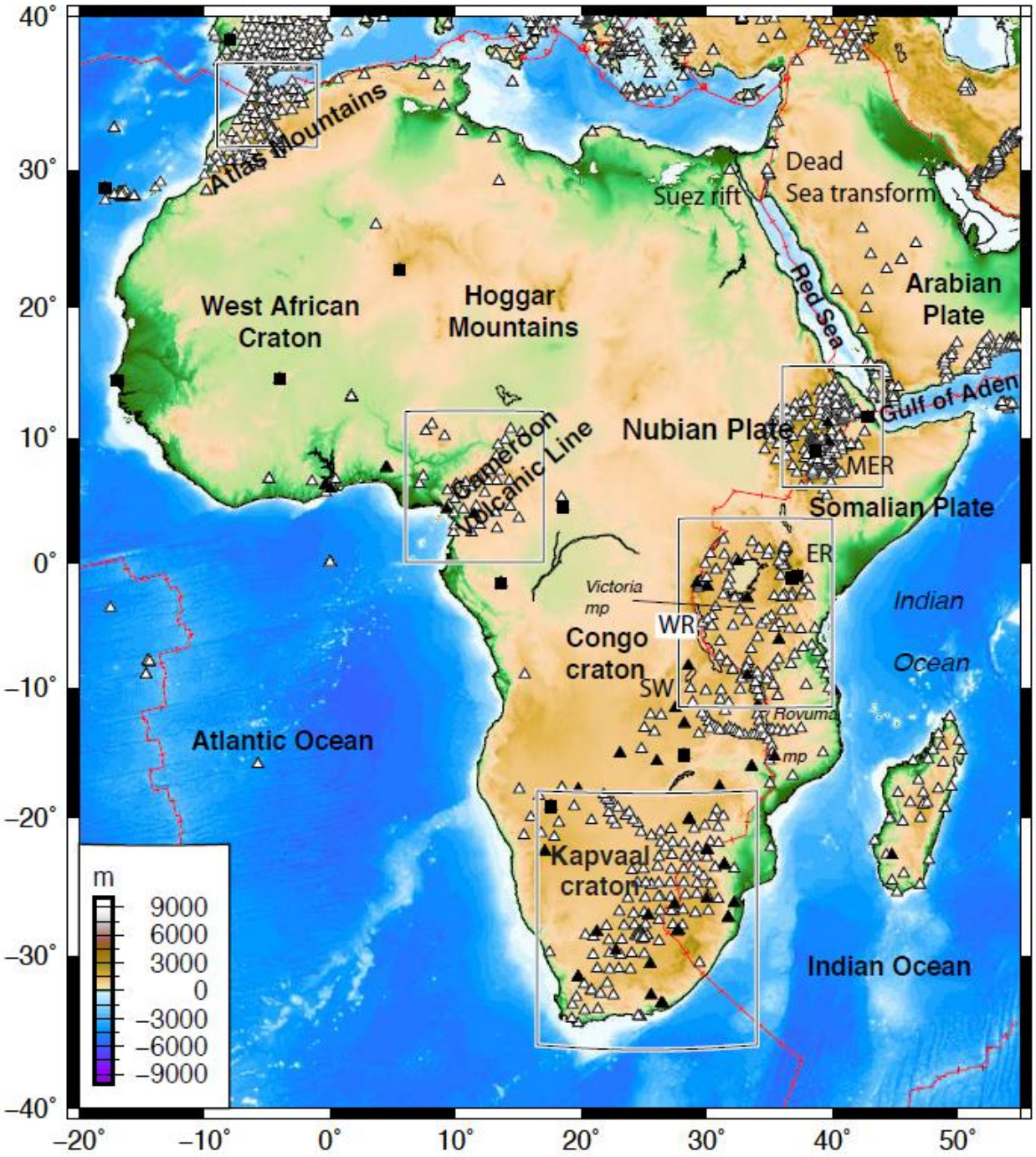

Figure 1. Topography of Africa with major plates (after Bird, 2009). Landforms and tectonic features labelled. White triangles are temporary seismic networks, whereas solid black shapes are permanent seismic stations. Stations used in controlled source experiments shown in Figures 5 and 7. Boxes enclose regions with crustal thickness information constrained from receiver functions in Figures 2 and 3. Sub-regions are explored in more detail in subsequent figures. SW = Southwestern rift; WR = Western rift; ER = Eastern rift; MER = Main Ethiopian rift; Rovuma mp = Rovuma microplate; Victoria mp = Victoria microplate.

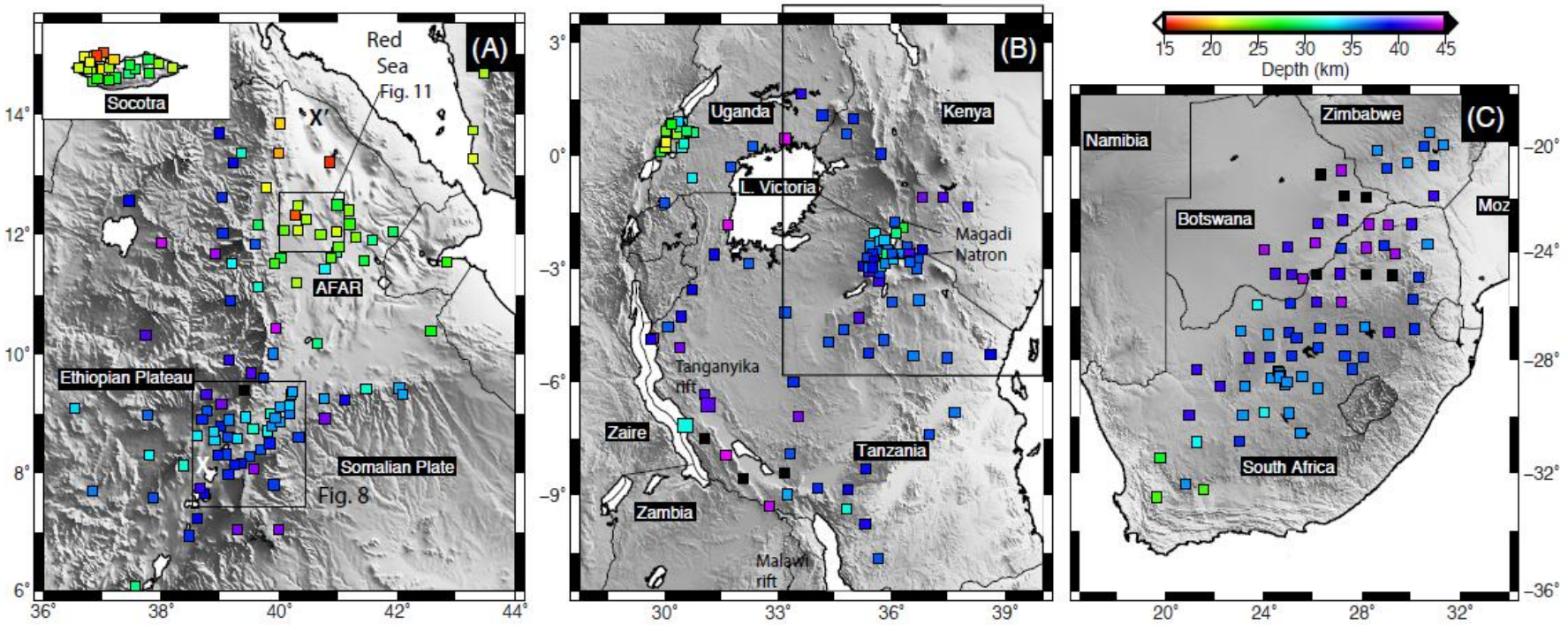

Figure 2. Crustal thickness in East Africa constrained using receiver function analysis. Boxes in 2a enclose area of Fig. 8 and Fig. 11. Box in 2b encloses area shown in Figure 4. Data are sourced from (A) Ethiopia-Yemen plateau regions and the Gulf of Aden Island of Socotra (Stuart et al., 2006; Dugda et al., 2006; Hammond et al., 2011; Ahmed et al., 2013, 2014); (B) East Africa (Tugume et al., 2012; Dugda et al., 2005; Wölbern et al. 2010; Plasman et al., 2017; Hodgson et al., 2017) (C) Southern Africa (Nguuri et al., 2001; Kgaswane et al. 2009).

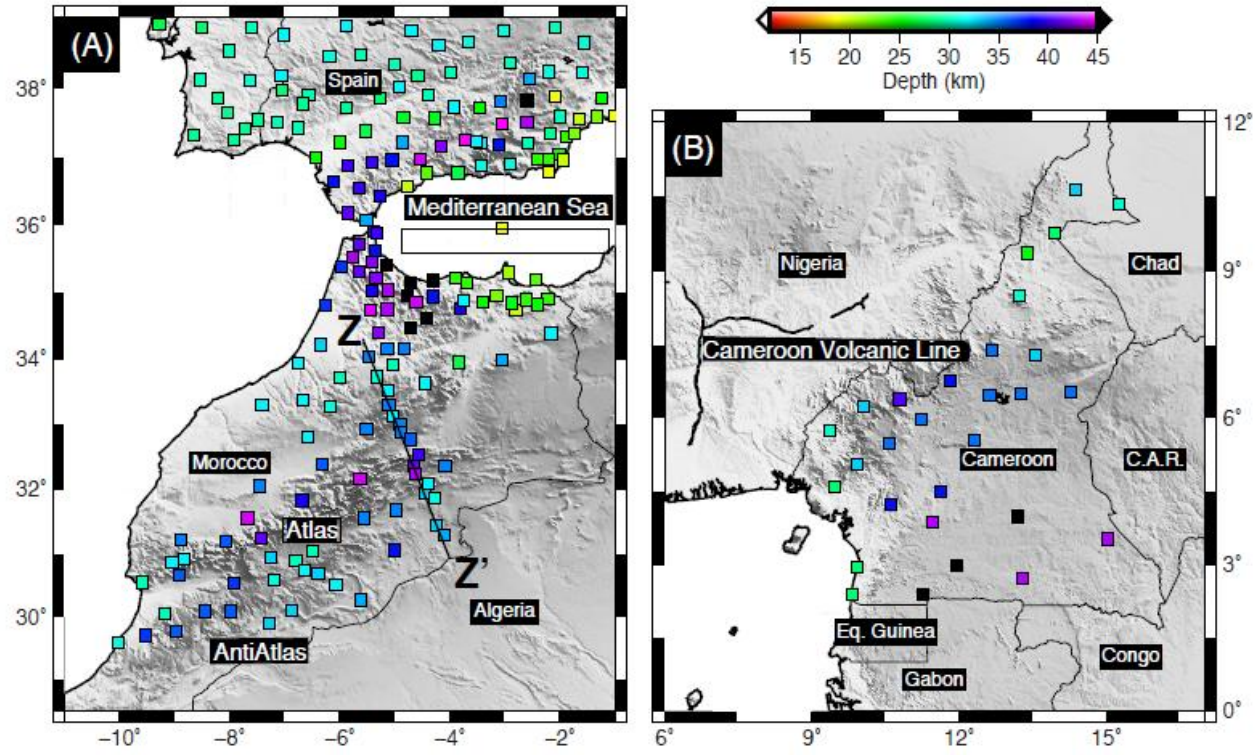

Figure 3: Crustal thickness in (a) the Atlas orogen (Africa-Eurasia collision) and (b) Cameroon Volcanic Line constrained using receiver function analysis. Z-Z' denotes location of profile shown in Figure 14. Data from (A) Mancilla et al., (2012); Miller and Becker (2014); Cooper and Miller (2015); Jessell et al. (2016); Spieker et al. (2014). (B) are sourced from Tokam et al. (2010) and Gallacher & Bastow (2012).

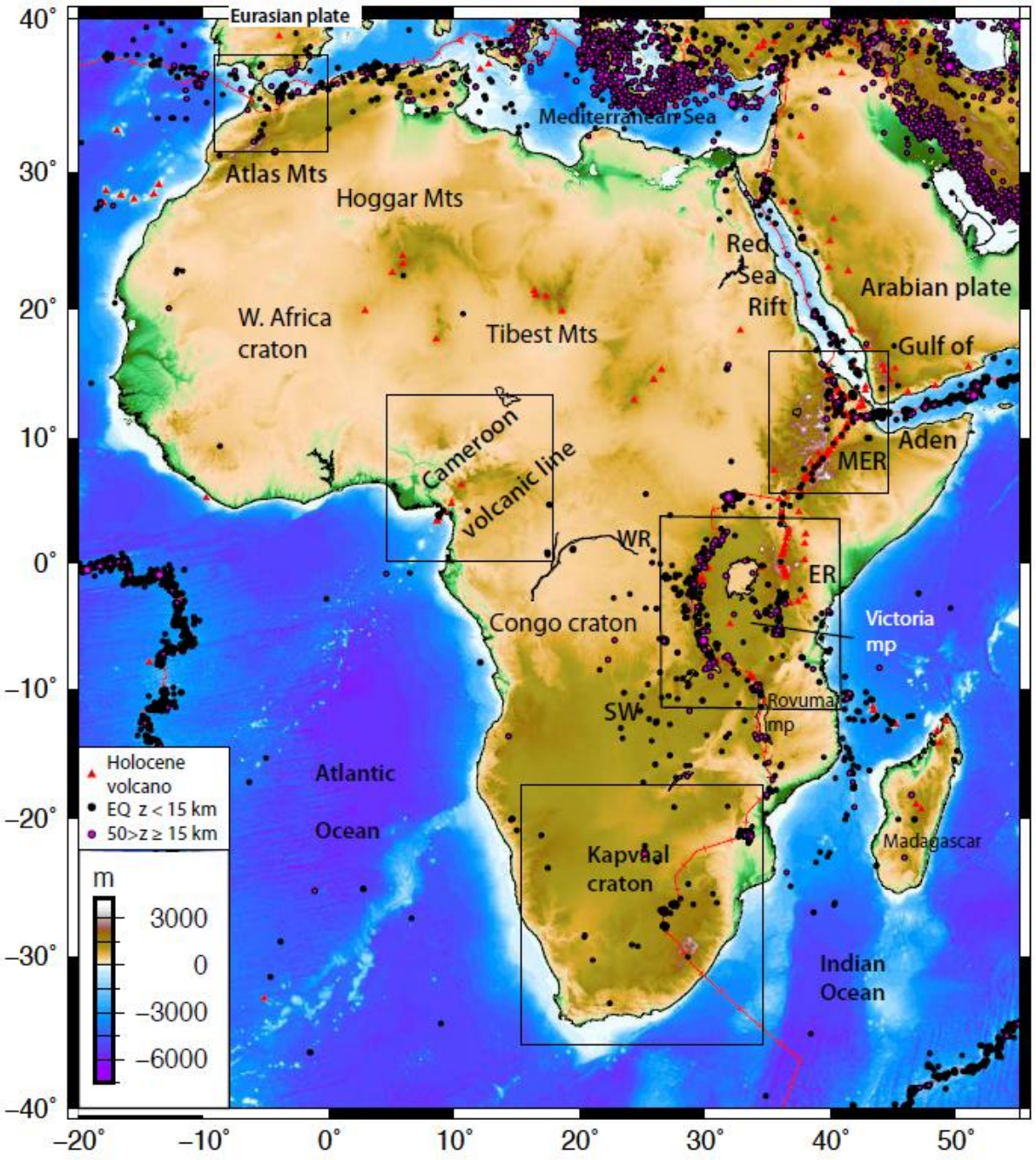

Figure 4: Topography of Africa with major plates, and 1976-2016 seismicity from the NEIC catalogue, and Holocene to Recent volcanoes from the Global Volcanism Program (http://volcano.si.edu/). ER = Eastern rift; WR = Western rift; SW = Southwestern arm; Rovuma mp = Rovuma microplate; Victoria mp = Victoria microplate. Large Archaean cratons with deep roots labelled; small Tanzania craton lies between the ER and WR. Lower crustal earthquakes with depths greater than 15 km are highlighted in magenta. Boxes enclose regions with crustal thickness information constrained from receiver functions in Figures 2 and 3.

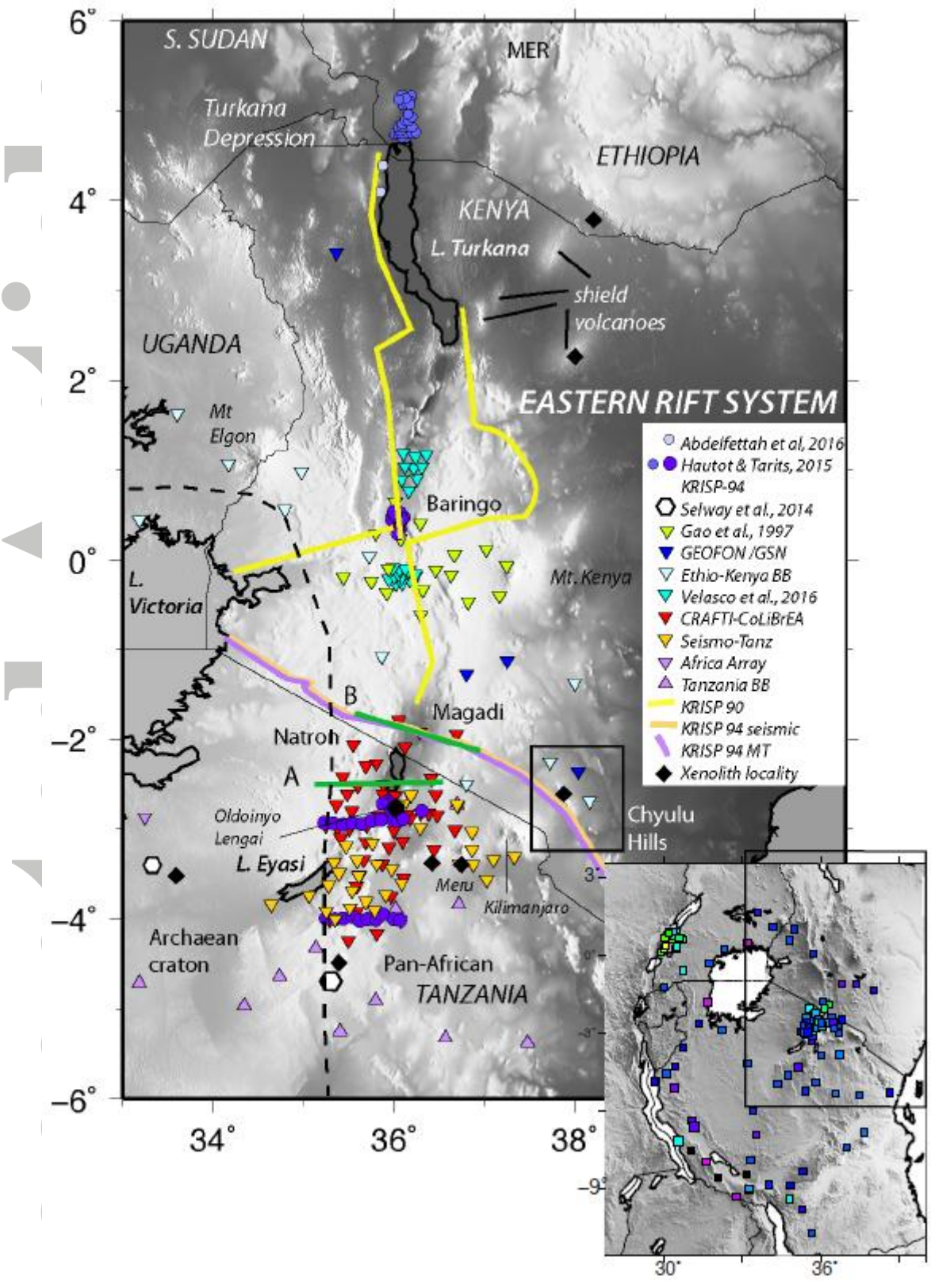

Figure 5. Compilation of seismic and magneto-telluric (MT) data sets from the Eastern rift system, with respect to crust and mantle xenolith localities. Inset places study area within context of region shown in Figure 2b. Bold green lines show the locations of cross sections of the Natron (A-A') and

Magadi (B-B') basins shown in Figure 6. Magadi and Natron are Early-Stage magmatic rift basins described in the text. Black box encloses the Chyulu Hills off-rift magmatic zone. Dashed black line is the approximate surface contact between Archaean and Pan-African crust. Triangles and inverted triangles are locations of broadband seismic data sets (Gao et al., 1997; Last et al., 1997; Dugda et al., 2005; Tugume et al., 2012; Albaric et al., 2014; Velasco et al., 2011; Plasman et al., 2017; Weinstein et al., 2017), and circles and hexagons are locations of intermediate and long-period MT recordings (Selway et al., 2014; Hautot et al., 2000; Simpson, 2000; Sakkas et al., 2002; Hautot and Tarits, 2015; Abdelfettah et al., 2016). Bold lines are approximate locations of the Kenya Rift International Seismic Project (KRISP) wide angle reflection/refraction and MT profiles as outlined in Prodehl et al. (1994) and Khan et al. (1999).

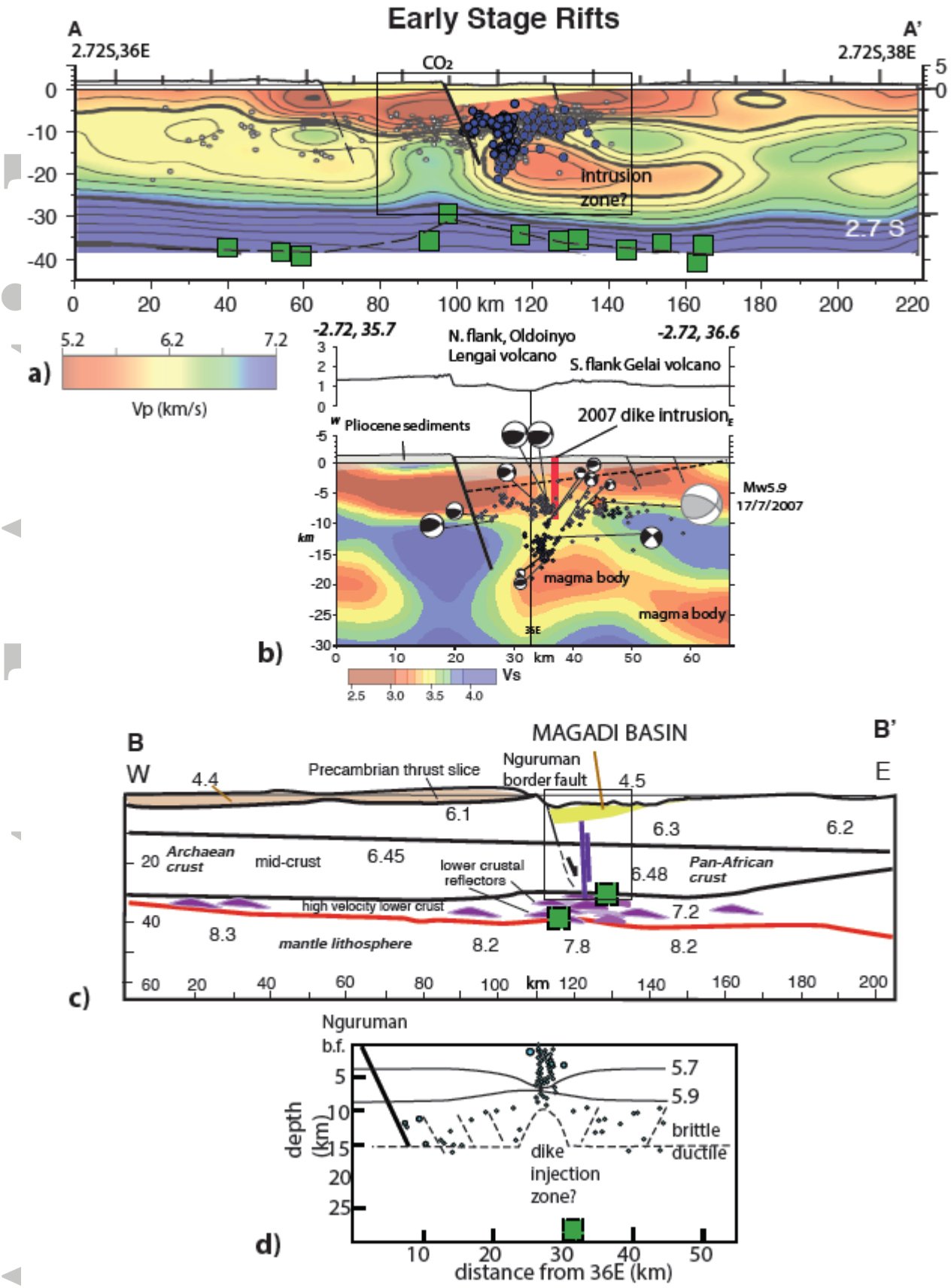

Figure 6. Cross-sections of crustal structure illustrating evolutionary changes in rift structure (see Fig. 5 for profile locations). With each diagram, we show a detailed velocity model with seismicity across

the active rift zone, from a variety of tomographic studies. Bold red line is refraction/reflection Moho. Purple lozenges indicate zones of underplate, or mafic lower crustal sills. For simplicity, dikes are sourced from the mantle, and shallow magma chambers, although multiple magma reservoirs may exist. Green squares are receiver function estimates of crustal thickness. A) Early-stage rifting in the ~3 My-old Natron basin. P- and S-wave Velocities from joint ambient noise, arrival time and gravity inversion (Roecker et al., 2017). Precise earthquake locations lying within 5 km of the line of section projected onto the line of the profile from Weinstein et al. (2017); receiver function crustal thickness estimates from Plasman et al. (2017). B) Increasing modification in the adjoining, ~ 7 My Magadi basin region (Birt et al. 1997). Bottom upper crustal section from arrival time tomography study of Ibs-von Seht et al. (2001), with earthquakes within 20 km projected onto the line of profile. Receiver functions from Plasman et al. (2017).

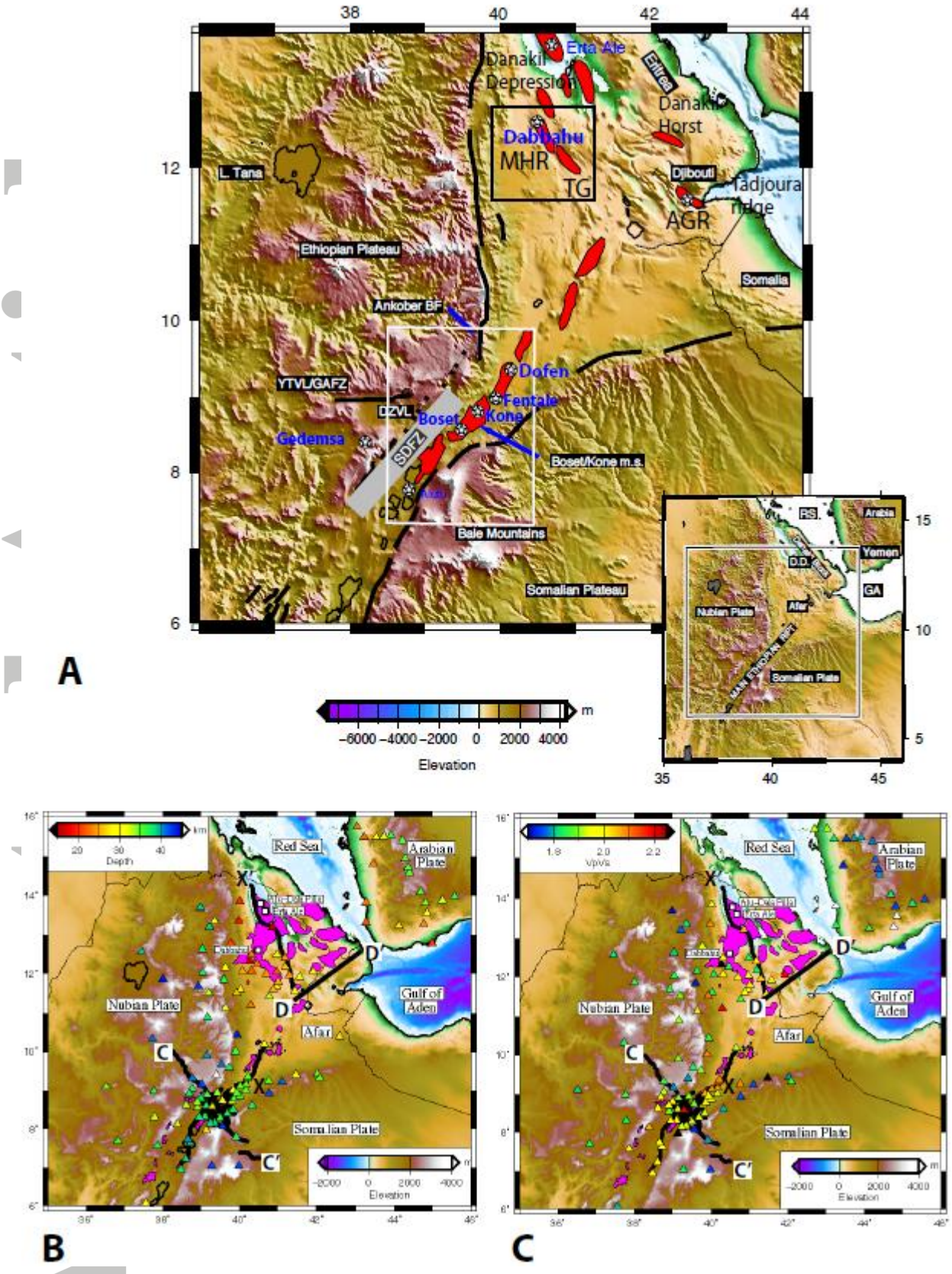

Figure 7. a) Topography and bathymetry of the Horn of Africa region. Red shapes are Quaternary to Recent magmatic segments along the rift axis. Black lines are Oligocene to Recent border faults. White circles are Holocene volcanoes named in the manuscript. SDFZ is Silti Debre Zeit Fault Zone and DVZL is Debre Zeit Volcanic Lineament. YTVL: Yerer Tullu-Wellel Volcanic Lineament. GAFZ:

Guder Ambo Fault Zone. MHR: Manda Harraro rift. TG is Tendaho Graben. AGR is Asal-Ghoubbet Rift. C-C' and D-D' indicate endpoints of crustal profiles shown in Figures 9 and 10. White box encloses area shown in Figure 8, and black box encloses area shown in Figure 11. X-X' indicate endpoints of crustal profile shown in Figure 12. c) Variations in crustal thickness with magenta indicating Quaternary lava flows. c) Variations in V_P/V_S in the region determined from receiver function analysis with magenta indicating Quaternary lava flows (Stuart et al., 2006; Dugda et al., 2006; Hammond et al, 2011; and Ahmed et al., 2012).

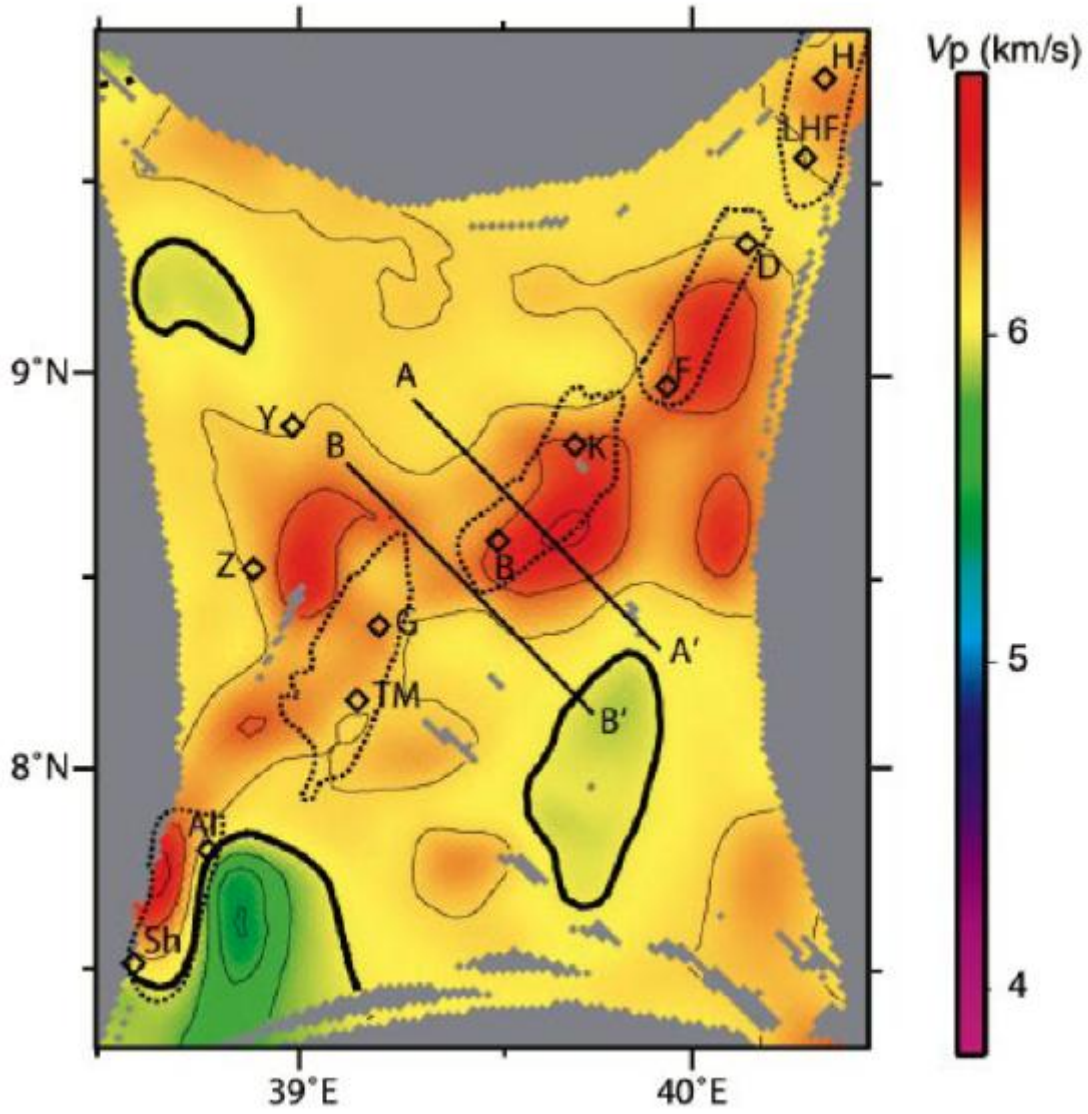

Figure 8. High velocity zones underlying magmatic segments of the central MER as imaged in horizontal slice of V_P at 10 km below rift topography, from controlled source and earthquake arrival time tomography (Keranen et al., 2004). Location of box shown in Figure 7a. Dashed lines enclose Quaternary-Recent magmatic segments. Diamonds denote locations of Quaternary-Recent eruptive centers: Sh = Shala; Al = Aluto; TM = Tullu Moje; G = Gedemsa; B = Boset; K = Kone; F = Fentale; D = Dofen; LHF = Liyado-Hayk field; H = Hertale. A-A' notes the location of the velocity profile shown in Figure 10b. Profile C-C' (Fig. 9) is centered on A-A', and it continues NW and SE of Profile A–A'. B-B' is shown in the original Keranen et al. (2004) paper.

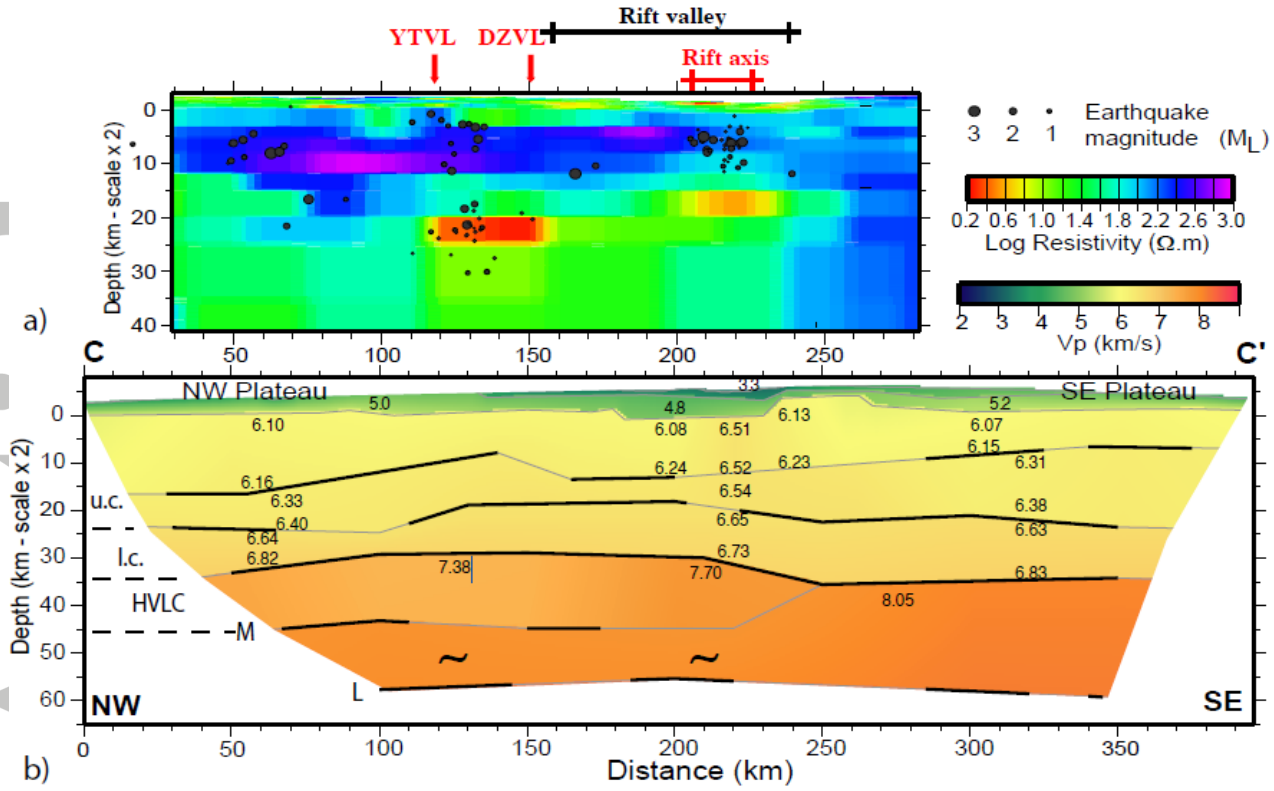

Figure 9. Rift cross-sections comparing several geophysical properties of the crust across the MER. The position of C - C' is labelled on Figure 7a. a) 2-D resistivity structure of the crust along a portion of A - A' determined using MT methods (Whaler and Hautot, 2006). The shallow low velocity parts of the model are interpreted as sediments and volcanic and volcaniclastic rocks filling in the subsiding basins of the MER, extending between ca. 150 and 250 km of C-C' (Keranen et al., 2004; Mackenzie et al., 2005). b) Profile C - C' is the P-wave velocity model of the crust determined using controlled source reflection / refraction (Mackenzie et al., 2005) with earthquake hypocenters (dark grey circles) recorded during Oct. 2001 - Jan. 2003 and located within 20 km either side (dashed lines) of the profile projected onto the section. Labels are u.c., upper-crust; l.c., lower-crust; HVLC, high velocity lower-crust; M, Moho.

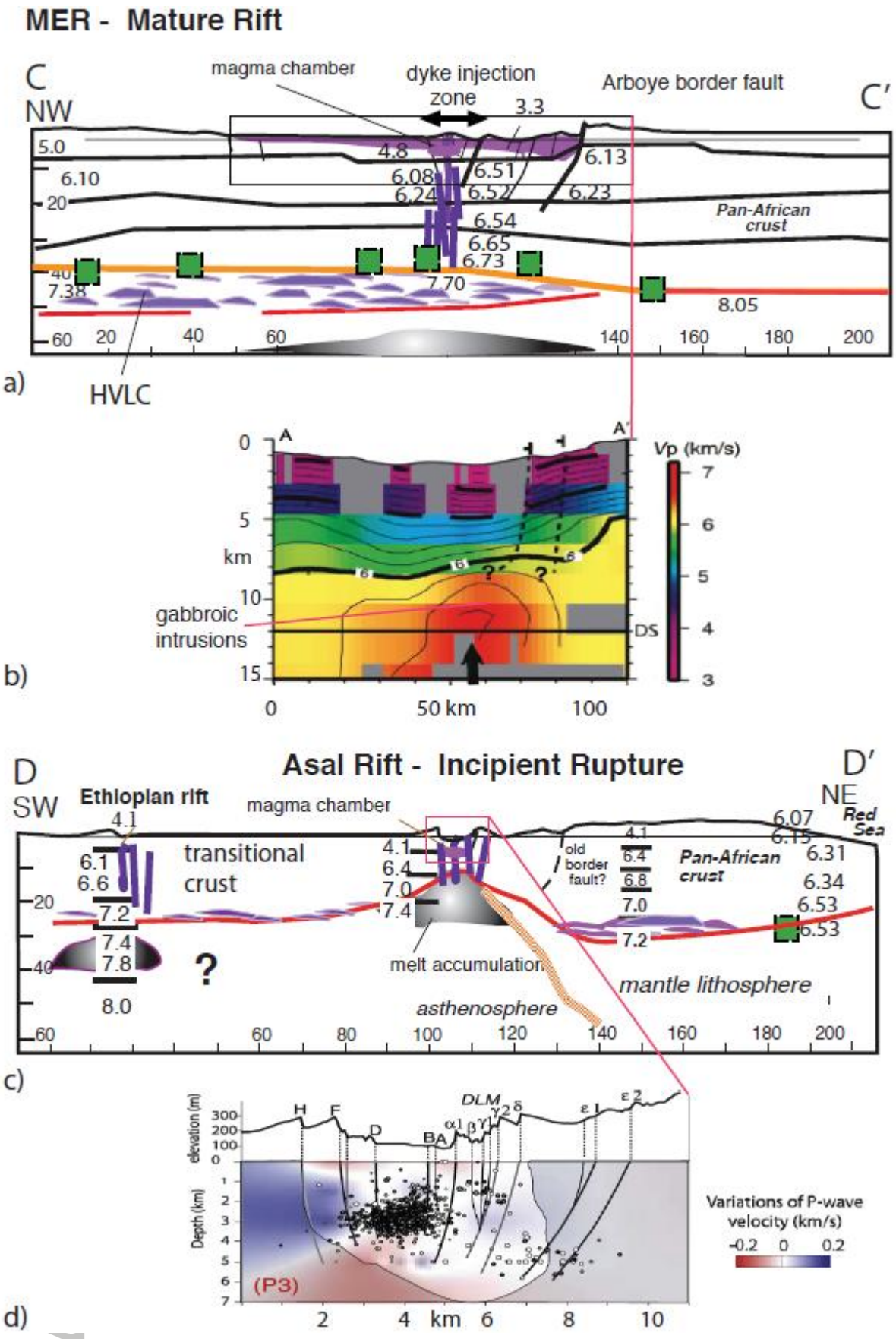

Figure 10: Cross-sections of crustal structure illustrating evolutionary changes between the mature Main Ethiopian rift and incipient seafloor spreading in the Asal rift (see Fig. 7a for profile locations).

With each diagram, we show a detailed velocity model with seismicity across the active rift zone. Bold red line is refraction/reflection Moho; orange line indicates top of thick underplate zone marked by. Purple lozenges (mafic lower crustal sills). For simplicity, dikes are sourced from the mantle, and shallow magma chambers, although multiple magma reservoirs may exist. Green squares are receiver function estimates of crustal thickness (Fig. 2A). a) Cross section C-C' of the ~12 My-old MER sector transitional between continental and oceanic rifting. Flood magmatism prior to rifting may contribute to the thick underplate. b) Shorter profile through 3D V_P tomography model (A-A', Fig. 8) shows gabbroic intrusions into lower and middle crust beneath the magmatic segment (Keranen et al., 2004). c) Incipient seafloor spreading in the Asal rift at the westernmost end of the Gulf of Aden rift based on velocity data from Makris and Ginzburg (1987) and Ruegg (1975) and structure from Doubre et al. (2007). d) Shorter profile from 3D V_P tomography model shows detail across rift. Greek letters refer to specific faults with measured slip rates, and colors from Doubre et al. (2007).

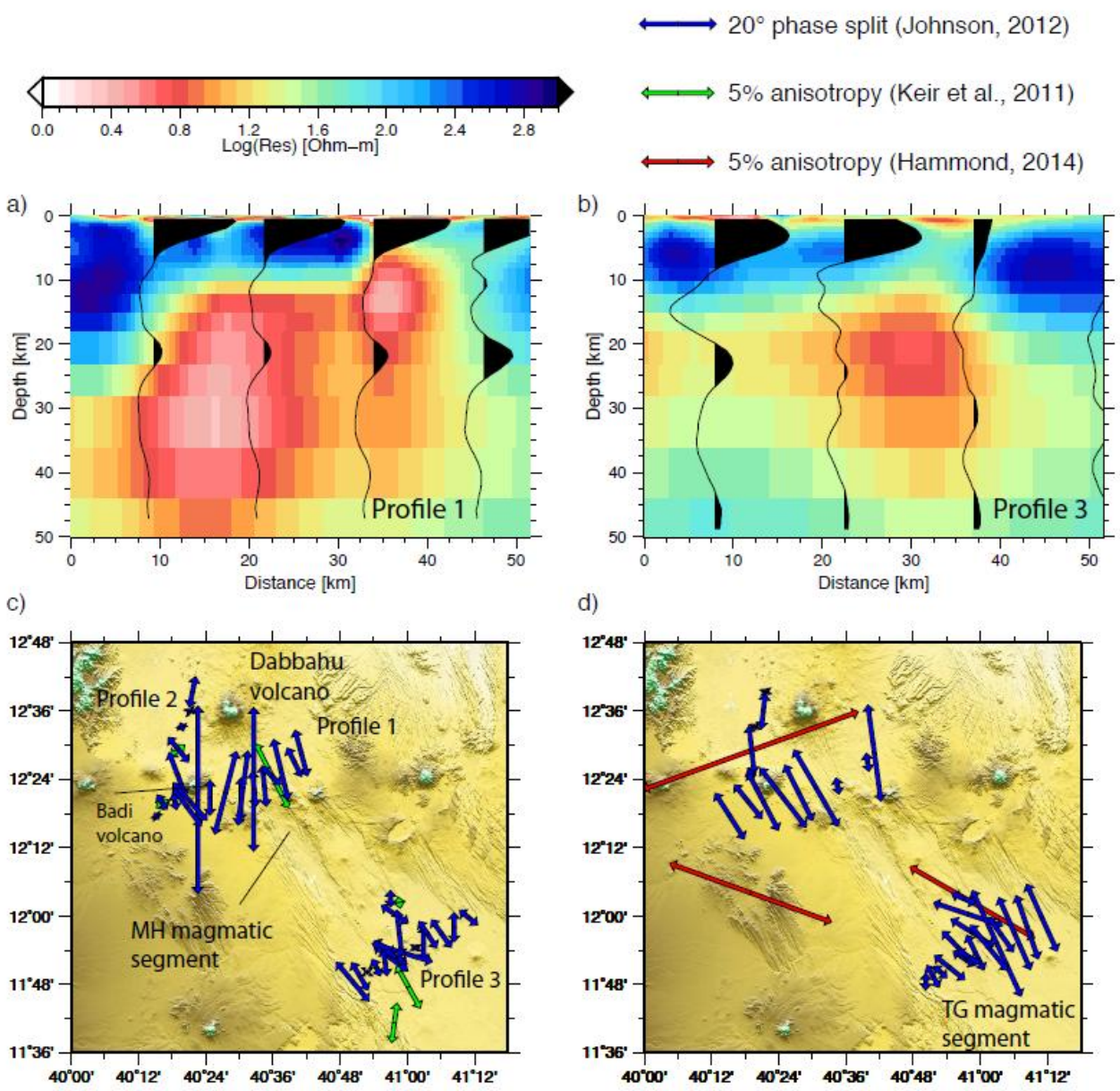

Figure 11. Comparison of MT and seismic models of crustal structure and anisotropy: a) Magnetotelluric results for Profile 1 (Desissa et al., 2013); b) Magnetotelluric results for Profile 3 (Johnson et al., 2016), with instrument locations shown in 11C. Location of study region shown in Figure 7a. Seismic traces on both plots show receiver function migrations from Hammond et al. (2011). c) Comparison of seismic anisotropy in the upper crust from shear-wave splitting (green arrows; Keir et al., 2011) and geoelectric strike from MT (blue arrows) for periods related to the low conductive (blue) areas shown in a, b (1-10 s) (Johnson, 2012). d) Comparison of seismic anisotropy in the whole crust from receiver functions (red arrows) (Hammond, 2014 and geoelectric strike from MT (blue arrows) for periods related to the highly conductive (red) areas shown in a,b (100-1000 s) (Johnson, 2012).

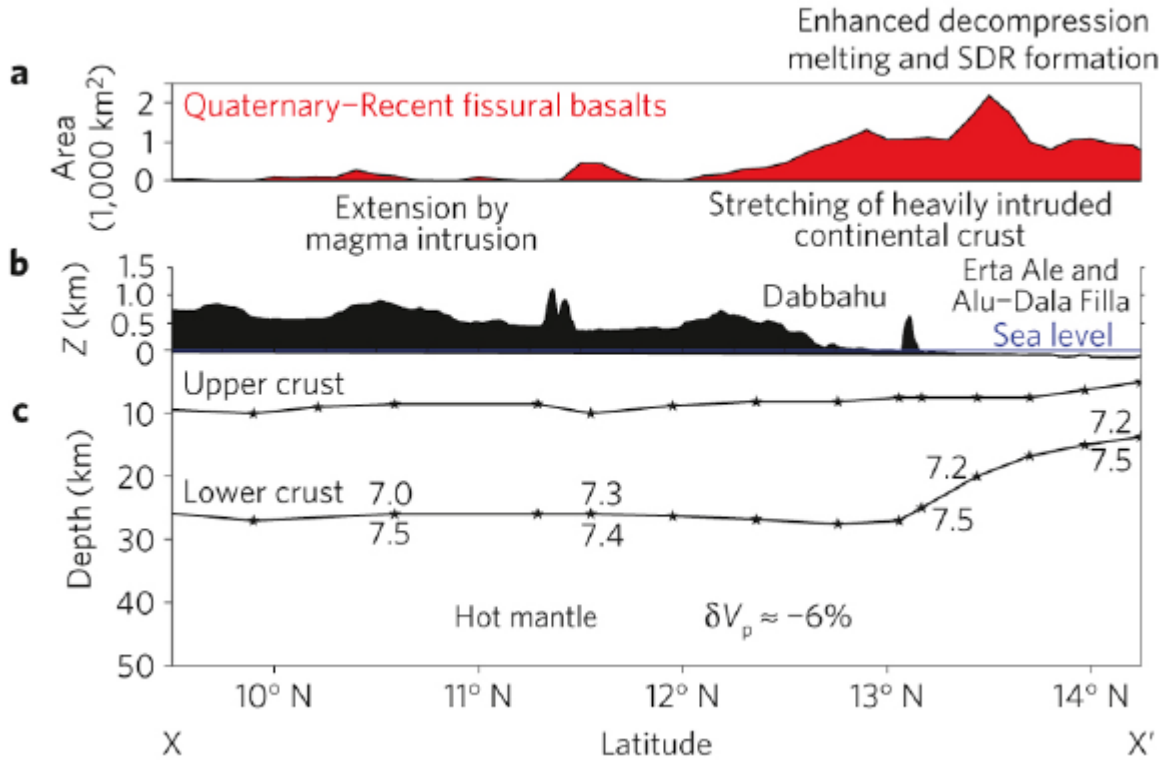

Figure 12. Panel a) Variation in Quaternary–Recent basaltic volcanism exposed every 0.1 latitude along strike in the Red Sea rift in Afar, with crustal velocity structure largely based on the EAGLE along-axis seismic profile (Maguire et al., 2006) and location shown in Fig 7A. Panel b shows elevation and Panel c shows crustal thickness. Seismic velocities are in km/s. Note the abrupt thinning of the crust in northern Afar (>13^{o} N), which coincides with subsidence of the rift valley below sea level and a marked pulse in Quaternary–Recent volcanism (after Bastow and Keir, 2011). SDR = seaward-dipping reflector; δV_P indicates regional velocity reduction relative to global norm.

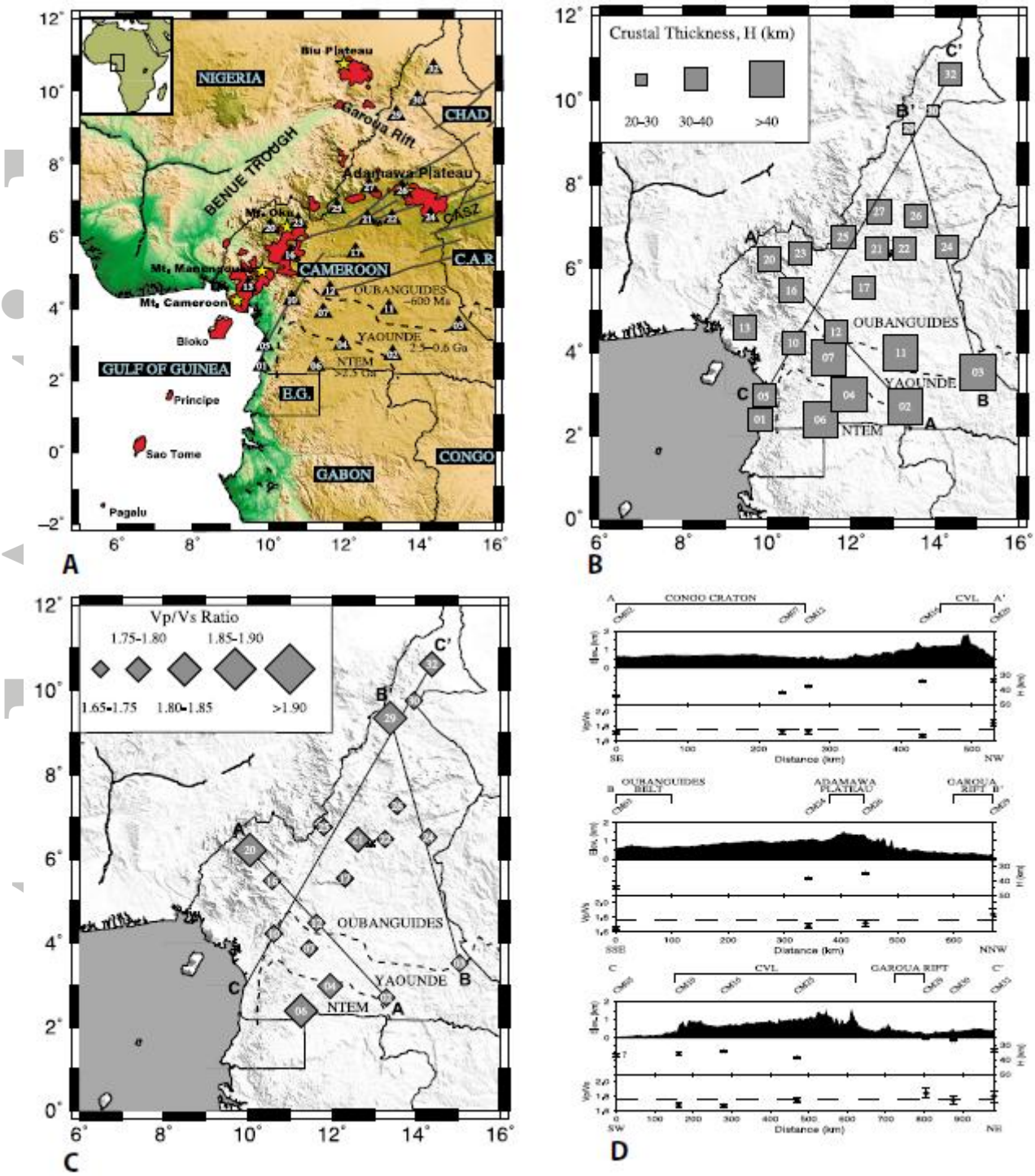

Figure 13. Panel A: Location map of the CBSE seismograph stations (triangles) superimposed on regional topography. Numbers are station codes. The Ntem Complex boundary and the Yaoundé domain boundary are after Toteu et al. (2004). Stars are selected CVL volcanoes. C.A.R.: Central African Republic; CASZ: Central African Shear Zone; E.G.: Equatorial Guinea. The red areas are regions of Cenozoic volcanism along the CVL taken from Tokam et al. (2010). Panel B:. Variations in crustal thickness. Panel C: Variations in V_P/V_S ratio across Cameroon from receiver function analysis. The thick black lines A-A′, B-B′, and C-C′ show the orientation of transects in Panel D. After Gallacher & Bastow (2012).

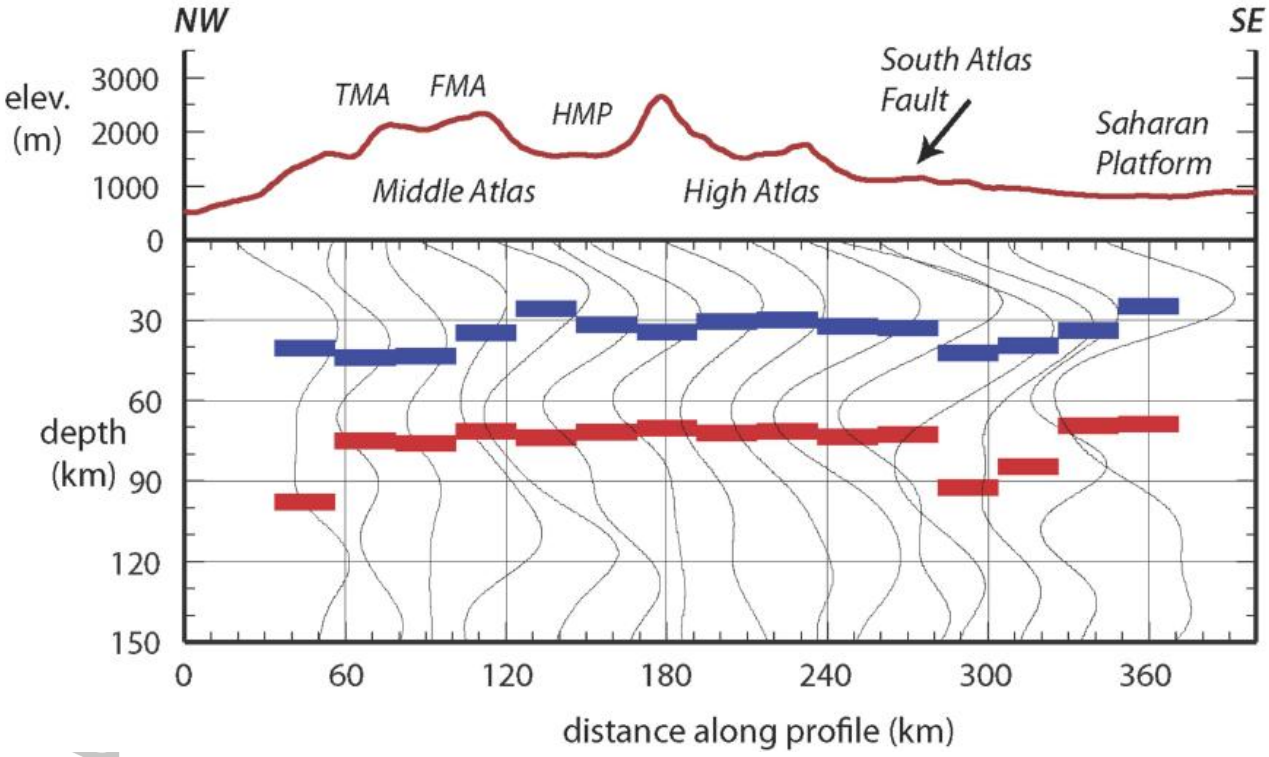

Figure 14. S-receiver function profile across Atlas Mountains from northwest to southeast as indicated in Figure 3A. Top panel indicates the elevation and primary tectonic features (HMP-High Moulouya platform; FMA-folded Middle Atlas; TMA-Tabular Middle Atlas). S-receiver function stacks at 40 km spacing are shown for all stations within 20 km of profile and plotted evenly spaced for clarity. Blue and red dashes indicate Moho and lithosphere-asthenosphere boundary, respectively.